Agent-based Modeling of Immunological Synapse Dynamics

Von der Fakultät für Lebenswissenschaften
der Technischen Universität Carolo-Wilhelmina zu Braunschweig
zur Erlangung des Grades
eines Doktors der Naturwissenschaften
(Dr. rer. nat.)
genehmigte
D i s s e r t a t i o n

von **Anastasios Siokis**
aus **Kastoria / Griechenland**

1. Referent: Professor Dr. Michael Meyer-Hermann
2. Referent: Professor Dr. Klemens Rottner
eingereicht am: 06.02.2019
mündliche Prüfung (Disputation) am: 25.06.2019

Druckjahr 2019

Vorveröffentlichungen der Dissertation

Teilergebnisse aus dieser Arbeit wurden mit Genehmigung der Fakultät für Lebenswissenschaften, vertreten durch den Mentor der Arbeit, in folgenden Beiträgen vorab veröffentlicht:

Publikationen

- Siokis, A, Robert, PA, Demetriou, P, Dustin, ML & Meyer-Hermann, M (2018). F-actin-driven CD28-CD80 localization in the immune synapse. Cell reports, 24(5), 1151-1162.
- Siokis, A, Robert, PA & Meyer-Hermann, M (2017). Mathematical Modeling of Synaptic Patterns. In The Immune Synapse (pp. 171-182). Humana Press, New York, NY.

Tagungsbeiträge

- Siokis, A, Robert, PA, Demetriou, P, Dustin, ML & Meyer-Hermann, M. An agent-based model for the F-actin driven spatial organization of the immunological synapse. 4th International Symposium on Image-based Systems Biology & InfectoOptics, 5-7 September 2018, Leibniz Institute for Natural Product Research and Infection Biology – Hans-Knöll Institute (HKI), Jena, Germany.
- Siokis, A. An agent-based model for the F-actin driven localization of TCR, LFA-1 and CD28 in the immunological synapse. Workshop on Computational Models in Biology and Medicine 2018, 8-9 March 2018, University of Regensburg, Germany.
- Siokis, A. Mathematical modeling of the Immune synapse formation. Molecular Immunology Symposium, 18 July 2016, Wolfson College, University of Oxford, United Kingdom.

Posterbeiträge

- Siokis, A, Robert, PA, Demetriou, P, Dustin, ML & Meyer-Hermann, M. Agent-based modeling of the F-actin driven spatial organization of the immunological synapse. Imaging the Immune System, 19-21 September 2018, Institut Pasteur, Paris, France.
- Siokis, A. Implications of actin dynamics in the immune synapse formation. Lymphocyte Antigen Receptor Signalling (EMBO Conference), 3-7 September 2016, Pontignano, Siena, Italy.

This research project (2015-2019) was supported by:

- the Human Frontier Science Program (HFSP) funding project: "Cooperation strategy and information processing in and between germinal centre reactions" (2015) for the first and second year of PhD

- an SFB project funding: "Molecular organisation of cellular communication within the immune system" (2018) for the third and fourth year of PhD

Abstract (English)

Adaptive immune responses require the exchange of information between T cells and Antigen Presenting cells (APCs). T cell receptors (TCRs) search and bind to processed antigen peptide bound to major histocompatibility complexes (pMHC) on the APC surface. During this process the surface molecules of the two cells are re-organized into a characteristic spatial pattern, known as Immunological Synapse (IS). The contact interface is segregated in three distinct regions, the central, peripheral and distal supramolecular activation clusters (c, p and dSMAC), occupied by different molecules. The formation of a stable IS leads to key events during the immune response, including T cell activation, fate decision and effector function such as killing of infected cells.

An agent-based model based on TCR-pMHC and LFA-1-ICAM-1 interactions was developed in order to investigate the mechanisms leading to the characteristic IS formation. Size-based segregation (SBS) for different sized complexes and coupling of molecules to the centripetal flow of F-actin are the considered mechanisms, and are discussed for additional molecules, such as the costimulatory CD28 and CD2, as well as the CD45 phosphatase, all important for TCR signaling.

SBS and centripetal flow resulted in the accumulation of TCR-pMHC in the center of the IS and the emergence of a peripheral LFA-1-ICAM-1 gradient which acted as an exclusion mechanism of molecules and complexes from the IS. The model predicted a mechanism of CD28/CD2 movement, according to which CD28/CD2 complexes passively follow TCR-pMHC movement. The characteristic annular CD28-CD80 pattern around the cSMAC only emerged with a particular CD28-actin coupling strength that induced a centripetal motion, whereas the CD2 *corolla* pattern formation required a CD2-CD2 self attraction but no interaction with the actin network.

The centripetal flow of TCR-pMHC complexes acted as a mechanism of TCR cooperativity, while active modulation of the association rate by F-actin foci showed that the global affinity of TCR toward pMHC molecules can be positively modulated.

The efforts to understand the mechanisms of IS formation can help in developing therapeutic targets aiming the formation of stable synapses, in cases like cancer and autoimmune diseases where impaired and unstable synapses and therefore defects on T cell activation are observed.

Keywords: Immune synapse formation, Agent-based modeling, Molecular localization, Pattern formation, TCR cooperativity, F-actin foci

Zusammenfassung (Deutsch)

Adaptive Immunreaktionen erfordern den Informationsaustausch zwischen T-Zellen und Antigen Presenting-Zellen (APCs). T-Zell-Rezeptoren (TCR) suchen und binden an prozessierte Antigenpeptide, die auf pMHC auf der APC-Oberfläche gebunden sind. Während dieses Vorgangs werden die Oberflächenmoleküle der beiden Zellen zu einem charakteristischen räumlichen Muster reorganisiert, das als Immunologische Synapse (IS) bekannt ist. Die IS ist in drei verschiedene Bereiche unterteilt, die zentralen, peripheren und distalen supramolekularen Aktivierungscluster (c, p und dSMAC), die von verschiedenen Molekülen besetzt sind. Die Bildung einer stabilen IS führt zu Schlüsselereignissen während der Immunreaktion, wie der T-Zell-Aktivierung oder Differenzierung zu Subtypen wie der zytotoxischen T-Zelle.

Ein Agenten-basiertes Modell wurde entwickelt, das TCR-pMHC und LFA-1-ICAM-1 Wechselwirkungen beschreibt, um die Mechanismen der Bildung von IS zu untersuchen. Die größenbasierte Segregation (SBS) für unterschiedliche große Komplexe und die Ankopplung von Molekülen an den zentripetalen Fluss von F-Aktin wurden implementiert und für die TCR-Signalvermittlung wichtigen kostimulatorischen Moleküle CD28 und CD2 sowie die CD45-Phosphatase diskutiert.

SBS und F-Aktin Zentripetalfluss führten zur Ansammlung von TCR-pMHC im Zentrum der IS und zur Entstehung eines peripheren LFA-1-ICAM-1-Gradienten, der als Ausschlussmechanismus von Molekülen und Komplexen aus der IS fungierte. Das Modell sagte einen neuen Mechanismus vorher, nach dem CD28/CD2 den TCR-pMHC-Komplexen passiv in Microclustern folgen.

Das ringförmige CD28-CD80-Muster um den cSMAC erfordert deren zentrale Bewegung mit einer bestimmten CD28-Aktin-Kopplungsstärke. Die CD2 corolla-Bildung erfordert eine CD2-CD2-Selbstanziehung aber keine Kopplung an F-Aktin.

Der Zentripetalfluss von TCR-pMHC-Komplexen wirkte als Mechanismus der TCR Kooperativität. Die aktive Modulation der Assoziationsrate durch F-Aktin-Foci ermöglicht eine Modulation der globale Affinität von TCR und pMHC-Molekülen.

Das verbesserte Verständnis der Mechanismen der IS-Bildung kann helfen, Therapien zu entwickeln, die auf die Bildung stabiler Synapsen abzielen, beispielsweise bei Krebs und Autoimmunerkrankungen, bei denen beeinträchtigte und instabile Synapsen und daher Defekte bei der T-Zellaktivierung beobachtet werden.

Schlüsselwörter: Immunologische Synapse, Agenten-basierte Modellierung, Molekulare Lokalisierung, Musterbildung, TCR-Kooperativität, F-Aktin

Dedicated to Calypso
for always being next to me
during tough and good moments
mentally supporting me whenever required
and enjoying the successes together.

Acknowledgements

The time is over. That's it. Many memories and many more stories to be told. These stories of course exist thanks to certain people, who made my PhD life and my life in Braunschweig in general a lot easier.

Philippe Paul August Robert, not only the best supervisor one can ask for but also a very good friend. Always there to help at work when needed, and always there when it comes to fun. Always willing to go for a beer, where we could discuss everything...form science and economy to politics and our lives and dreams. But we were not alone, Ananya Rastogi was also there. We started the same day at the lab, and we had to do all the lovely paperwork together! We had the same fears and this created a very good friendship. We teased her a lot for her diet choices, but it was all coming from our hearts!

Michael Meyer-Hermann. I have to admit I was lucky. You don't find a boss like him every day. Lively discussions, amazing ideas but most importantly a person you feel familiar with. Working with him gave me motivation to become better every day and deliver the best I can. I would also like to thank the rest of the lab members for creating a nice atmosphere.

I would also like to thank my collaborators from the University of Oxford and especially Michael Dustin. Working and discussing with him helped me understand the nature and importance of the synapse and also improve the modeling with his intellectual input.

I can not leave my family out of this...can I? Of course not! My mother, Eleni, and my father, Menelaos for supporting me all the years of my studies and believing in me. My brother Nikos, whose words back in winter of 2007, boosted my ego and motivated me to pursue becoming a Mathematician. He is still one of my biggest fans you know! Of course, I could never forget my late grandfather, Anastasios (yes we have the same name), who talked about me full of pride, trying to explain to my grandmother, Iordana, what the hell I am doing in Germany!

Last but not least, the person who motivates me every single day, the person who was always by my side, supporting me, creating a lovely environment and calming me down whenever I was over the edge, my other half and partner, Calypso!

To all YOU people, a big thanks from the depths of my heart!

Abbreviations

TCR	T cell receptor
pMHC	Antigen peptide bound to major histocompatibility complex
LFA-1	Lymphocyte function-associated antigen 1
ICAM-1	Intercellular adhesion molecule 1
CD28	Cluster of differentiation 28
CD80	Cluster of differentiation 80
CD2	Cluster of differentiation 2
CD58	Cluster of differentiation 58
CD45	Cluster of differentiation 45
APC	Antigen Presenting Cell
SLB	Supported Lipid Bilayer
SBS	Size-based segregation
IS	Immunological synapse
AM	Arbitrary molecule
c, p & dSMAC	central, peripheral & distal supramolecular activation cluster
SD	Standard deviation

Contents

Chapter 1

Introduction

1.1 The immune system

Billions of bacteria, viruses, fungi and parasites are constantly attacking our bodies in order to make it their home. The high energy concentration of our bodies is the perfect environment for these microorganisms in order to thrive. Thankfully humans have developed a multifaceted and complex defence army, the so called immune system. The immune systems consists of a complex network of cells, tissue and organs that work together in order to keep us healthy. Organs and tissue include the skin, mucous and membranes, the bone marrow, the thymus, lymph nodes and lymphatic vessels, tonsils and the spleen (Figure 1.1). These organs utilize, assist and promote the presence of different cell types, such as granulocytes, macrophages (MΦs), neutrophils, dendritic cells (DCs), natural killer (NK) cells, as well as B and T lymphocytes, in order to properly repel the attacks.

The foreign substances entering our bodies have developed evasion mechanisms to hide from the immune system. Luckily, the immune system has also "evolved" and developed ways to recognise and clear such foreign microorganisms. All jawed vertebrates, including humans, have developed a very diverse and sophisticated two-layered defence system, the innate or non-specific immunity and the adaptive or acquired or specific immunity [1–3]. The first line of defence is by blocking the entrance of these microorganisms to the body with the help of skin and mucous. If this barrier is breached and the microorganisms manage to enter the body, innate immune responses are initiated. This is a non-specific and immediate defence against all the foreign organisms entering the body [4]. One can simply think of the innate immune system as a detection mechanism. If the pathogens manage to break through the innate immune barrier too, adaptive immune responses take over, this time in a specific manner [3, 5].

Randomly generated pattern recognition receptors (PRRs) identify microorganisms entering the body and rapidly initiate the innate immune response. Phagocytes, such us macrophages and neutrophils, are recruited to the area of foreign invasion and begin to kill or inactivate the foreign objects. In this way the spread of the microorganisms throughout other parts of the body

is stopped or at least delayed [4, 6, 7]. The innate immune response though is short lived, but essential to "buy time" for the second, "smarter" way of defence, the adaptive immune response, to take over. The adaptive immune response involves two types of immunity, the humoral and the cell-mediated immunity [8–18]. Humoral immune response is mediated by B lymphocytes, while cell-mediated immunity comes in the form of T lymphocytes. The cells taking part in the defence system are depicted in Figure 1.2.

B cells can recognise 3D structures, such as proteins, lipids and native antigens. Their B cell receptor (BCR) can even detect soluble antigen. When encountering foreign antigen (Ag), B cells endocytose it, process it and present parts of it on their surfaces. The Ag is bound to major histocompatibility complexes of class II in the form of peptide-Ag, annotated as pMHC. The B cells in this case act as antigen presenting cells, APCs. B cells then migrate to the lymph nodes and interact with T helper cells (T_H) [19]. This interactions will lead to T_H activation which in turn release some special molecules called cytokines that induce rapid B cell proliferation [20–23]. The new B cell clones will become either plasma or memory cells. The plasma cells produce antibodies that on one hand can bind to foreign cells in order to inhibit their functions and on the other hand can attract phagocytes and killer cells in order to eliminate the invaders [24–26]. Memory cells remain inactivated and the next time they encounter the same antigen, they produce new plasma cells, starting in this way a faster immune response [27–31]. Other kinds of APCs include dendritic cells and macrophages [32–37]. DCs are also considered mediators of communication between innate and adaptive immune responses [38].

The cell-mediated immune response requires the recognition of Ag by the T cells, which will lead to further action. As mentioned before, Ag is processed by APCs, such as B cells, dendritic cells, macrophages and in general all innate immune cells, and presented on their surfaces through a non foreign Ag, bound to MHC. T cells can only recognise Ag by binding their T cell receptor (TCR) to MHC complexes and different T cell types recognize the presented Ag in different ways [39].

When TCR binds to Ag presented through class I MHC, we refer to killer or cytotoxic T cells [40], whereas when binding to class II MHC, we refer to helper and regulatory T cells. In order to get activated, killer T cells need additional signals from a co-receptor of TCR known as CD8, and therefore these cells are also called $CD8^+$ T cells. Similarly, helper and regulatory T cells need the assistance of the CD4 co-receptor and are known as $CD4^+$ T cells [4]. Other types of T cells such as natural killer T (NKT) cells, that share the properties of natural killer (NK) and T cells are not considered as classical T cells [41, 42].

Once cytotoxic T cells get activated, they travel through the body in search of the same Ag that they initially recognized. When a cell with this Ag is found, they release toxins in order to kill it. The killing is performed either by release of perforin which disrupts the infected cell membrane or by release of granulysin that induces the apoptosis of the infected cell [43–46].

Helper T cells on the other hand instead of killing, are the commanders of the body's defence, by instructing other cells, such as cytotoxic and natural killer (NK) cells [47, 48], to perform this job. Once helper T cells get activated due to the Ag recognition, cytokines are released which

drive the other cells to either kill or in the case of B cell to produce antibodies [4, 49–52].

One role of regulatory T cells (Tregs) is, as their name suggests, to regulate the activation state of other cells, in order to avoid excessive and uncontrolled killing [53–56]. These are Foxp3 expressing T cells. Interestingly, it is suggested that $CD4^+Foxp3^+$ Tregs accumulate in skeletal muscle shortly after acute injury and assist in muscle repair [57, 58].

Natural killer (NK) cells are considered innate immune cells, which can also recognise *Ag* bound to MHC [59–61]. A behaviour of NK cells, which shows that their surface receptors are tuned to grasp abrupt changes in the stimulus that they receive instead of the absolute level of stimulus, is proposed as the "discontinuity theory of immunity" [62, 63]. This theory can be supported by the fact that when infected cells manage to escape the surveillance of B and cytotoxic T cells, are being attacked by (NK) cells.

The functions of B and T cells are presented in Figure 1.3. While B cells can access *Ag* in the extracellular environment, they fail to detect intracellular pathogens, such as viruses or bacteria. Thus, through the production of specific antibodies, B cells support the extracellular defence. T cells on the other hand, have to scan the surfaces of APCs, bind to the presented *Ag*, and subsequently get activated in order to perform their respective tasks, cytotoxic T cells to kill and helper T cells to boost B and cytotoxic T cell function as well as recruit other immune cells. In contrast to B cells, T cells cannot recognize extracellular and soluble antigen, but only processed antigen, presented by APCs.

In this thesis, I will focus on the interactions between T cells and APCs during antigen recognition. This process leads to the reorganization of the surface molecules of these cells resulting in the appearance of a characteristic pattern known as immunological synapse (IS). The IS pattern formation is of great importance for T cell activation. Here, I will focus on the mechanisms leading to the emergence of different, characteristic IS patterns.

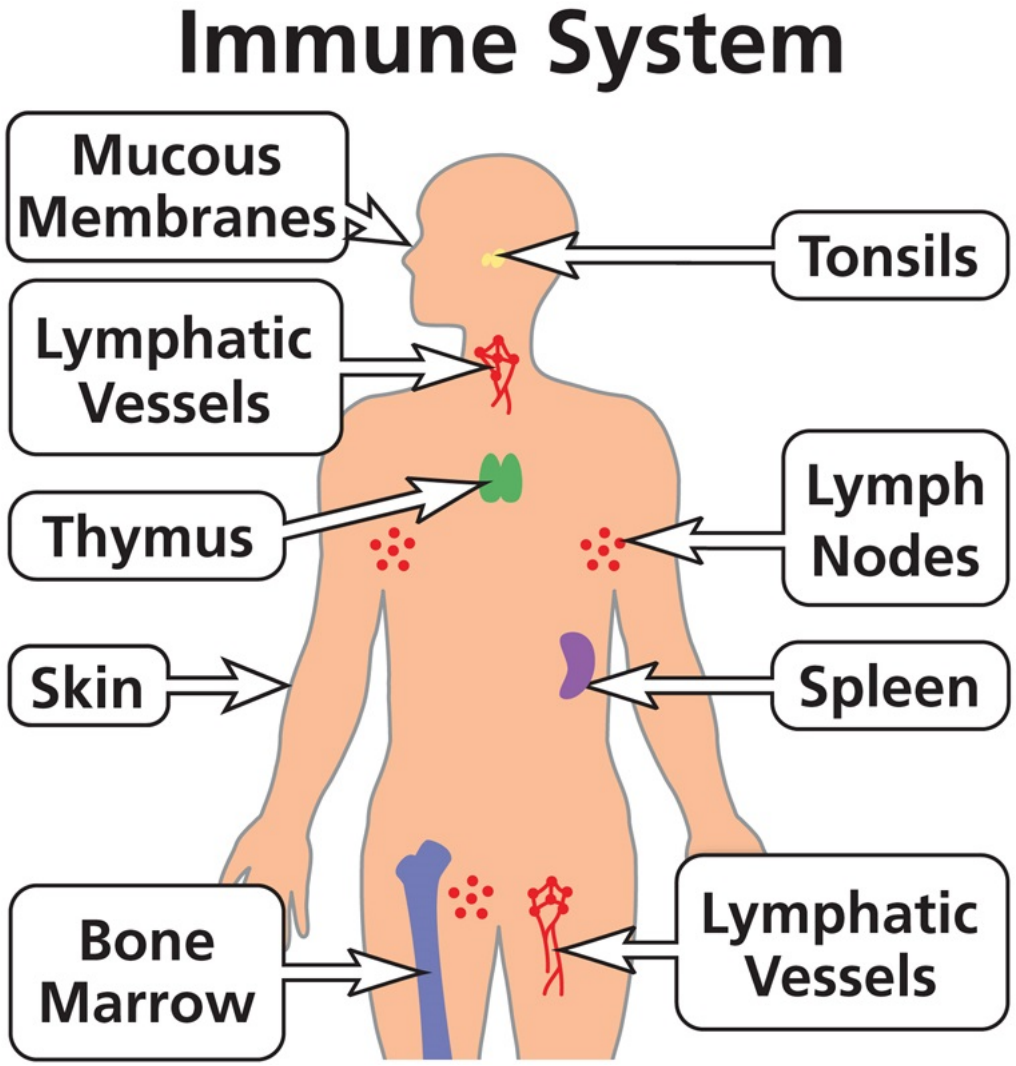

Figure 1.1: The organs of the immune system. Skin, mucous and membranes block the majority of pathogens to enter the body. When the first barrier falls, the rest of the organs, thymous, bone marrow, lymph nodes, tonsils and spleen, produce and train immune cells. Figure taken from: US Department of Health and Human Services, NIH, URL: `https://tinyurl.com/y78ejau3`.

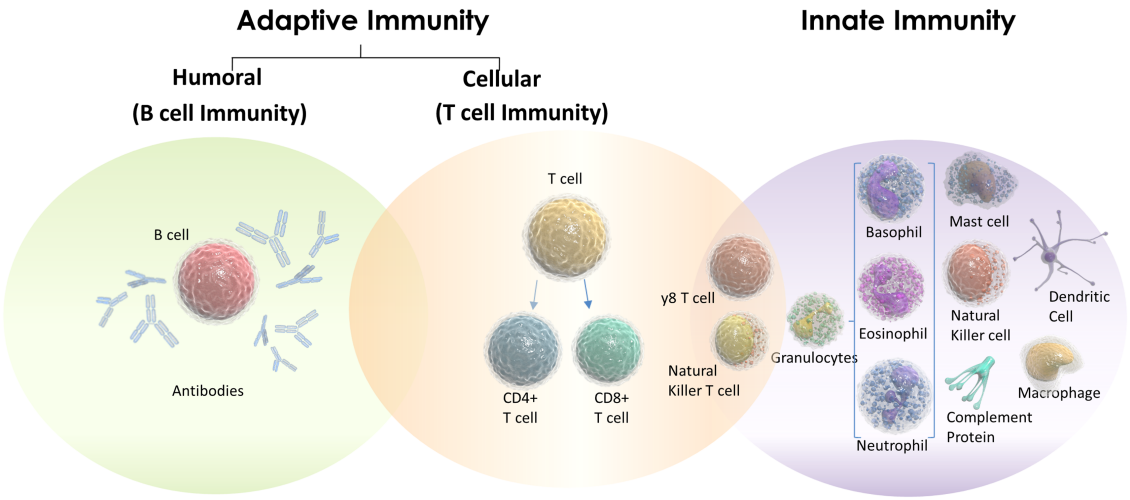

Figure 1.2: The cell types of innate and adaptive immune system. Adaptive immune responses come in the forms of humoral and cellular immunity. Figure taken from: Oxford Immunotec, URL: `http://www.oxfordimmunotec.com/international/science/technology-2`.

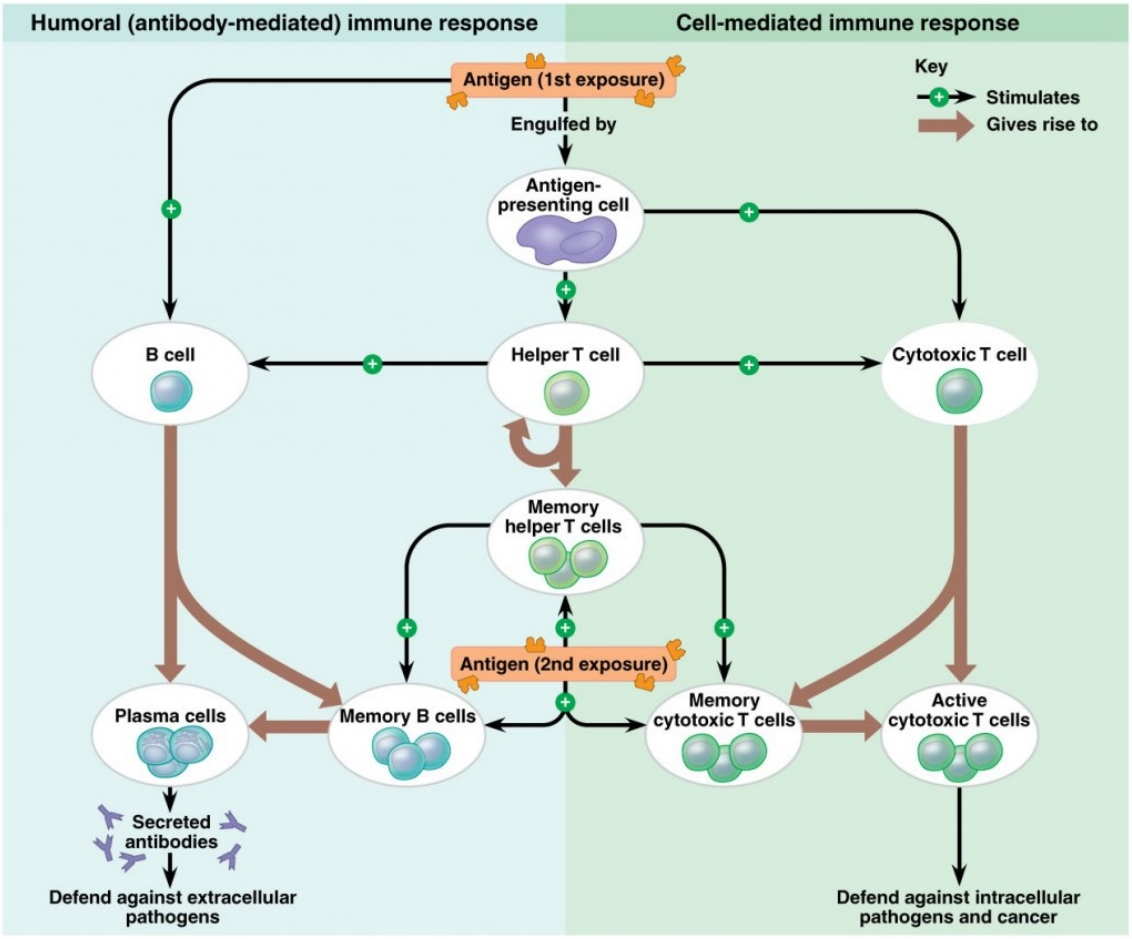

Figure 1.3: Functions and interactions of the immune cells during an adaptive immune response. Upon antigen uptake, B cells can get activated and produce memory and plasma cells, which defend against extracellular pathogens. During antigen presentation by APCs, cytotoxic and helper T cells get activated. Cytotoxic T cells defend against intracellular pathogens, whereas helper T cells boost the effector function of B and cytotoxic T cells. Figure taken from: University of Leicester, as was adapted from Biology, 8th Edition, Campbell and Reece, 2008 [64], URL: `https://www2.le.ac.uk/projects/vgec/highereducation/topics/microbial-genetics-1/vaccines-1`.

1.2 The immunological synapse

Formation of the immunological synapse. Dendritic cells (DCs), and more generally APCs, collect antigen roaming the body by taking up large amounts of fluid and engulfing host or pathogenic particles. They degrade pathogen proteins into peptides which in turn bind to MHC complexes and are presented at the surface of the cells as these APCs move toward the lymph nodes. In lymph nodes, they come into contact with thousands of naive T cells. Naive T cells are the ones that were never in contact with antigen before (antigen inexperienced). In this way, the T cells carrying TCRs become antigen specific which in turn leads to T cell proliferation. These T cells then exit the lymph node and migrate either to the site of infection via the blood stream or to the B cell follicles. The T cells that move to the site of infection will on one hand start killing, in the case of cytotoxic T cells (CD8 T cells), or on the other hand, boost and coordinate other cells to perform the killing and other immune compartments to clear the pathogen, in which case they are called helper T cells (CD4). The phenotype of the T cells depends on the signals received by the interactions with APCs in the thymus. In the particular case of antibody responses, B and T cells need to meet in follicles and germinal centres, where T cells propagate important signals to resident B cells. These signals define the fate of B cells, by either leading to B cell selection and consequent high affinity antibody generation or B cell death. The interaction of a T cell with an APC, i.e. B cell, dendritic cell, macrophage etc., is depicted in Figure 1.4.

Therefore, it begins to become obvious that antigen recognition by T cells is a key event during an immune response. During the antigen recognition process T cells come in close contact with DCs, B cells or in general professional APCs, i.e. APCs that present the peptide antigen bound to MHC complexes of class II (Figure 1.4). TCRs search the APC surface for the presented antigen, which are annotated as pMHC. Once the initial binding events happen, additional molecules bind their respective ligands. One characteristic example is the lymphocyte function associated antigen-1 (LFA-1) which is a cell adhesion molecule and binds to intercellular adhesion molecule-1 (ICAM-1), present on the APC surface [65, 66]. This process leads to the stabilization of the contact interface and the re-organization of the surface molecules into the characteristic pattern known as the immunological synapse (IS). Therefore, the IS is a dynamic cell-cell interface with binding of molecules, spatial activation of signaling pathways and reorganization of the cytoskeleton.

It was initially observed that TCR bind to pMHC molecules, the term TCR-pMHC complexes will be used. TCR-pMHC accumulate in the center of the contact region between the two interacting cells [68, 69]. This region was named central supramolecular activation cluster or cSMAC. This central TCR-pMHC region is surrounded by a ring of LFA-1-ICAM-1 called the peripheral SMAC (pSMAC). There are many more molecules and receptors taking part in the process of this dynamic pattern formation, such us CD4/CD8 which define the function of the T cell (helper or cytotoxic T cells respectively), the costimulatory molecules CD28 and CTLA4 which compete for the same ligands, CD80 and CD86, that also reside in the cSMAC, while other characteristic examples include CD2 molecules on T cells that bind to CD58 in humans and CD48 in rodents and

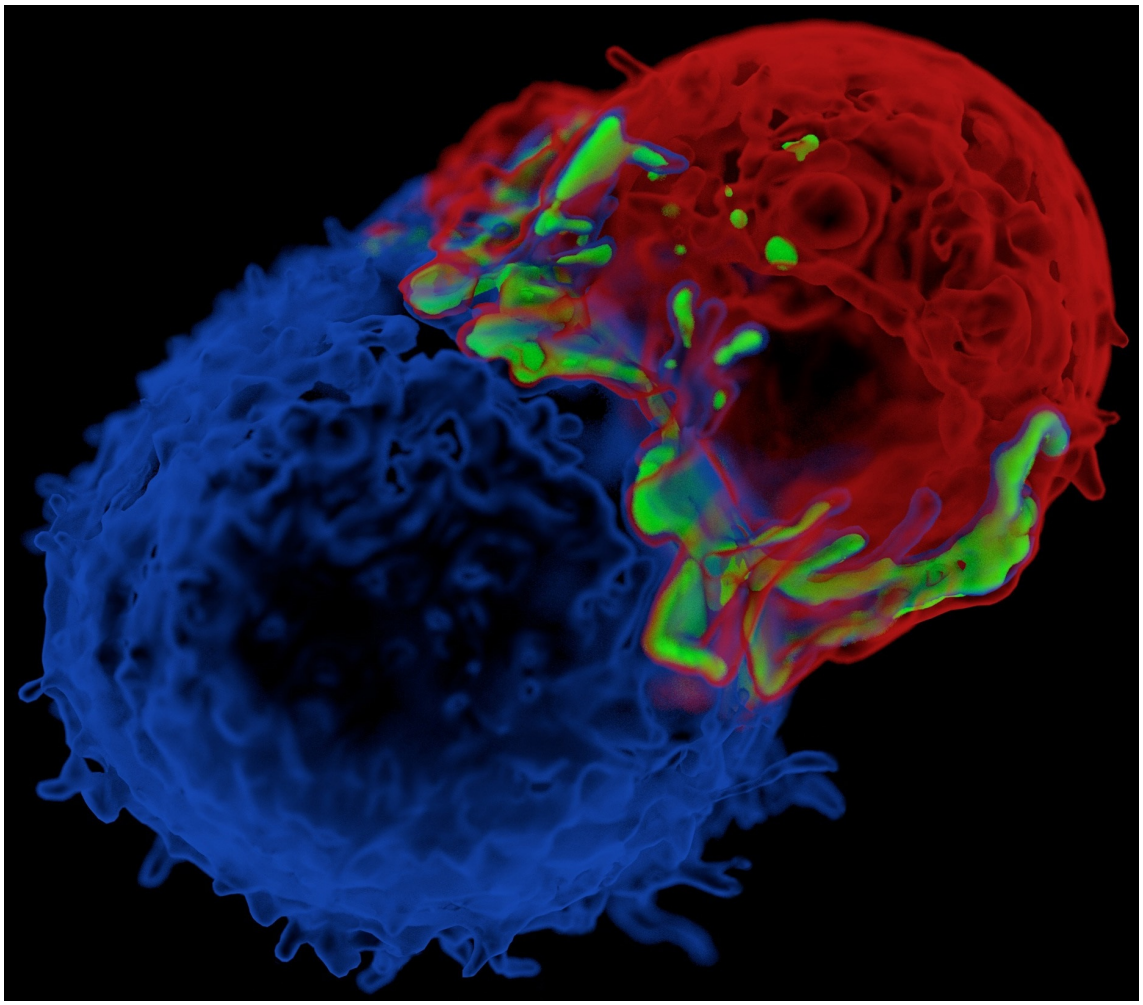

Figure 1.4: The interaction of an engineered T cell (red) with an antigen presenting cell (blue). This interaction leads to the recruitment of signaling molecules such as ZAP70 (green) to the contact interface. Figure taken from : Vale's Lab URL: `https://valelab.ucsf.edu/`, as created for the publication: James and Vale, Nature, 487, 64-69, 2012, DOI: `https://doi.org/10.1038/nature11220` [67].

the CD45 molecules for which there is no discovered ligand, that accumulate to the outer pSMAC region, referred as distal SMAC (dSMAC) [70]. The pattern depicted in Figure 1.5, is the widely studied immunological synapse (IS), also known as "bull's eye" pattern.

Proposed mechanisms behind immunological synapse formation This characteristic IS structure impacts on T cell activation, signaling and fate decision [71–78]. A lot of attention has been placed toward understanding the mechanisms behind the surface molecules re-organization which leads to characteristic IS formation [79–83]. During early time points of IS formation, the specific TCRs which are bound to pMHC, form *islands* known as TCR-pMHC microclusters. The contact interface is stabilized by integrin complexes, formed between LFA-1 and ICAM-1 molecules. These complexes assist in the adhesion between the two interacting cells. TCR-pMHC microclusters move to the central region of the contact interface, while LFA-1-ICAM-1 complexes encircle these microclusters. Later, the two kinds of complexes completely segregate from each other and form two distinct areas in the synapse: the TCR-pMHC cSMAC and the LFA-1-ICAM-

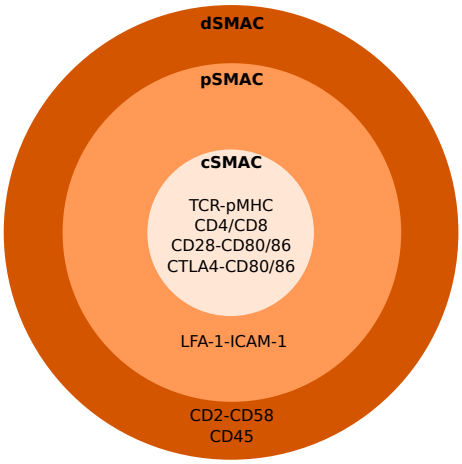

Figure 1.5: The accumulation of different free and bound molecules in different regions of the contact interface between T cells and APCs.

1 pSMAC [79]. The third, outer ring called dSMAC consists of other molecules and complexes, which are excluded from the central and peripheral regions. Of course, many more molecules are part of an IS, and they may reside to one of the three regions.

It has to be noted that the physiological interaction between two immune cells harbors very complex mechanisms that are hard to study. The interacting cells build a complex 3D interface with undulating membranes [84–88]. The difficulty of analysing and imaging the real life 3D cell-cell contact led scientists to construct artificial systems, which try to mimic it. One such example is the supported lipid bilayer (SLB). This system was developed to mimic cell membranes and tissue [89, 90]. In the study of the IS, SLBs are widely utilized since they offer an ideal setting for optical observation by microscope, such as total internal reflection (TIRFM) [91,92], and more recently stochastic optical reconstruction (STORM) microscopy [93, 94].

SLBs are coated with molecules which are laterally mobile. In this way, when the receptors of the T cell bind to their ligands on the artificial APC (i.e. the SLB), the IS can still be reproduced (Figure 1.6). Experimentalists have used this technique to observe how TCR-pMHC and LFA-1-ICAM-1 accumulate to their respective regions at the later time points of the IS formation. An obvious drawback of this technique is the absence of the APC, whose membrane is also dynamically changing [95], similar to T cells. These dynamic changes may also assist TCR-pMHC central accumulation or even lead to different patterns in the cell-cell junction, as observed for germinal center B cell synapses by Nowosad et al. [96].

But what are the mechanisms that lead to TCR-pMHC microcluster formation? And how do the microclusters accumulate in the central area of the contact region? The length of TCR-pMHC complex spans at around 13 nm, whereas LFA-1-ICAM-1 complexes can be around 45 nm in length. When TCR-pMHC complexes form, they tend to bring the two interacting cells very close to each other. Thus, the longer LFA-1-ICAM-1 complexes don't fit in these "close" contact areas. In these regions, high membrane tension occurs which leads to membrane bending, and consequently to steric exclusion of these two types of complexes (Figure 1.6). Similarly, other molecules can

be clustered and segregate from one another due to their size [68, 97, 98]. This is referred to as size-based segregation (SBS). There might be additional mechanisms that can lead to exclusion of molecules from certain areas of the IS. One such example is the proposed kinetic segregation model (KSM) [99]. This model suggests that molecules, such as CD45, can get excluded due to intracellular signaling events. The ability of CD45 to interfere with the intracellular tail of TCR and alter its signaling have led to proposition of this exclusion mechanism. The steric exclusion or the exclusion due to KSM though are not able to explain alone the accumulation of the different interacting molecules to one of the three different IS regions, central, peripheral and distal SMAC (Figure 1.5). Therefore, biologists tried to shed light on the driving forces behind the characteristic patterns observed.

The initial experimental observations focused on the movement of TCR-pMHC complexes, since they are the most important players of T cell activation. It is observed that during antigen recognition, there is a large scale reorganisation of the T cell actin cytoskeleton [101–104]. Actin activation leads to T cell spreading on top of the APC, and at the same time there is continuous polymerization leading to the formation of actin filaments (F-actin). The actin filaments form bundles and move from the periphery of the cell-cell contact surface toward the center of it. In the pSMAC region, F-actin filaments interact with myosin IIa molecules and are reorganized into concentric arcs. The continuous F-actin polymerization at the periphery pushes these arcs toward the cSMAC where it depolymerizes (Figures 1.7 & 1.8) [104–107]. This continuous flow of F-actin arcs is believed to be the driving mechanism of TCR-pMHC accumulation in the cSMAC by interacting with the intracellular tails of bound TCR molecules, pulling them toward the central region and finally depositing them in the cSMAC [100, 104, 108–114].

In order to prove this theory, DeMond et al performed experiments with mazes of barriers on the SLB surface and showed that TCR-pMHC movement is based on frictional coupling to F-actin centripetal flow [100]. TCR-pMHC microclusters in Jurkat T cells are shown to be transported in the IS due the retrograde flow of F-actin and the contraction of actomyosin-II arcs (Figure 1.8) [105, 107, 115]. Moreover, TCR microclusters and the actomyosin arcs were found to travel together at a similar speed [104].

Additionally to TCR-pMHC, it has been observed that the F-actin flow in the IS drives the spatial organization of LFA-1-ICAM-1 complexes. This process leads to the opening of the intracellular tail of LFA-1 in regions close to the cSMAC, a process called affinity maturation of LFA-1, and leads to LFA-1 activation [104, 115–117]. Furthermore, F-actin polymerization and retrograde flow have been shown to be critical for the movement of sinaling microcluster [102, 112] and PLCγ1 signaling [111]. In the case of cytotoxic T and NK cells, actin depletion in the center of the IS is shown to lead the event of granule secretion in order to perform killing of the infected target cell [43, 118, 119]. It is also shown that the formation of an IS improves the killing efficiency by three to four times, compared to cytotoxic T cells that failed to form IS with infected target cells [120].

A centrally directed transport is likely not restricted to TCR-pMHC and LFA-1-ICAM-1 com-

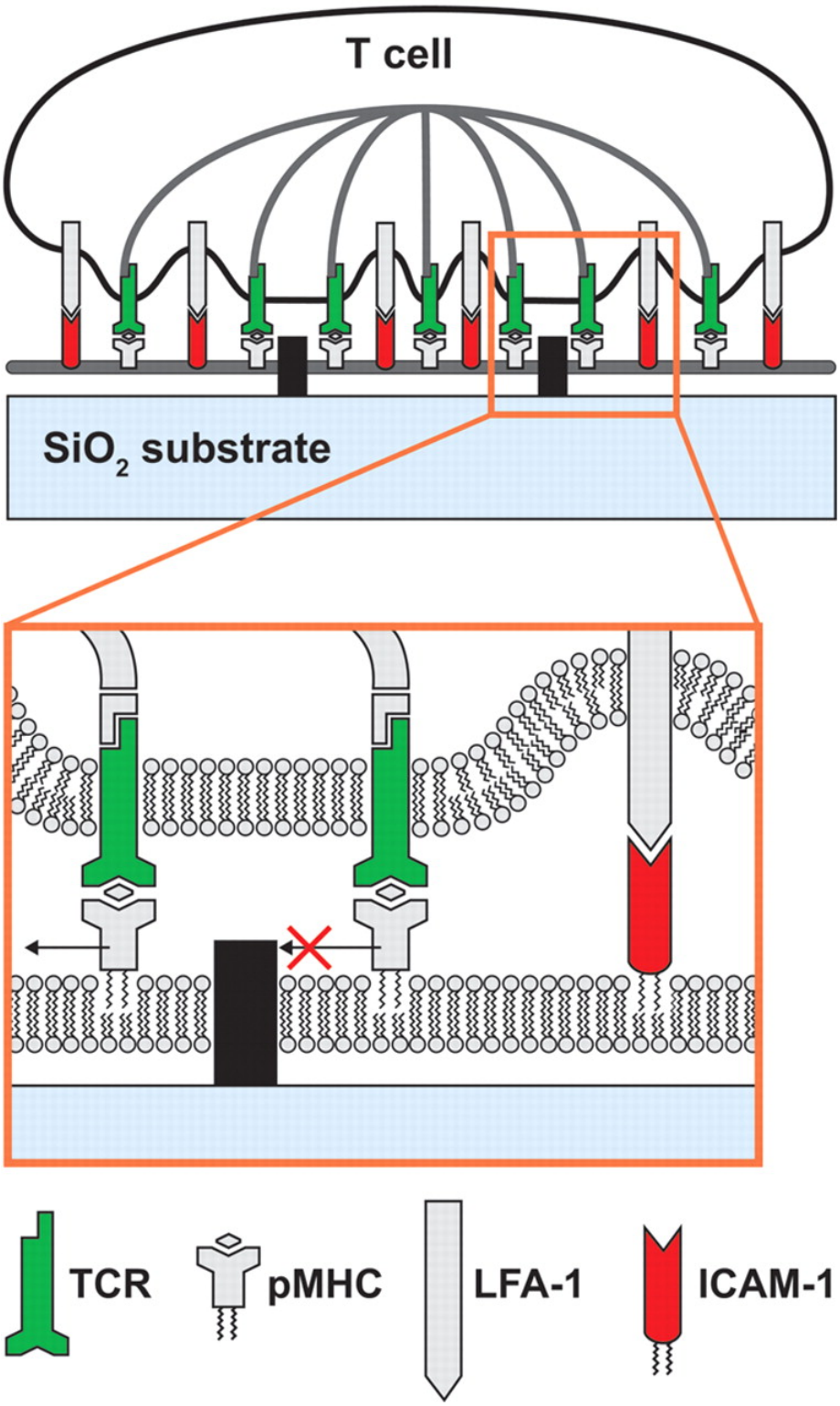

Figure 1.6: T cell-SLB system. SLB is coated with laterally mobile molecules, such as pMHC and ICAM-1. T cell roams the SLB surface and upon TCR-pMHC binding comes in close contact. The longer LFA-1-ICAM-1 complexes forming do not fit in the close contact regions, and membrane bending occurs, which leads to steric exclusion between TCR-pMHC and LFA-1-ICAM-1 complexes. The SLB system has also been used to study geometrically repatterned synapses, either for signaling [71] or for localization mechanism studies [100]. Figure taken from: Mossman et al., Science, 310, 1191-1193, 2005, DOI: `DOI:10.1126/science.1119238`, [71].

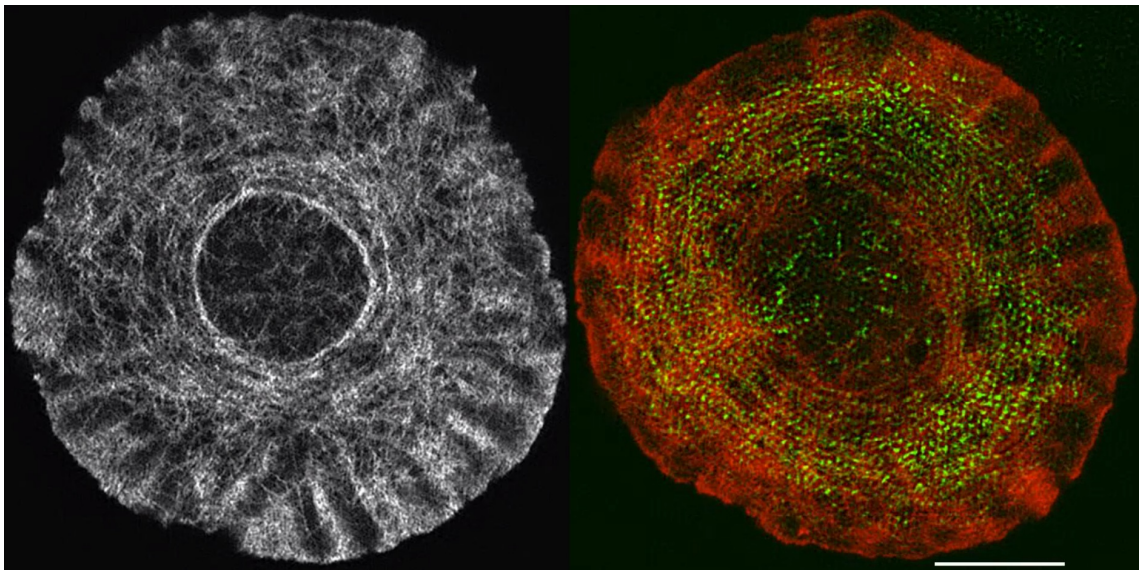

Figure 1.7: The F-actin network during IS formation. Left: F-actin filaments characteristically show the three IS regions, the dSMAC where bundles of F-actin appear, the pSMAC where the concentric arcs are observed and finally, the cSMAC void of F-actin. Right: The F-actin filaments (red) interact with myosin IIa molecules (green) in the pSMAC and are re-oriented into concentric arcs, which are depolymerized in the cSMAC region. Figure taken from: Murugesan et al., J Cell Biol, 215, 383-399, 2016, DOI: DOI:10.1083/jcb.201603080 [104].

plexes, and it is not clear whether other molecules in the IS are also coupled to F-actin. This is one of the questions I will try to answer in this work. For the sake of simplicity, and to be able to use the majority of the experimental data, the *in silico* investigation of the IS dynamics and mechanisms leading to formation of different characteristic patterns will be based on observations made on SLBs.

The actin cytoskeleton except for its central role in IS pattern formation, is shown to affect TCR signaling too. Characteristic polymerized actin structures in the sites of TCR-pMHC engagement, called F-actin foci, are shown to recruit and phosphorylate PLCγ, a critical point of TCR signaling [121].

Apart from the dynamics of the F-actin cytoskeleton, recent advances in imaging started to elucidate the importance of microrubules in IS formation. Microtubules are microscopic, hollow tubes formed by the polymerization of tubulin proteins. They are responsible for the cell shape and the organization of the cell's organelles [122]. Some of their roles include cell division, movement and transport of materials within the cell. The microtubules are organized by the microtubule organization center, or MTOC. During IS formation, the MTOC re-organizes the T cell microtubules on top of the IS region (Figure 1.9a) [123–126]. It has been observed that TCR-pMHC microclusters move along microtubules (Figure 1.9b), while inhibition of the microtubule organization, leads to impaired IS pattern [127–129]. Additionally, microtubules are considered important for T cell signaling by assisting calcium flux [123,130–132]. Therefore, it is clear that the entire cytoskeleton is taking part, if not being completely responsible, for the organization of the surface molecules during IS formation.

Functions of the immunological synapse. As it was discussed so far, the formation of the

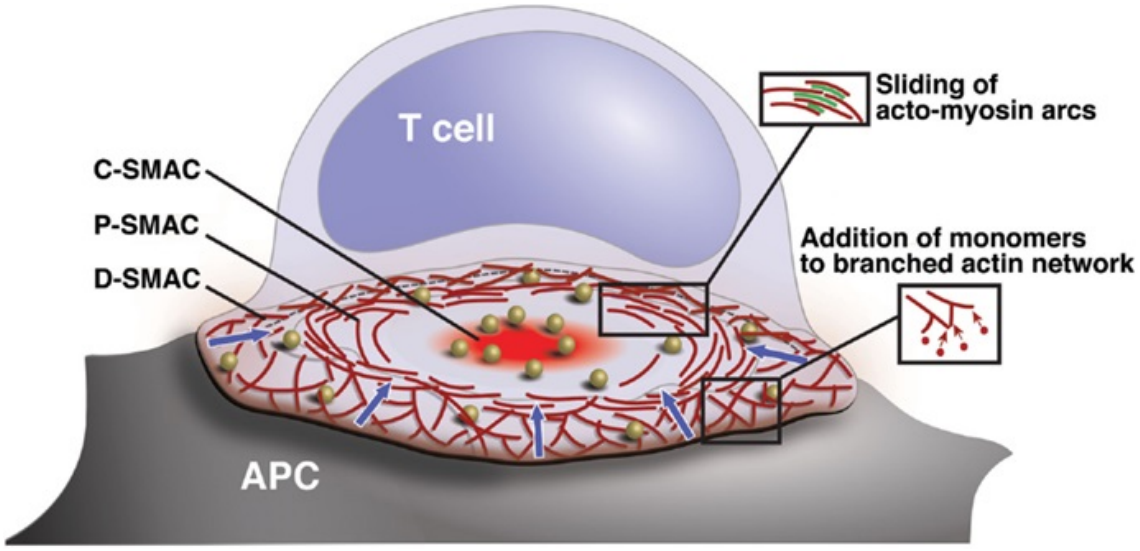

Figure 1.8: Organization of actin dynamics in the IS. Actin polymerizes at the periphery of the IS, and travels toward the center of the IS. In the pSMAC region, actin reorganizes into concentric arcs with the help of myosin II molecules and continues toward the cSMAC, where it depolymerizes. In the cSMAC accumulation of TCR-pMHC complexes together with many signaling molecules (gold spheres) is observed. Figure taken from: Comrie and Burkhardt, Frontiers in immunology, 7, 68, 2016, DOI: `https://doi.org/10.3389/fimmu.2016.00068` [107].

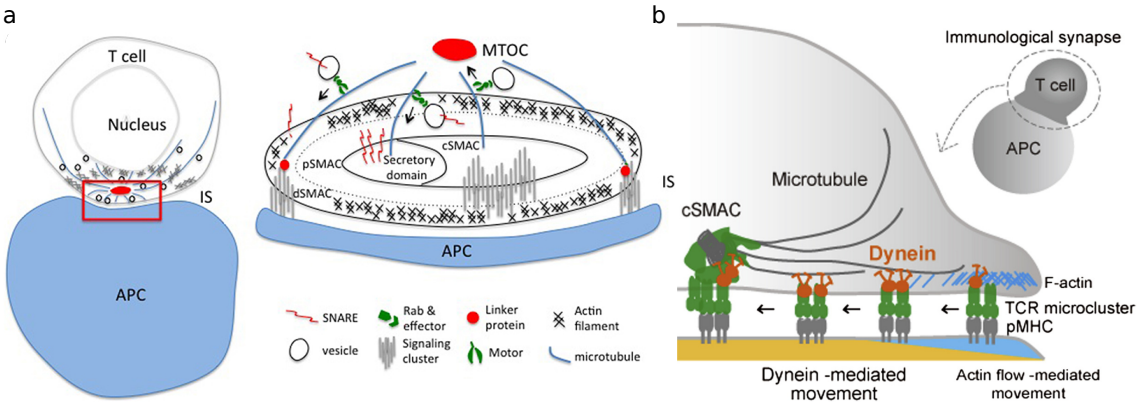

Figure 1.9: Microtubule organization during IS formation. **(a)** TCR-pMHC microclusters attach to dynein motors which in turn are attached to actin and microtubules. In this way TCR-pMHC microclusters are transported to the center of the IS. **(b)** MTOC organizes microtubules, which are attached to signaling TCR-pMHC microclusters. Figure taken from: **(a)** Lou et al.,Front Cell Dev. Biol., 4, 77, 2016, DOI: `https://doi.org/10.3389/fcell.2016.00077` [124]. **(b)** Hashimoto-Tane et al., Immunity, 34, 919-931, 2011, DOI: `https://doi.org/10.1016/j.immuni.2011.05.012` [128].

IS is important for many different reasons, such as killing of infected cells or boosting the functions of other immune cells. In order to achieve such behaviour, T cells need to receive the appropriate signals from the APCs they come in contact with. During the IS formation, very complex signaling cascades in the T cell get activated. There are several theories of how the T cell receptor gets activated. CD45 has a double effect on TCR signaling, through interaction with the Src family kinase Lck [133]. CD45 controls the activation of $p56^{lck}$, by either phosphorylating the Y505 site which leads to closed Lck conformation and therefore signal inhibition, or by phosphorylating the Y394 site, which results in the opening of Lck and consequently signal amplification [134, 135]. Davis

and Merwe suggested that the exclusion of CD45 molecules from TCR-pMHC sites results in signal amplification, which can lead to T cell activation [99], in a model called kinetic segregation (KS). It is also shown that inhibition of an enzyme known as tyrosine protein kinase Csk or c-terminal Src kinase, can trigger TCR signaling [136–138]. Others suggested that during TCR and pMHC interactions, conformational changes happening on TCR molecules can affect signaling [139–143]. Additionally, it has been observed that TCRs respond to forces induced by catch bonds or by the actin network interactions, and increase the interaction strength with pMHCs, contributing to signal amplification [144]. Signaling cascades starting from triggered TCR molecules consist of a very complex network of interacting receptors, kinases, enzymes, transcription factors, phosphatases and many more (Figure 1.10). All these molecules and mechanisms are orchestrated by the received signals during antigen recognition which eventually result in the desired effector function of the T cell [131, 145–149].

There are many interesting mechanisms by which the two interacting cells communicate during the IS formation. On the T cell side, engulfing of interacting TCR-pMHC complexes and endocytosing them leads to three key events. The internalized active TCR together with the antigen can lead to additional intracellular signaling (Figure 1.11) [150,151]. The complex can be also degraded or recycled to the surface of the T cell. The T cell can also engulf TCRs into microvesicles. These microvesicles are then released in the cell-cell junctions, and can be phagocytosed by the APC (Figure 1.11) [152–154]. The internalized TCRs can then interact with intracellular pMHC, which enhances APC signaling. These complex trafficking dynamics, as well as recruitment of molecules to the IS from the rest of the cell surface were not considered in the development of the model, which will be presented in the following sections.

Importance of the immunological synapse. IS formation is an important step for the body's defence against pathogens. There are defects though in IS formation. Synapses can show non-conventional patterns and it is not clear how this affects TCR signaling and T cell activation. The stable, radially symmetric synapses are considered as the normal cases (Figure 1.12 (top)). There are cases where the symmetry brakes and the T cells are moving on top of the APC or SLB surfaces. In these cases, the lamellipodium takes the place of the dSMAC and is the leading edge of the moving T cell. The lamella region takes over the role of the pSMAC, with adhesion molecules residing there and the uropod is a kind of moving cSMAC. In addition, the microtubule organization changes drastically (Figure 1.12 (bottom)). Synapses like this are known as kinapses [155–159]. Schubert et al. showed that T cells formed normal synapses with influenza-infected cells, but the IS formation was impaired in the case of multiple sclerosis (MS) and type-1 diabetes (T1D) [160]. They quantified the effectiveness of the IS formation for different T cell clones (Figure 1.13 (top line)) and showed that in the cases of MS and T1D synapses failed to form (Figure 1.13 (yellow and beige blocks)). These two examples, MS and T1D, elucidate the importance of the synapse, since impaired formation and function can be a leading cause for autoimmune diseases.

In the case of breast cancer, it has been observed that T cells are highly motile in the tumour region. This means that the interactions with the tumour cells are transient and therefore the T

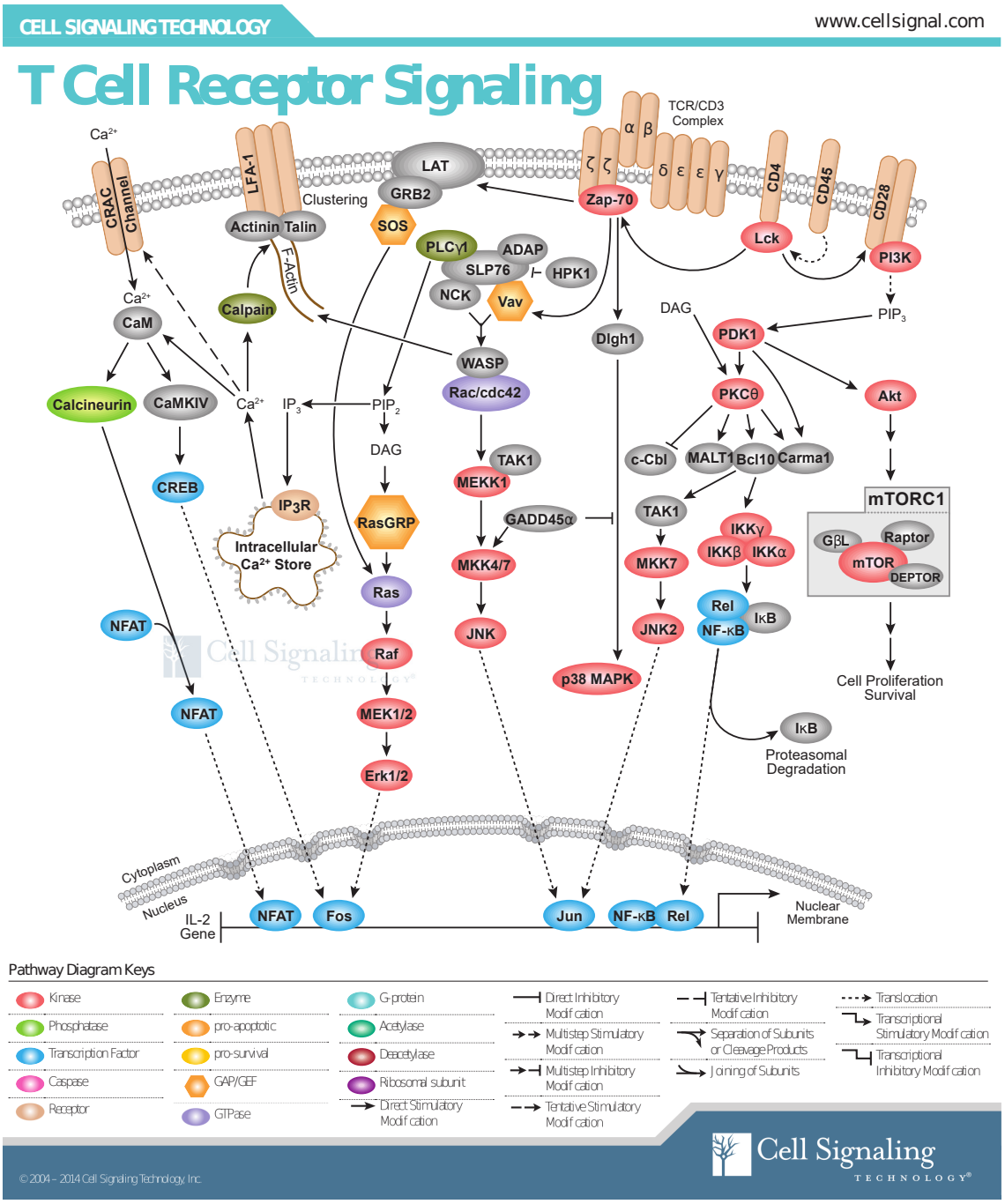

Figure 1.10: T cell signaling pathways, include an enormous variety of receptors, kinases, phosphtases, enzymes, transcription factors and many more. Figure taken from: Cell Signaling Technology, URL: `https://www.cellsignal.com`.

cells form kinapses instead of synapses. In these cases, tumours continue to grow and there is high metastasis potential. Techniques to combine T cell anti-CTLA-4 treatment, a common treatment against different types of cancer [161–164], with radiation therapy showed that T cells are arrested in the tumour area, forming stable synapses. This T cell behaviour led to tumour shrinkage and low metastasis potential [165].

To conclude this part, experiments have shown the importance of immunological synapse formation in many different settings, such as viral infections, autoimmune diseases and cancer. Both

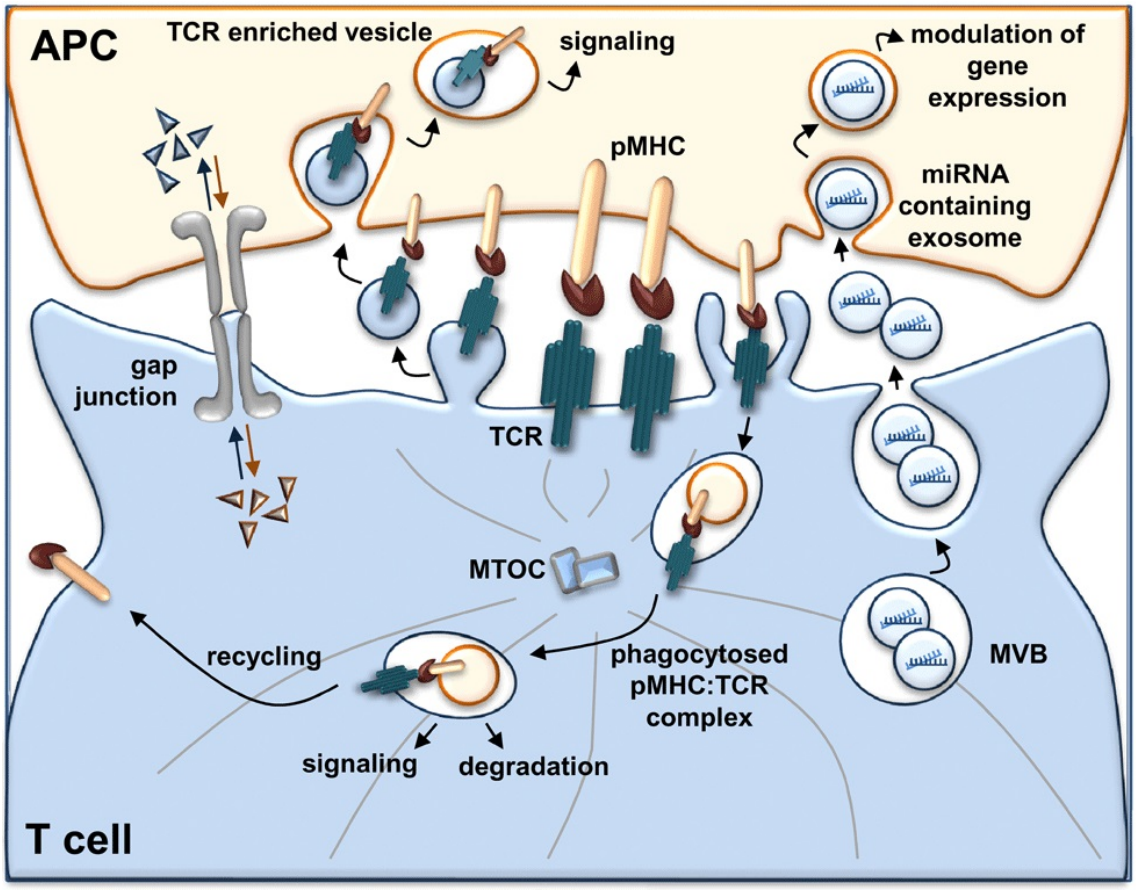

Figure 1.11: Communication of the two interacting cell, T cell and APC, during IS formation. When TCR-pMHC complexes are endocytosed by the T cell, the antigen is being processed which leads to (i) signaling initiation, (ii) degradation of it or (iii) recycling back to the surface. Similarly, TCR-pMHC complexes can get endocytosed by the APC. Additionally, the T cell generates microvesicles which contain T cell receptors. The microvesicles are released in the IS region and taken up by the APC, which again leads to activation of signaling cascades. Figure taken from: Finetti et al., F1000Research, 6, 2017 , DOI: `10.12688/f1000research.11944.1` [151].

the interacting cells, T cell and APC (macrophage, dendritic cell or B cell) exchange information which leads to different behaviours. In T cells, the formation of the IS leads to activation, proliferation, cytokine and lytic granule secretion, apoptosis, differentiation and TCR signaling. The transmitted signals from the T cell lead to boosted APC functions, such as killing in the case of macrophages and production of antibodies in the case of B cells. Given these conclusions, it is not surprising that IS formation is so widely studied, not only from biologists but also from the mathematical and physical community, as I will discuss in the following section.

1.3 Modeling of immunological synapse formation

Apart from biologists, many scientists in the fields of physics and mathematics showed great interest in understanding a system as complex as IS formation. Different modeling approaches have been developed to understand the IS spatial formation from mechanistic forces, with the majority focusing on the mechanisms of microcluster formation. There are different approaches,

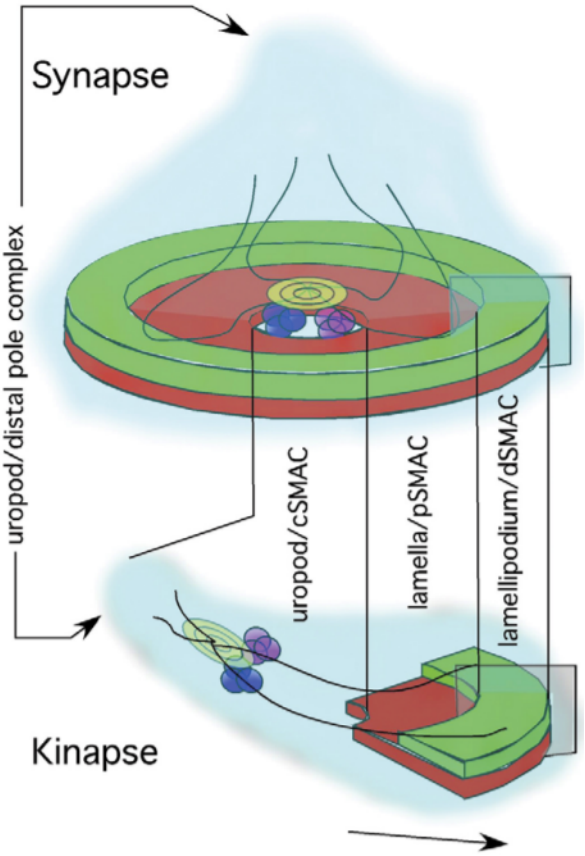

Figure 1.12: Synapse versus kinapse formation. Synapses are radially symmetric whereas in kinapses the symmetry is lost and the T cell moves in the direction of the arrow. The organization of microtubules is also drastically changing between the two cases. Figure taken from: Dustin, Curr opin cell biol, 19, 529-533, 2007 , DOI: `10.1016/j.ceb.2007.08.003` [155].

including partial differential equation (PDE), statistical mechanics and agent-based models, which I am going to discuss below.

Partial differential equation models. Qi et al. established a PDE model in order to examine whether the formation of the synapse could be driven by self-assembly involving extracellular receptor interactions and membrane bending [166, 167]. A set of reaction diffusion equations coupled to one that describes potential motion toward a free energy minimum for the membrane shape changes constitute the model [167]. In this work, the authors concluded that the formation of the IS may simply emerge from self-assembly processes. This model could be extended to test different systems, such as multiple different peptides on the APC surface or NK cell synapses, instead of T lymphocytes, with the limitation that receptors and ligands were embedded into opposed, deformable membranes whose properties could be derived from the cytoskeleton [168].

Burroughs and Wülfing created another PDE model, trying to prove that the mechanism of IS formation is supported by the length difference in the different kinds of complexes (TCR-pMHC and LFA-1-ICAM-1), namely the size-based segregation (SBS), by incorporating reaction kinetics, thermodynamics, and elasticity of the complexes and the membranes [169]. They concluded that the different bond lengths induce a significant contribution to the free energy of the interaction,

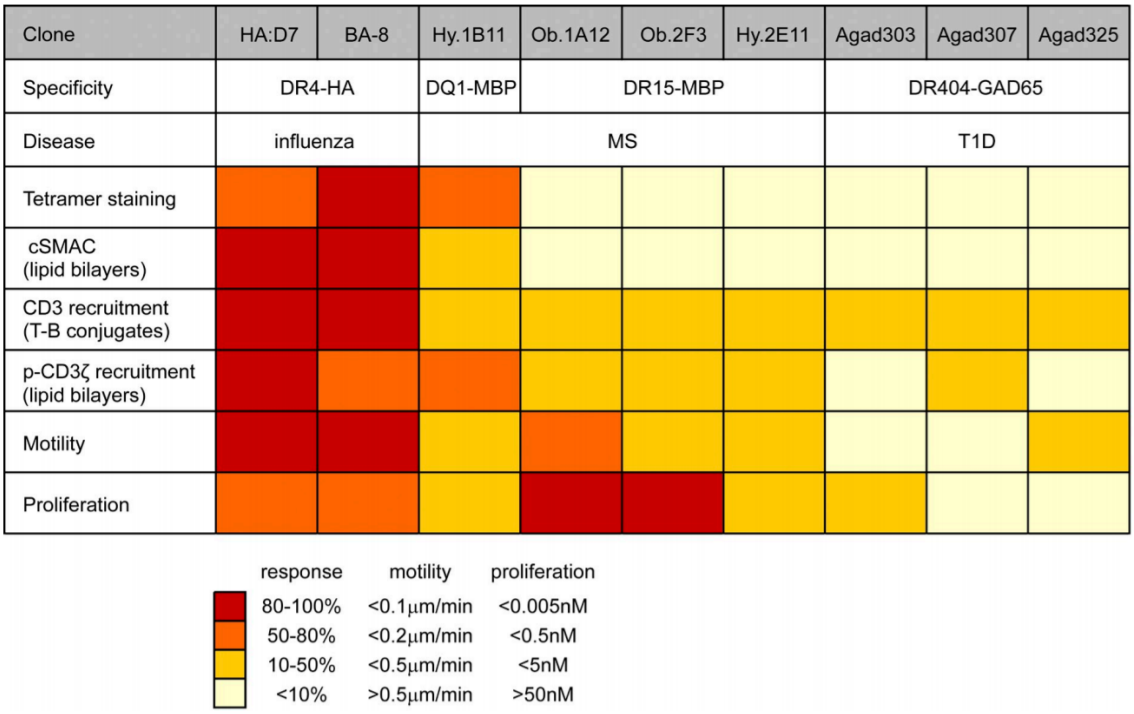

Figure 1.13: Efficiency of IS formation for different T cell clones (top line) in different settings, such as influenza infected cells, multiple sclerosis (MS) and type 1 diabetes (T1D). The stability and radial symmetry of the IS is defined as a response value. In red and orange the formed synapses are considered very good, whereas yellow and beige show defects in the IS patterns. Figure taken from: Schubert et al., JEM, 209, 335-352, 2012 , DOI: `10.1084/jem.20111485` [160].

which means that the membrane deformations are important for the dynamics of IS formation.

More recently, Carlson and Mahadevan introduced an updated PDE model [170]. This model takes into account the membrane mechanics, the protein binding kinetics and motion, as well as the fluid flow in the synaptic cleft in the contact interface between the two interacting cells. In comparison with experimental data, the authors were able to show that passive elastohydrodynamics and protein binding kinetics are able to describe the formation and organization of protein clusters. Interestingly, this model does not invoke active cytoskeletal transport processes.

In all the above models, size-based segregation (SBS) [82] explained the TCR microcluster formation, but was not sufficient to confer the formation of a "bull's" eye pattern. Additional assumptions were required for the reproduction of the TCR-pMHC cSMAC formation in accordance with the experimental observations [68].

Statistical mechanics models. Weikl et al. introduced a statistical mechanics model [171, 172], which includes thermal fluctuations. This model incorporates different forces, including membrane deformations, in an energy-dependent manner, which describes the global configuration of densities at each site of the lattice. Densities are locally updated by virtue of a Monte Carlo simulation and depend on the variation in the free energy. An extension of this model would be to explicitly distinguish agents, which would not change the outcome of the simulations. The authors observe that the "bull's eye" pattern is initially reversed, with TCR-pMHC complexes forming at the periphery of the contact region, while LFA-1-ICAM-1 complexes are present in the cSMAC.

They confirm the findings of [166, 167], but in contrast to other theoretical studies, this model needs the cytoskeletal transport process, in order to obtain the final pattern of the IS.

Lattice gas model. A recently developed lattice gas model containing three types of sites, empty sites, mobile TCR-pMHC sites and immobile sites representing the F-actin sites respectively, investigates only the aggregation of TCR-pMHC complexes to the central IS region. The model concludes that the TCR-pMHC cSMAC accumulation is driven by a combination of membrane mediated attraction, actin retrograde flow and transport of dynein motors [173]. This model though lacks the presence of the essential adhesion complexes, LFA-1-ICAM-1.

Agent-based models. The basis of an agent-based model is that individual interacting agents represent molecules that form patterns in the IS and follow specific rules. Figge and Meyer-Hermann formulated an agent-based model taking into account the motion and interactions of individual agents/molecules, as well as the binding kinetics of TCR-pMHC and LFA-1-ICAM-1 complexes [174, 175]. The authors discussed the differences between a long-range, attractive force between TCR-pMHC complexes versus a centrally directed transport of these molecules. Their computer simulations [174] were based on the geometrically re-patterned experimental observations introduced by Mossman et al. [71]. In this setting, chromium barriers that block the diffusion of molecules on SLBs, showed that signaling can be sustained if the TCR-pMHC microclusters are blocked form reaching the cSMAC. The authors' predictions where tested experimentally by [100], by introducing mazes of barriers on SLBs and monitoring TCR-pMHC movements. The corresponding experimental results suggested a coordinated centripetal transport of TCRs linked to the centripetal cortical actin flow. They also showed that the diversity of molecular patterns, such as dynamic and multifocal structures, is directly related to the TCR-pMHC binding affinity [175].

Similar methodology was used by [176, 177]. In this case, the B cell-APC interaction was modeled. The authors investigated whether the transport of molecules by the cytoskeleton toward the center is a potential mechanism for IS formation. The working hypothesis of this model was investigated with a Monte-Carlo approach with biased centrally directed diffusion of the complexes. This model reproduces the experimentally observed IS for realistic time and affinity levels.

These above mentioned models were limited to microcluster formation and central forces on the TCRs and did not investigate the effect of actin on other functional molecules.

In the following chapters, I will introduce a new agent-based model, which takes into account SBS, binding kinetics and centrally directed motion due to F-actin coupling of complexes. I will discuss potential mechanisms for the localization of a variety of molecules, which are important for T cell activation, signaling, function and fate decision.

Chapter 2

Agent-based modeling of the dynamics of immunological synapse formation

2.1 Experimental setting.

Immunological synapses (IS) are complex three dimensional (3D) T cell-Antigen presenting cell (APC) junctions that involve many molecular interactions leading to the formation of characteristic spatial patterns. In order to investigate their formation dynamics, biologists produced artificial systems where APCs are being replaced by Supported Lipid Bilayers (SLBs) [79]. SLBs are two dimensional (2D) surfaces coated with laterally mobile and fluorescently tagged molecules, which act as ligands for the receptors on T cells. This set-up allowed for the usage of confocal (CF) [178], total internal reflection fluorescence (TIRFM) [91, 92] and more recently stochastic optical reconstruction (STORM) [93, 94] microscopy, leading to a more detailed insight of the T cell-SLB contact interface in general and the molecular movement and localization more specifically. Another advantage of the SLB system is that the number of molecules in the bilayer and the number of interactions with receptors can be quantified, or even more important, can be controlled.

2.2 Setting-up the T cell and SLB surfaces

I developed an agent-based model based on the simplified T cell-SLB experimental set-up [79]. Initially, a representation of the two interacting surfaces was needed. This is accomplished by creating a lattice for both of them [179]. I further simplified the experimental setting, implementing both lattices in 2D, where each lattice is represented as a square mesh (Figure 2.1). The nodes of these meshes are called gridpoints, which are initially empty. The lattice constant, $\alpha = 70\,\mathrm{nm}$, represents the closest distance between two neighboring gridpoints [175, 179, 180]. This constant

is varied between $\alpha = 100\,\text{nm}$ and $\alpha = 17\,\text{nm}$, in order to investigate IS formation within the resolution range of currently used microscopy techniques, i.e. TIRFM at $\simeq 100\,\text{nm}$ and STORM at $\simeq 20\,\text{nm}$. The gridpoints outside a radius $R > 4.9\,\mu\text{m}$ from the central point of the two lattices are blocked as inaccessible by agents. In this way, the initial square lattice, is transformed into a circular surface, representing an established contact surface between the two interacting cells.

For the two *in silico* cells, I used a Moore neighborhood, meaning that each gridpoint on the lattices has eight neighbors, four on the vertical and horizontal direction, called the "nearest neighbors", and the other four, the diagonal neighbors, which are the "next-nearest neighbors". The movement of the agents that will be introduced later will be confined to these gridpoints [179]. Of course there are other possible approaches to represent the two surfaces. On the one hand, a similar lattice to the one used here, but with movement being restricted only to the four nearest neighbors (von Neumann neighborhood). In this case, a diagonal movement would require that an agent performs two moves, horizontal and then vertical or vertical and then horizontal, compared to the one diagonal movement of the Moore neighborhood. In such a case, more computational time would be required for the same movement. On the other hand, one could even use a square plane where the agents can move in any random direction. This case would require the use of a collision detection algorithm. Therefore, the usage of square lattices with Moore neighborhoods has the advantage of being computationally fast but requires some measures that repair the artificial discretization of space which bears the risk of generating artifacts.

2.3 Introducing the agents

Now that the *in silico* cell surfaces were ready, I had to introduce the agents. These agents will represent the different kinds of molecules that are present on the surface of each cell. The agents are randomly distributed on the gridpoints, while each gridpoint can acquire one and only one agent. The densities used for each agent are taken from literature and can be found in Table 2.1.

2.4 Agent diffusion

Molecules diffuse on the surface of cells due to thermally induced stochastic motion, meaning that it is a random process that can happen toward any direction. However, in the *in silico* setting, diffusion can only happen toward one of the eight "nearest" and "next-nearest" neighbors, due to the Moore neighborhood representation (Figure 2.1). Therefore, a random direction generator will choose one of these neighbors in a probabilistic manner, provided the selected position is empty, such that the movement can be accomplished. Diffusion is represented as a random walk in the lattice, where the probability to move is defined as the ratio of the simulation time step to the time an agent needs to diffuse on a neighboring gridpoint on the 2D lattice with a type-specific diffusion constant D_{X} [175, 179]. Here X denotes one of the molecules or complexes under consideration. The formation of complexes will be discussed in detail later.

Since the diagonal movements are longer than the horizontal or vertical ones, a diagonally moving agent will cover bigger distance than an agent moving on the horizontal or vertical direction in a specific time interval. In order to take into account the distance between different gridpoints, the probabilities of moving to a diagonal neighbor is reduced by the geometrical factor of $1/\sqrt{2}$ [174,175]. Further, in order to account for adhesive behaviours between agents, a phenomenological adhesive factor, $f(N_{nn})$, which further reduces the diffusion probability is introduced to the model [175, 179], given by:

$$f(N_{nn}) = \begin{cases} 1/(1+N_{nn}), & N_{nn} \leq 4 \\ 0, & N_{nn} > 4 \end{cases},$$

where N_{nn} is the actual number of "nearest neighbors" occupied by the same kind of agent with the agent under investigation. One such example of adhesive force could be the cross-linking of engaged TCR molecules, where their intracellular tails get entangled [181]. Finally, the maximum estimated simulation time step is given by the ratio of the lattice constant squared, α^2, to the diffusion coefficient of a free molecule, D_{m}, where m denotes an arbitrary molecule, and should be smaller than $t > 0.0012$ seconds.

2.5 Agents/Molecules present in the IS

The agents studied in this work, are considered some of the most important molecules for T cell activation, function and fate decision, and include the following, on the T cell lattice together with their respective ligand on the SLB lattice:

(a) T cell receptor (TCR), which binds to peptide antigen bound to major histocompatibility complexes (pMHC).

(b) Lymphocyte function-associated antigen 1 (LFA-1), which binds to intercellular adhesion molecule 1 (ICAM-1).

(c) Cluster of differentiation 28 (CD28), which binds CD80 and CD86. Here only CD80 is considered in order to be in accordance with experimental settings.

(d) Cluster of differentiation 2 (CD2), also known as T cell surface antigen, LFA-2, LFA-3 receptor, erythrocyte receptor and rosette receptor, which binds to CD58 in humans and CD48 in rodents.

(e) Cluster of differentiation 45 (CD45), originally called leukocyte common antigen (LCA), which does not have a known ligand.

The association, dissociation rates, sizes, interactions are presented in Table 2.1, together with other characteristic parameters of the model, such as diffusion constants, lattice size and agent densities.

Name	**Parameter**	**Value**
Radius of contact region	$R\,(\mu\mathrm{m})$	4.9
Lattice constant	$a\,(\mu\mathrm{m})$	0.07
Free molecule diffusion constant	$D_{\mathrm{m}}\,(\mu\mathrm{m}^2/\mathrm{s})$	0.10
Complex diffusion constant	$D_{\mathrm{c}}\,(\mu\mathrm{m}^2/\mathrm{s})$	0.06
Size of TCR-pMHC	(nm)	12
Size of LFA-1-ICAM-1	(nm)	45
Size of CD28-CD80	(nm)	10
Size of CD2-CD58	(nm)	11
Size of CD28-CD80	(nm)	10
Size of CD45	(nm)	45
Radius of SBS between TCR-pMHC and LFA-1-ICAM-1	$R_{\mathrm{SBS,TM-LI}}\,(\mu\mathrm{m})$	0.425
Weight of SBS	$W_{\mathrm{SBS,TM-LI}}$	-1.0
Radius of SBS between CD28-CD80 and LFA-1-ICAM-1	$R_{\mathrm{SBS,CC-LI}}\,(\mu\mathrm{m})$	0.425
Weight of SBS	$W_{SBS,CC-LI}$	-1.0
Radius of SBS between CD28-CD80 and TCR-pMHC	$R_{\mathrm{SBS,CC-TM}}\,(\mu m)$	$0.000 - 0.210$
Weight of SBS	$W_{\mathrm{SBS,CC-TM}}$	$(-1.0,\, 0.0)$
Radius of SBS between CD2-CD58 and LFA-1-ICAM-1	$R_{\mathrm{SBS,CD2C-LI}}\,(\mu\mathrm{m})$	0.425
Weight of SBS	$W_{\mathrm{SBS,CD2C-LI}}$	-1.0
Radius of Attraction between CD2-CD58 and CD2-CD58	$R_{\mathrm{Att,Self}}\,(\mu\mathrm{m})$	$0.00 - 0.35$
Weight of Attraction	$W_{\mathrm{Att,Self}}$	$0.2 - 1.0$
Radius of Attraction between CD2-CD58 and CD28-CD80	$R_{\mathrm{CD2CD28}}\,(\mu\mathrm{m})$	$0.00 - 0.35$
Weight of Attraction	W_{CD2CD28}	1.0
Dissociation rate TCR-pMHC	$k_{\mathrm{off,TM}}\,(1/\mathrm{s})$	0.1
Association rate TCR-pMHC	$k_{\mathrm{on,TM}}\,(1/\mathrm{Ms})$	2×10^4
Dissociation rate LFA-1-ICAM-1	$k_{\mathrm{off,LI}}\,(1/\mathrm{s})$	0.03
Association rate LFA-1-ICAM-1	$k_{\mathrm{on,LI}}\,(1/\mathrm{Ms})$	3×10^5
Dissociation rate CD28-CD80	$k_{\mathrm{off,CC}}\,(1/\mathrm{s})$	1.6
Association rate CD28-CD80	$k_{\mathrm{off,CC}}\,(1/\mathrm{s})$	4×10^5
Dissociation rate CD2-CD58	$k_{\mathrm{on,CD2C}}\,(1/\mathrm{s})$	4
Association rate CD2-CD58	$k_{\mathrm{off,CD2C}}\,(1/\mathrm{Ms})$	6×10^5
TCR-pMHC centrally directed force	C_{TM}	1.00
LFA-1-ICAM-1 centrally directed force	C_{LI}	0.06
CD28-CD80 centrally directed force	C_{CC}	0.20
CD2-CD58 centrally directed force	C_{CD2C}	0.00
Fraction of occupied gridpoints in T cell		$30 - 80\%$
Fraction of occupied gridpoints in SLB/APC		$30 - 80\%$
Fraction of TCR, pMHC		6%
Fraction of LFA-1, ICAM-1		15%
Fraction of CD28, CD80		$7.5 - 15\%$
Fraction of CD2, CD58		$0.075 - 36\%$

Table 2.1: Reference parameter values.

2.6 Chemical kinetics

So far the two lattices are not interacting with each other, meaning that the two cells are not interacting. These interactions happen when agents from the one lattice bind to agents on the other lattice. This should happen in a way similar to real life, thus chemical kinetics were introduced to the model. While molecules diffuse on the lattices, they are allowed to check the agent at the exact same position on the opposite lattice. If the agent is the appropriate, a receptor-ligand binding probability is formulated. This probability is based on the association rates for the specific molecules under consideration, k_{on}, Avogadro's number, and the volume of the grid mesh where the complex is about to form and is given by [175]:

$$p_{\text{on}} = \frac{\tau}{\tau_{\text{on}}}, \qquad \tau_{\text{on}} = \frac{V \times N_{\text{A}}}{k_{\text{on}}}. \tag{2.1}$$

On the other hand, the probability of unbinding a complex into free molecules is based on the dissociation rates, k_{off}, of each individual type of complex and is given by [175]:

$$p_{\text{off}} = \frac{\tau}{\tau_{\text{off}}}, \qquad \tau_{\text{off}} = \frac{1}{k_{\text{off}}}. \tag{2.2}$$

The association and dissociation rates are taken from literature for the different kinds of molecules and complexes I will discuss throughout this work. When a complex diffuses, its two agents (one on each lattice) need to move in the same direction, which happens less often, thus the diffusion rate of the complexes is assumed lower than that of free molecules, $D_{\text{c}} < D_{\text{m}}$, where c denotes complex and m molecule [179, 180].

2.7 Complex interactions

In the forming immunological synapse, the membranes of the cells are highly undulating and in addition, the sizes of the forming complexes are highly variable. The different complex sizes lead to surface tension, which further leads to membrane bending. Despite the elasticity that the complexes can have, membrane bending forces the longer complexes to segregate from the shorter ones, only based on their sizes. This behaviour is called size-based segregation (SBS).

Now this rule must be applied to the agents, but because the whole model is in 2D, membrane bending cannot be included. As a phenomenological approach, another way to impose membrane bending is to model a repulsive force between the different kinds of complexes. This force is modeled as a weighted vector from a complex toward all its interacting neighbors, within a radius R_{force} [175]. The weight of each vector, W_{force}, represents the strength of the force relative to diffusion, where negative weights represent repulsion and positive ones attraction. All vectors are summed, and the resulting vector points to the direction of movement (Figure 2.1). The direction is attributed to one of the eight neighbors, based on a probabilistic function explained in the following section (Movement discretization) and in [179].

2.8 Movement discretization

There are several options to convert the unit vector direction of a force into the movement to a gridpoint, which bears the risk of introducing unphysiological biases into the simulation:

(a) As a first strategy, a rounding scheme can be used: If the final vector points from (x, y) to a position $(x + \delta, y + \epsilon)$, the two coordinates are rounded to the closest integer leading to $\delta, \epsilon = \pm 1$ or $\delta, \epsilon = 0$. This technique could be used in meshless lattices, but here the resulting synapse formation is affected by the square mesh, and is not in accordance with experimental observations [179].

(b) Another technique is to use the factor $1/\sqrt{2}$, as was done for the probabilities to move diagonally by diffusion, but now for the angle θ of the force. This technique allows choosing a position with a higher chance of moving vertically or horizontally compared to diagonally. Still though, the effect of a the square mesh on the lattice will be clearly visible and far away from the experimental observations [179].

(c) The previous two methods are deterministic, meaning that if an agent followed the same force for several time steps, it would move to the same direction of the eight possible neighbors each time, which would make it follow a straight movement into a direction imposed by the lattice rather than by the direction of the force vector. In order to avoid this problem, a new function is introduced, which decides where an agent will move in a probabilistic manner.

This function gives the probability to move from (x, y) to a potential new position $(x+\delta, y+\epsilon)$, where $\delta, \epsilon = -1, 0, 1$. For example, if the forces that act on a complex in position (x, y) point to a position between 0 and 45 degrees, there are two options for the agent to move. Either it will move to position $(x + 1, y)$ or to position $(x + 1, y + 1)$. Thus, the probability of $\delta = 1$ is $P(\delta = 1) = 1$. On the other hand, ϵ can either be $\epsilon = 0$ or $\epsilon = 1$.

The way to decide between the two options is to project the force vector to the base vectors formed by the two possible movement vectors. It gives the ratio on how many times they should be used in order to follow the direction of the force, on average. Here, it leads to $P(\epsilon = 1) = \dfrac{\sin(\theta)}{\cos(\theta)} = \tan(\theta)$. In accordance, if, for example, the vector of the forces points into the interval $45° \leq \theta \leq 90°$, then $P(\epsilon = 1) = 1$ and $P(\delta = 1) = -\dfrac{\cos(\theta)}{\sin(\theta)} = -\dfrac{1}{\tan(\theta)}$. The formula giving the probabilities for δ and ϵ is depicted in Figure 2.2a, b and is derived from the tangent and the cotangent of the angle θ, which is the angle of the force vector with respect to the $x-$axis. Finally, as the diagonal movements cover more distance, and because the ratio between diagonal and straight moves has to be kept, the probability to move by forces is reduced from 1 to $1/L$ where L is the length of the "average movement vector" generated by this method. It is following the unit vector force but its length depends on the angle, Figure 2.2c [179].

2.9 Centripetal transport of complexes

In recent years, the formation of a mature IS has been attributed to molecules binding to cortical filamentous actin (F-actin). F-actin forms concentric arcs in the T cell during the antigen recognition process, which move symmetrically toward the center of the contact region. By contraction, these arcs can pull the intracellular domains of different molecules, leading to the formation of the characteristic IS pattern known as "bull's eye" pattern [100, 104, 105, 115]. A new rule has to be introduced to the model, in order to recapitulate this inward transport of molecules. For simplicity, and since the model is in 2D, the transport of complexes by the centripetal contraction of F-actin arcs is modeled as a centrally directed empirical force (Figure 2.1). This new force will be added to the SBS force vector with weight $C_{\mathrm{X}} > 0$, where X denotes the specific complex. C_{X} now reflects the strength by which molecules bind to F-actin, or in other words, the strength of the centripetal force exerted on complexes due to the coupling with F-actin.

2.10 F-actin foci model

F-actin foci are dynamically polymerized structures resulting from local nucleation of F-actin, and appear at TCR-pMHC sites [112, 121]. For the implementation of the F-actin foci model, a third square 2D lattice is created. This lattice represents the T cell membrane. As shown in Figure 2.3, TCR-pMHC complexes from the T cell lattice can create F-actin nucleation points on the F-actin lattice. In this way, the two lattices are now communicating and interacting with each other. Similarly, nucleation points can get polymerized, called nucleation polymerized points, if they colocalize with LFA-1-ICAM-1 complexes. In further presence of LFA-1-ICAM-1 in the neighborhood, defined by $R_{\mathrm{neighborhood}}$, around either nucleation or nucleation polymerized points, polymerization of F-actin foci happens, creating polymerization points. These polymerization points form clusters representing the experimentally observed F-actin foci.

This model will be implemented on the final chapter, where I will be discussing TCR cooperativity during pMHC amount titration. In this case, foci act as positive regulators of the probability of TCR binding, allowing to simulate active modulation of the association rate of TCR-pMHC complexes.

2.11 Exchange algorithm

In order to avoid artificial inhibition of motility by local crowdedness, a local exchange algorithm was implemented [180, 182]: Agents that failed to move by active forces (SBS or actin coupling) to an occupied node are stored in a list. At the end of each time step, the agents on this list retry to perform the movement. If the target position is free, then the agent moves on it. If the target position is occupied by an agent with a force pointing toward the moving agent, the two agents are exchanged. Otherwise, the agent remains in its initial position.

2.12 Optimization of simulation speed

To optimize the speed, all the agents are separately stored in a list, which is shuffled, and at each time step, all the agents are picked in a random order and updated. Each of the steps described above, i.e. diffusion, binding kinetics, interactions between complexes and centripetal transport, are tested once per time step per agent.

2.13 Model implementation

The model is programmed using object-oriented programming in *C++* language. The code is separated in two classes: one representing the agents and, the other, the lattices including the rules applied to these agents. The completion time of a simulation takes about 6-8 hours of CPU time (using a 3.47 GHz CPU) for 30 minutes of IS formation. The random generator used is *mersenne twister engine (mt19937)*, and the IS plots were generated using the *Qt* framework.

2.14 Model readouts

Except for the visualization of the IS pattern using the *Qt* framework, the model allows more data to be stored in text files for further analysis.

(a) **Density plots.** The density of complexes and molecules was computed inside equally spaced concentric rings as the fraction of occupied grid points by each type of complex. The standard deviation (SD) of at least $n = 10$ simulations is plotted. Absence of SD in density plots was justified by the robustness of simulations.

(b) **Localization plots.** Utilizing the density plots, and by considering boundaries for each one of the areas of the IS, central, peripheral and distal supramolecular activation clusters (SMACs), the percentages of each molecule and complex in each SMAC are plotted.

(c) **Radial distribution functions.** The radial distribution function, RDF, (or pair correlation function), describes the density as a function of distance from a reference particle. In this study, I implemented the RDF as the local density of agents (complexes or molecules) inside a ring of width dr, at a distance r from a reference particle, normalized by the total density of the particle under consideration [180]. The plotted RDF represents the frequency of finding a particle of a specific type in a particular distance from a reference particle. This representation is useful to show the mean size of TCR-pMHC microclusters, the distribution of LFA-1-ICAM-1 away from a TCR-pMHC microcluster, and the degree of colocalization of CD28-CD80 and TCR-pMHC in microclusters.

(d) **Agent colocalization.** The model further calculates the amount of molecules or complexes within a defined radius $R_{\mathrm{col}} = 0.21\,\mu\mathrm{m}$. If a minimum number, $\min(X, Y)$, of the two different kinds of molecules or complexes, X and Y, is found, the model returns the colocalization [180].

(e) **In situ dissociation constant.** The model stores the density of the free and complexed agents. The in situ dissociation constant, ${}^{\text{cell}}K_{\text{D}}$, is calculated by:

$$ {}^{\text{cell}}K_{\text{D}} = \frac{[Receptor_{\text{free}}][Ligand_{\text{free}}]}{[Receptor - Ligand_{\text{pair}}]}, \tag{2.3} $$

as was experimentally presented by Pielak et al. [183].

The presented agent-based simulations could also be implemented as a PDE model by treating the IS on a macroscopic population level. I was choosing an agent-based model because this approach allows to go down to the single molecule level, which might become relevant in small structures and at high resolution. In this limit, agent-based approaches appear as the better choice [180].

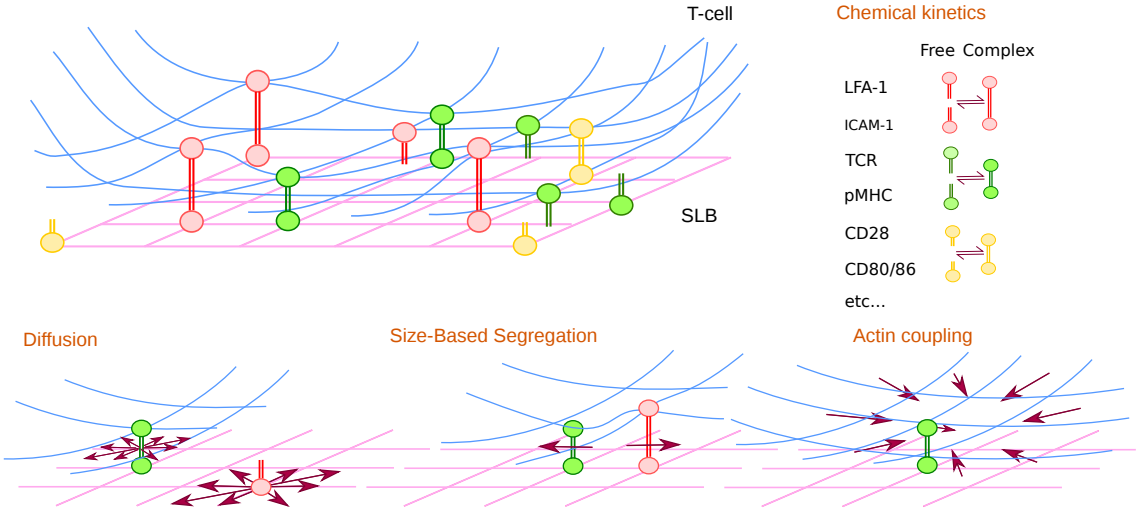

Figure 2.1: List of mechanisms included in the IS model. The membrane of the T cell (blue) and the SLB (pink) carry molecules. Opposite molecules bind or unbind by chemical kinetics. Free and complexed molecules move by diffusion or forces: centripetal forces reflecting actin coupling and SBS representing the effect of membrane bending.

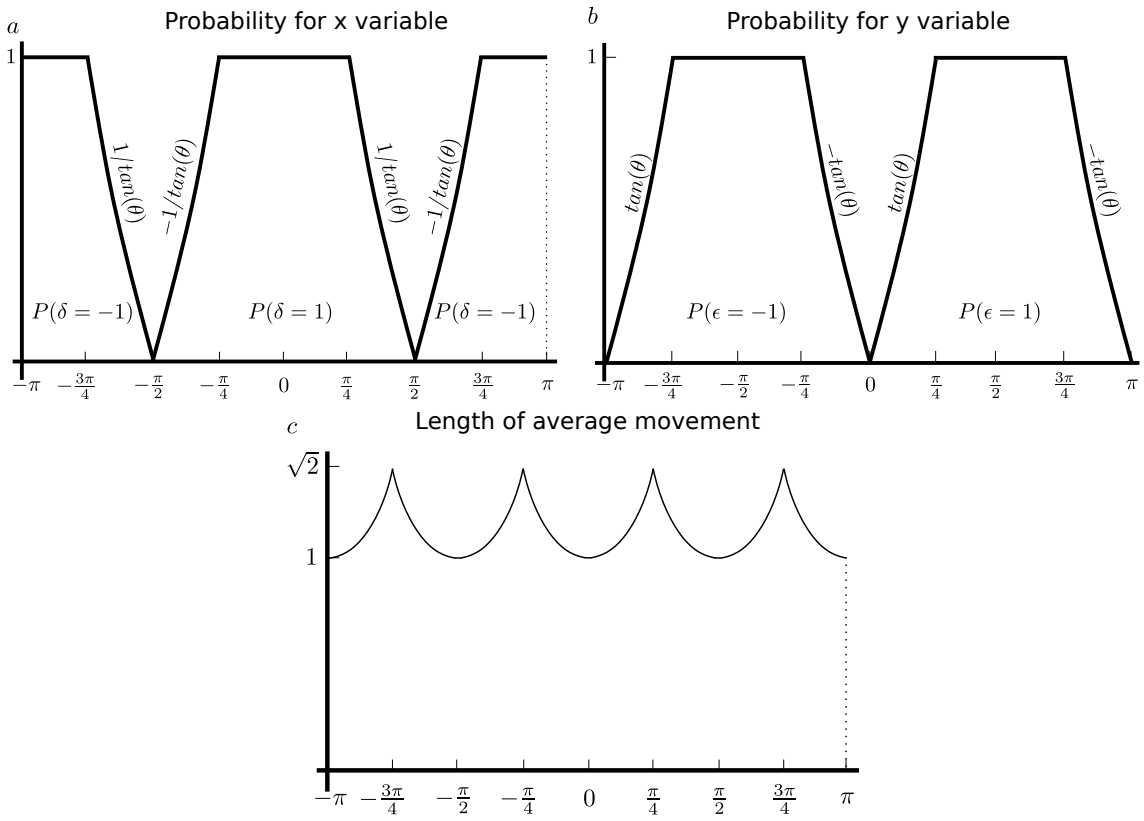

Figure 2.2: The probability functions for δ and ϵ variables, for the movement of the agents. **(a)** Probability function for x variable, given by $\pm 1/\tan(\theta)$, where θ is the angle of the vector force in the x direction. **(b)** Probability function for y variable, given by $\pm\tan(\theta)$, where θ is the angle of the vector force in the y direction. **(c)**The length of the average movement vector, L.

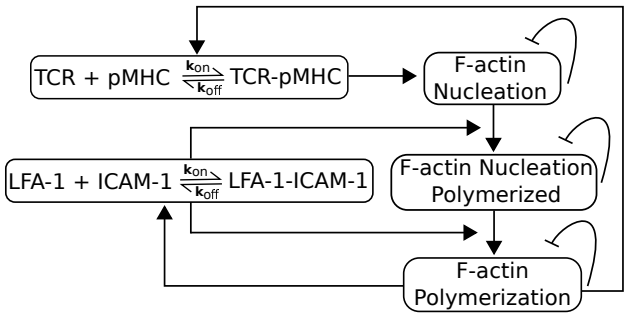

Figure 2.3: Model for F-actin foci formation. TCR-pMHC binding leads to F-actin nucleation, which in presence of LFA-1-ICAM-1 leads to polymerization of the nucleated actin. Consequently, this leads to the formation of F-actin polymerization, with a positive feedback on TCR-pMHC association constant.

Chapter 3

Immunological Synapse Formation

3.1 Introduction

The formation of immune synapses (ISs) is a central process for antigen recognition by T cells. The structure of the IS impacts on T cell activation, signaling, and fate decisions as I discussed so far [68, 71–78]. For these reasons, a lot of attention has been placed toward understanding the mechanisms of IS formation [79, 81, 82, 184]. During early IS formation, specific T cell receptors (TCRs) bind to peptide-bound major histocompatibility complexes (pMHC) of either class I or II and form islands of microclusters. Synapse formation and adhesion is stabilized by integrin complexes, formed between lymphocyte function-associated antigen 1 (LFA-1) and intercellular adhesion molecule 1 (ICAM-1). TCR-pMHC microclusters move to the central region of the contact interface, while LFA-1-ICAM-1 complexes encircle these microclusters. Later, the two kinds of complexes segregate from each other and form two distinct areas in the synapse: the central supramolecular activation cluster (cSMAC) occupied by TCR-pMHC complexes and the peripheral SMAC (pSMAC) formed by integrin complexes [79].

Together with the aforementioned molecules, T cells and APCs express hundreds of other receptor and ligands, which in turn play important roles in T cell activation and effector function. A characteristic example is the transmembrane protein phosphatase CD45. Interestingly, no ligand has been described for CD45 on APCs so far. Therefore, CD45 molecules do not communicate directly with the APC. Despite that, CD45 has been shown to exert a double effect on TCR signaling, either by positively regulating T cell activation through the dephosphorylation of p56lck and p59fyn [185–190], or by negatively regulating the autocatalytic tyrosine phosphorylation of src-kinase molecules and their ability to dephosphorylate components of the T cell complex [191, 192]. The double role of CD45 on TCR signaling comes with a specific localization. These molecules are observed to be excluded from the forming TCR-pMHC microclusters and eventually are completely excluded from the IS, and reside in the outer pSMAC region, called distal SMAC (dSMAC) [185]. Interestingly, there are reports suggesting that the exclusion of CD45 is not necessary in the case of high affinity TCR-pMHC interactions, at least at the early times of TCR activation [193]. In

this case too, CD45 slowly segregated from the sites of TCR-pMHC engagement. Therefore, it becomes clear that the particular localization and dynamics of CD45 are relevant to understand the regulation of TCR signaling in the synapse [108, 194].

In this chapter, I will examine possible mechanisms for the localization of the four basic molecules required for IS formation, namely TCR and LFA-1 on the T cell surface and pMHC and ICAM-1 on the APC surface. In the forming IS pattern, CD45 molecules will be introduced and I will try to shed light onto the mechanisms that lead to CD45 exclusion and the formation of the dSMAC.

3.2 Formation of the Immunological Synapse

In order to understand the mechanisms driving the spatial organization of molecules in the IS, I start from an agent-based model taking into account TCR, LFA-1, pMHC and ICAM-1 only [180]. Molecules are located in the two lattices representing the membranes of the two interacting cells. Free molecules may bind to their cognate ligands on the opposite lattice and already formed complexes can return to the free molecule state, according to their respective dissociation constants (see Table 2.1) [175,179,180]. First, molecules and complexes move only according to diffusion. As seen in Figure 3.1a, the diffusing complexes fail to form any particular pattern, and the IS region consists of intermixed TCR-pMHC and LFA-1-ICAM-1 complexes. This is a result of ignoring the bending of membrane due to lack of interactions between complexes.

It is known that TCR-pMHC and LFA-1-ICAM-1 have big differences in size, with TCR-pMHC being around 12 nm in length while LFA-1-ICAM-1 complexes have a size of about 45 nm. This size difference creates high tension in the regions where the smaller TCR-pMHC complexes reside, which leads to membrane bending and consequently, steric exclusion of the bigger LFA-1-ICAM-1. In order to phenomenologically represent the membrane bending in the two-dimensional (2D) system, size-based segregation (SBS) was modeled as a repulsive force between two complexes of different lengths [82]. The introduction of SBS generated TCR-pMHC microclusters, which failed to merge into the central supramolucular activation cluster (cSMAC) Figure 3.1b, and did not create the experimentally observed "bull's eye" pattern. This suggests that additional forces are needed for its formation.

A phenomenological centrally directed force was introduced into the model, which represents coupling of molecules to actin, inducing a centripetal flow. The strength of the force reflects the coupling strength to F-actin arcs. It was initially applied only to TCR-pMHC complexes Figure 3.1c [100, 104, 105, 115]. Microclusters formed within the first minute of contact between the cells, merged into bigger clusters, and finally formed the cSMAC Figure 3.1c. The mature synapse formed at ten minutes and remained stable, in agreement with experimental results [79,108]. This *in silico* framework recapitulates the major properties of the IS, and is suitable to further investigate the properties of additional mechanisms and regulatory molecules.

In Figure 3.1d, the density of complexes was computed inside equally spaced rings as the

fraction of occupied grid points by each type of complex. Here I observed the differences in the distribution of TCR-pMHC and LFA-1-ICAM-1 complexes throughout the cell-cell junction, in the three cases discussed above, (i) only diffusing complexes, (ii) addition of SBS and (iii) further addition of TCR-pMHC centripetal force due to actin coupling. When the characteristic pattern is formed, TCR-pMHC complexes reside in the central region of the IS, while LFA-1-ICAM-1 are homogeneously distributed outside the cSMAC, forming peripheral SMAC (pSMAC).

The relative positioning of molecules can be quantitatively described using Radial Distribution Functions (RDFs). The RDF between two types represents the frequency of finding a particle of type 2 in a radial neighborhood of type 1 particles. The peak of the RDF of TCR-pMHC complexes to themselves at 60 seconds reveals the formation of microclusters with a mean diameter of $d \simeq 0.3$ (Figure 3.2a). This diameter increased and ultimately led to a cSMAC with a diameter of $d \simeq 2.0 - 3.0\,\mu$m at 600 seconds [180].

The RDF of LFA1-ICAM-1 complexes around TCR-pMHCs (Figure 3.2b) also reflects the microclusters with $d \simeq 1\,\mu$m at 60 seconds, which evolve to larger structures of $d \simeq 3 - 4\,\mu$m at 600 seconds. These diameters are larger than those in the RDF of pairs of TCR-pMHC complexes, which reflects the halo around the microclusters and the cSMAC. This predicted halo is also found in experiments, and the model supports that this is a result of the membrane bending in these regions [195].

3.3 LFA-1 coupling to F-actin results in a pSMAC gradient toward the center of the IS

So far the model showed that the experimental observations of TCR-pMHC interacting with the F-actin flow [100,104,105] can act as a mechanism for TCR-pMHC accumulation in the central area of the synapse, the cSMAC. The question then was if other molecules exhibit the same behaviour. It has been suggested that LFA-1-ICAM-1 complexes can also be affected by the centripetal flow of F-actin arcs [116]. A centripetal force on LFA-1-ICAM-1 was added then to the *in silico* model, similar to TCR-pMHC complexes and the impact on IS formation was analysed and compared with the case were only TCR-pMHC complexes bind to actin (Figures 3.3).

The localization of TCR-pMHC microclusters and the "bull's eye" were mainly unaffected, though the microclusters moved slower to the cSMAC due to higher density of LFA-1 around the cSMAC. In contrast to Figure 3.3a, the model showed that the centripetal flow of LFA-1-ICAM-1 complexes leads to the formation of a LFA-1 density gradient in the pSMAC (Figure 3.3b, c): In comparison, without attachment to F-actin, LFA-1-ICAM-1 complexes were uniformly spread throughout the pSMAC (red solid line). Actin binding led to a higher concentration of LFA-1-ICAM-1 around the cSMAC that reduced as the distance from the center increased (red dashed line). This quantitatively illustrates the gradient observed in Figure 3.3b. Interestingly, the predicted LFA-1 gradient was also found in experiments [116, 196]. According to the model, the interplay of actin-mediated forces together with diffusion are responsible for the formation of

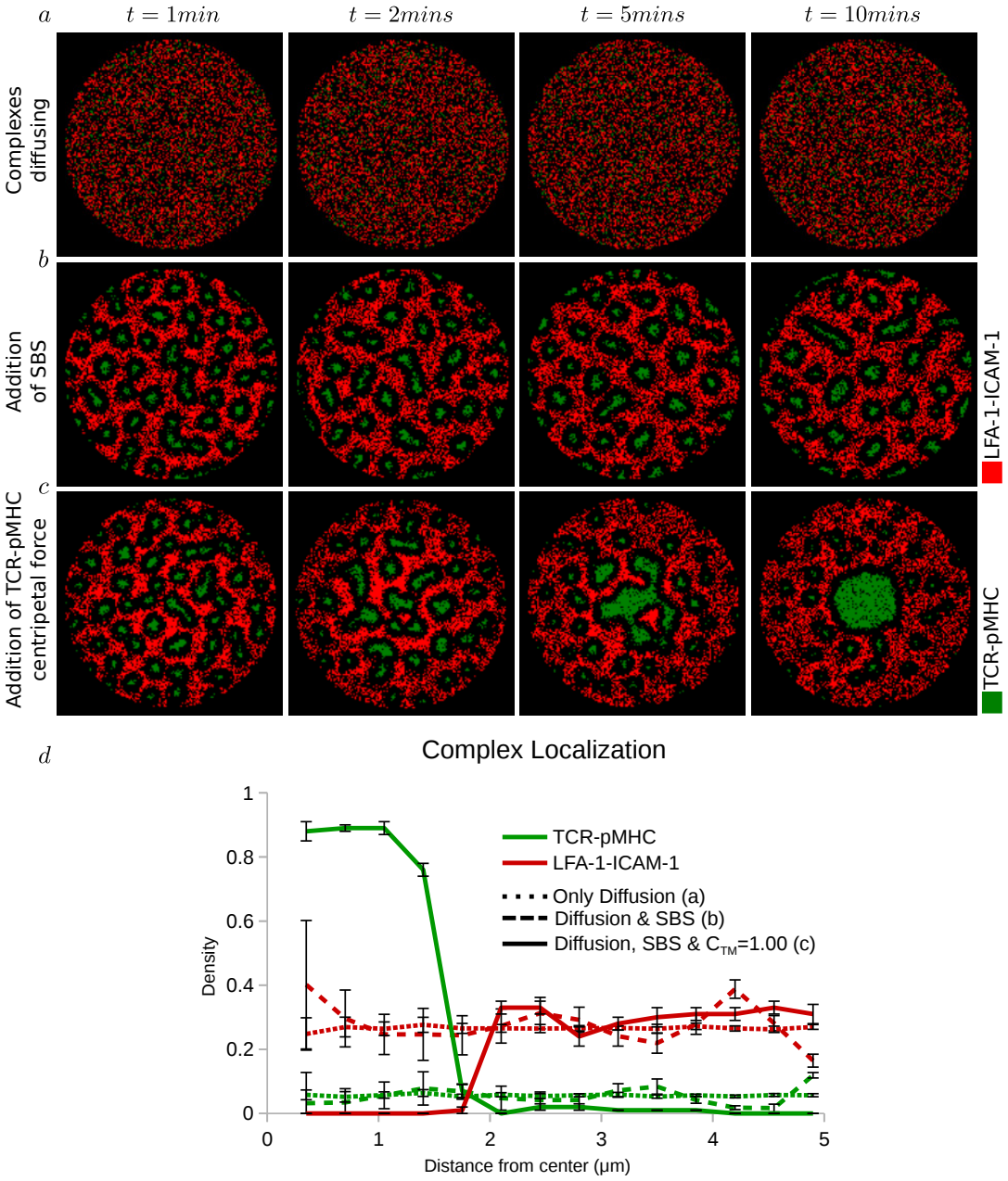

Figure 3.1: Formation of the immunological synapse. **(a)** TCR-pMHC and LFA-1-ICAM-1 complexes are only diffusing. **(b)** Addition of SBS between TCR-pMHC and LFA-1-ICAM-1 complexes. **(c)** Addition of TCR-pMHC coupling to actin, $C_{\mathrm{TM}} = 1.0$, and consequently centripetal force on TCR-pMHC. **(d)** Radial density profile of complexes along the distance from the center at 600 second, for (a) solid , (b) dashed and (c) dotted lines. Error bars represent the SD of $n = 10$ simulations. TCR-pMHC: green, LFA-1-ICAM-1: red.

an LFA-1 gradient in the IS.

I further analysed the RDFs between TCR-pMHC complexes and compared between presence and absence of LFA-1 gradient (Figure 3.4). There are no significant differences in the localization of TCR-pMHC in the two cases studied here. In the case of LFA-1 coupling to the F-actin flow, the TCR-pMHC microclusters at 60, 300, as well as at 600 seconds, seemed more densely packed than in the case of absence of LFA-1 interaction with actin (Figure 3.4a). This is observed by the higher values obtained for the first case, as a result of the combined exclusion of TCR-pMHC due to SBS

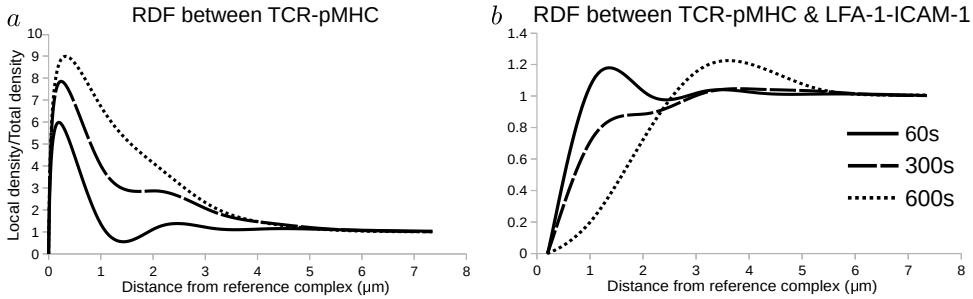

Figure 3.2: Radial distribution functions of Figure 3.1c at 60 (solid line), 300 (dashed line) and 600 seconds (dotted line), between (a) pairs of TCR-pMHC and (b) between TCR-pMHC and LFA-1-ICAM-1 complexes.

and LFA-1 centripetal flow. Nonetheless, these negligible differences showed that TCR-pMHC flow and accumulation in the cSMAC are not significantly affected by the emerging LFA-1 gradient.

On the contrary to TCR-pMHC, LFA-1-ICAM-1 localization with respect to TCR-pMHC complexes seemed to be highly affected. At the first moments of the IS formation (60 seconds) there were no significant differences between presence or absence of LFA-1-ICAM-1 coupling to actin (Figure 3.4b, solid lines). At 300 and 600 seconds though, LFA-1-ICAM-1 appeared at higher densities and closer to the TCR-pMHC complexes, when they were coupled to actin (Figure 3.4b, dashed and dotted lines). Eventually, the halo between central and peripheral SMACs persisted [195], but the density of LFA-1 in the inner pSMAC was a lot higher than before (Figure 3.3a, b).

The power of the model is that physiological parameters can be monitored or altered to make predictions. One such prediction is the importance of physiologically correct association and dissociation rates, as depicted in Figure 3.5, in absence or presence of LFA-1 gradient. The reference values are $k_{\mathrm{on,TM}} = 2 * 10^4\,\mathrm{M^{-1}s^{-1}}$, $k_{\mathrm{on,LI}} = 3 * 10^5\,\mathrm{M^{-1}s^{-1}}$, $k_{\mathrm{off,TM}} = 0.1\,\mathrm{s^{-1}}$, $K_{\mathrm{off,LI}} = 0.03\,\mathrm{s^{-1}}$ and will be used throughout this study. Decreasing the TCR-pMHC on-rates resulted in smaller cSMAC due to the difficulty in forming complexes, while increasing them, resulted in a bigger and denser cSMAC than before (Figure 3.5a, b (a-b)). Similarly, by decreasing the off-rates, the cSMAC becomes more dense, as it is more difficult for the complexes to return to the free molecule state (Figure 3.5a, b (c)). Accordingly, increasing the off-rate, led to a less dense cSMAC (Figure 3.5a, b (d)). Altering the association and dissociation rates of LFA-1-ICAM-1 complexes had similar effects on the pSMAC population. Reduction of the on-rates led to a less dense pSMAC, while increasing it, resulted in a higher density of complexes in the pSMAC (Figure 3.5a, b (e-f)). Finally, lower off-rates led to a denser pSMAC, while faster dissociation of LFA-1-ICAM-1 complexes resulted in a sparse pSMAC (Figure 3.5a, b (g-h)).

The model can also be extended to perform selective inhibition of different processes. Arrest of the coupling to F-actin experimentally would mean that no complex can be transported by interacting with it. However, I used the model so far to investigate the synapse when neither TCR-pMHC nor LFA-1-ICAM-1 couple to the F-actin centripetal flow (Figure 3.1b), or when only TCR-pMHC interact with it (Figure 3.1b) or finally, both TCR-pMHC and LFA-1-ICAM-1 are centrally transported (Figure 3.3b). But what would happen if the binding of TCR-pMHC to F-

actin was arrested while LFA-1-ICAM-1 could still bind to it (Figure 3.6)? SBS once again resulted in the emergence of a multifocal pattern, where TCR-pMHC microclusters failed to merge into the cSMAC, same as in Figure 3.1b. The centripetal transport of the LFA-1-ICAM-1 complexes led to their accumulation in the center of the contact region, and at the same time, TCR-pMHC microclusters were passively excluded toward the periphery ($t = 5$ minutes), where they ended up in a ring structure at the distal SMAC (dSMAC) ($t = 10$ minutes). Intuitively, from that *in silico* experiment, I concluded that for proper IS formation, the centripetal actin-driven force on LFA-1 must be lower than on TCR, and that the emerging radial LFA-1 gradient affects the localization of other molecules of the IS [180].

In conclusion, the model so far was able to recapitulate the dynamics of IS formation, with physiological parameters, as described experimentally [79, 108]. TCR-pMHC microclusters appeared from the first minutes of T cell-SLB interaction, which merged into bigger clusters before eventually accumulating in the center of the contact region, forming the cSMAC. Interstingly, the emergence of the pSMAC LFA-1-ICAM-1 gradient toward the cSMAC was also observed in accordance with experimental findings [116, 196]. The model explained so far is the basis of further investigations performed for the localization mechanisms and different spatial patterns appearing when different molecules are taken into consideration. The first thing to discuss will be the effect of the LFA-1 gradient on other molecules present during T cell activation.

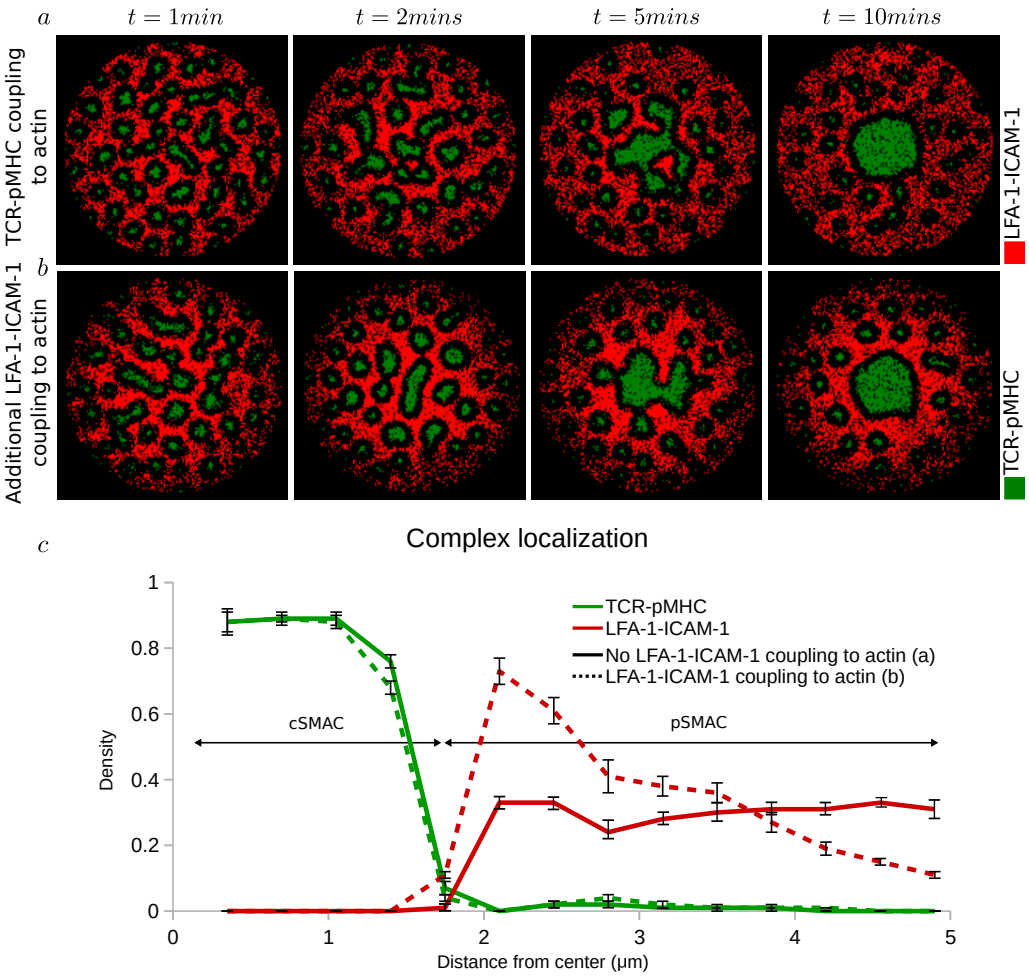

Figure 3.3: LFA-1 coupling to F-actin induces a gradient of LFA-1-ICAM-1 complexes. **(a), (b)** IS formation at 60, 120, 300 and 600 seconds (a) with TCR-pMHC coupling to F-actin, $C_{\mathrm{TM}} = 1.0$ (same with Figure 3.1c) and (b) with TCR-pMHC and LFA-1-ICAM-1 attachment to F-actin, $C_{\mathrm{TM}} = 1.0$ and $C_{\mathrm{LI}} = 0.05$, respectively. TCR-pMHC: green, LFA-1-ICAM-1: red. **(c)** Radial density profile of complexes along the distance from the center at 600 second, without (solid) or with (dashed) LFA-1 attachment to F-actin. Error bars represent the SD of $n = 10$ simulations.

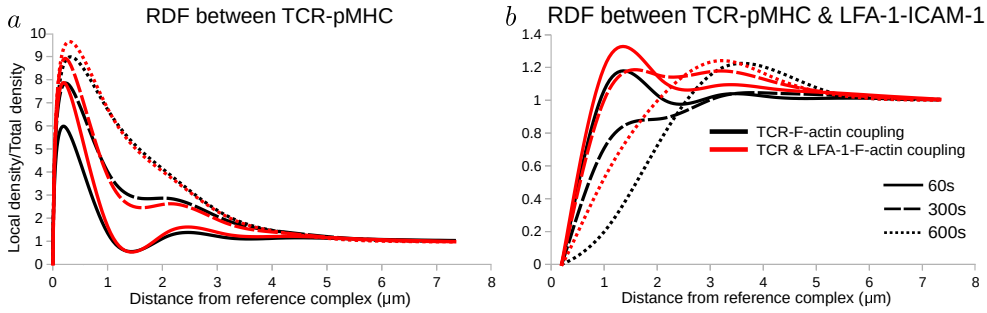

Figure 3.4: Radial distribution functions of Figure 3.3 at 60 (solid line), 300 (dashed line) and 600 seconds (dotted line), between (a) pairs of TCR-pMHC and (b) between TCR-pMHC and LFA-1-ICAM-1 complexes. Absence of LFA-1-ICAM-1 coupling to actin: black lines. Presence of LFA-1-ICAM-1 coupling to actin: red lines.

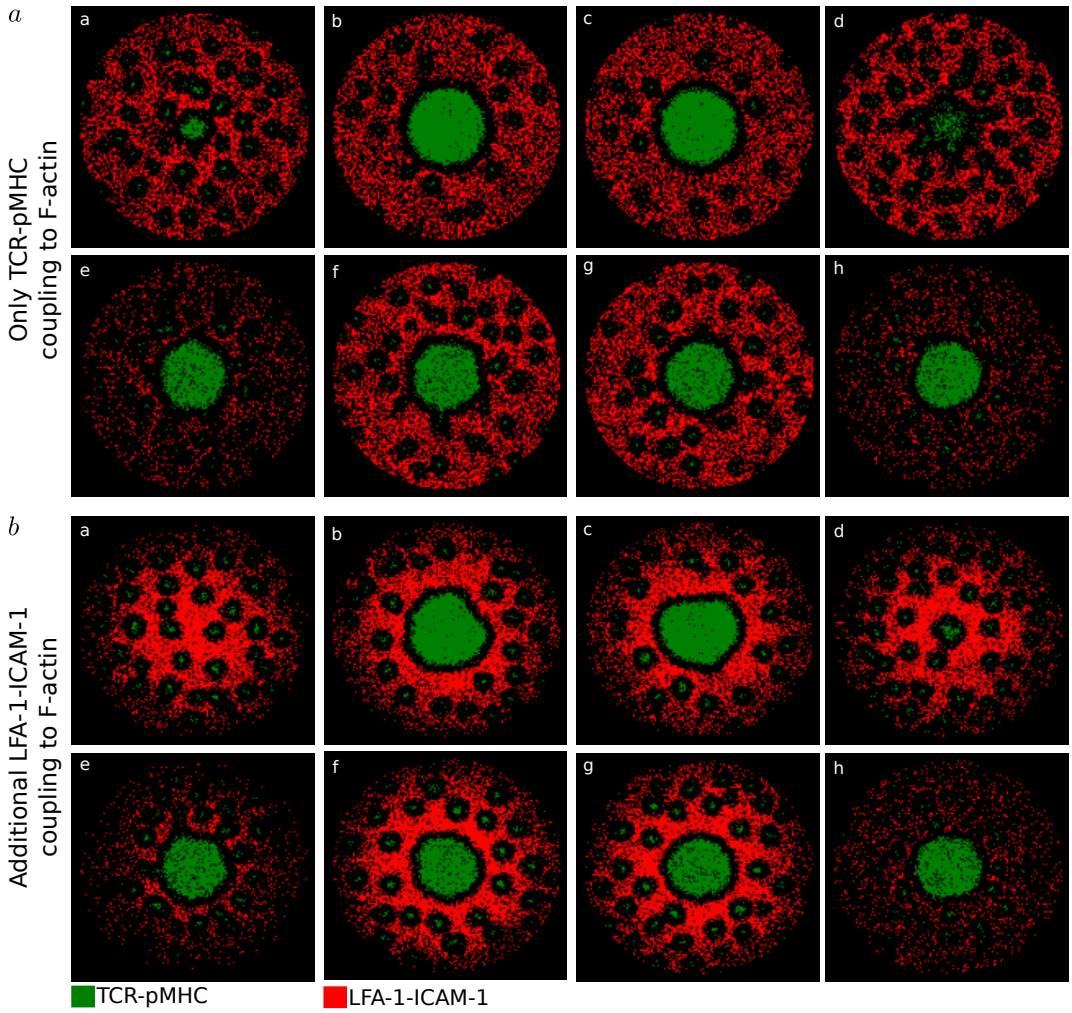

Figure 3.5: Effect of altering the association, k_{on}, and dissociation, k_{off}, rates for TCR-pMHC and LFA-1-ICAM-1 complexes, with (a) absence, $C_{\text{LI}} = 0.00$ or (b) presence of LFA-1 coupling to F-actin, $C_{\text{LI}} = 0.05$. Changes made to the basic parameters, $k_{\text{on,TM}} = 2 * 10^4\,\text{M}^{-1}\text{s}^{-1}$, $k_{\text{on,LI}} = 3 * 10^5\,\text{M}^{-1}\text{s}^{-1}$, $k_{\text{off,TM}} = 0.1\,\text{s}^{-1}$, $k_{\text{off,LI}} = 0.03\,\text{s}^{-1}$, are depicted: (a) $k_{\text{on,TM}} = 2 * 10^3\,\text{M}^{-1}\text{s}^{-1}$, (b) $k_{\text{on,TM}} = 2 * 10^5\,\text{M}^{-1}\text{s}^{-1}$, (c) $k_{\text{off,TM}} = 0.01\,\text{s}^{-1}$, (d) $k_{\text{off,TM}} = 1.0\,\text{s}^{-1}$, (e) $k_{\text{on,LI}} = 3 * 10^3\,\text{M}^{-1}\text{s}^{-1}$, (f) $k_{\text{on,LI}} = 3 * 10^7\,\text{M}^{-1}\text{s}^{-1}$, (g) $k_{\text{off,LI}} = 0.003\,\text{s}^{-1}$, (h) $k_{\text{off,LI}} = 3.0\,\text{s}^{-1}$. TCR-pMHC: green, LFA-1-ICAM-1: red.

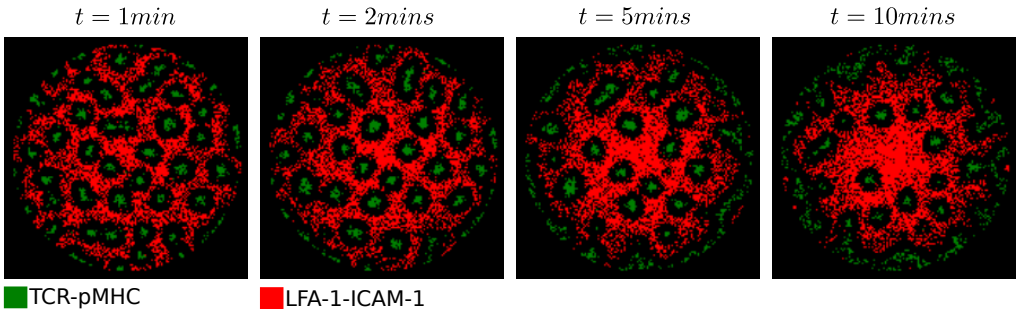

Figure 3.6: Blocking only TCR-pMHC centripetal motion and not LFA-1-ICAM-1 when the SBS is taken into account. As LFA-1-ICAM-1 accumulate in the central region due to F-actin coupling, TCR-pMHC are pushed to the outer part of the contact region, and eventually a ring of TCR-pMHC appears in the dSMAC. (a)-(d) 60, 120, 300 and 600 seconds. TCR-pMHC: green, LFA-1-ICAM-1: red.

3.4 The LFA-1 gradient relocates unbound molecules

In order to investigate the effect of the LFA-1 gradient on other molecules and complexes taking part in IS formation, extra agents will be introduced into model. What kind of agents should they be? Where to start from? First of all, I looked for experimental data where the effect of the LFA-1 gradient is discussed. One such example investigates the localization of the costimulatory molecule CD28 [196]. Luckily, in this article, the localization of both free and complexed CD28 molecules is studied. In the next chapter, I will focus on the localization mechanisms of CD28 complexes, but for now, the available data can be used to investigate how freely diffusing molecules move within the forming synapse. The model was updated and CD28 molecules were introduced in the T cell lattice. There were no interactions between the present TCR-pMHC and LFA-1-ICAM-1 complexes and free CD28 included, since the small free molecules should be able to move freely in the contact interface. Initially, no ligand was introduced in the SLB, in order to investigate the effect of the LFA-1 gradient on freely diffusing molecules. Experimentally, absence of ligand led to a uniform distribution of CD28 molecules throughout the IS, with a higher accumulation in the dSMAC region [196].

The model, in contrast to experiments, allows us to alter the strength with which LFA-1 couples to actin, C_{LI}. In the absence of LFA-1 coupling to actin, $C_{\mathrm{LI}} = 0.00$, free CD28 molecules were uniformly spread in the contact region (Figure 3.7a (left)), which is in qualitative disagreement with the experimental result. In contrast, LFA-1 coupling to actin, $C_{\mathrm{LI}} = 0.05 - 0.10$, split free CD28 into two populations, one into the cSMAC and another into the dSMAC (Figures 3.7a (middle, right)), in agreement with experiments. Stronger coupling of LFA-1 to actin excluded more CD28 to the dSMAC, but still a substantial amount remained dispersed throughout the contact region (Figure 3.7b) [180].

This result does not only apply to CD28, but to any small free molecule in the IS, which does not interact with the surrounding complexes. The modeling results reveal that the predicted LFA-1 gradient, induced by its coupling to the centripetal flow of actin, is a mechanism with the potential to divide free molecules in the IS into two populations, relocating them to the cSMAC and the dSMAC. The question raising is if the localization of molecules longer than CD28, will be affected in a different way. The characteristic example of CD45 molecules, which have the same size as an LFA-1-ICAM-1 complex, $\simeq 45\,\mathrm{nm}$, and therefore are considered very long, will be discussed in the following section.

3.5 CD45 localization is also affected by the LFA-1 gradient

Similar to free CD28 molecules, I considered the transmembrane protein phosphatase CD45. No ligand has been described so far for CD45, but its presence in the synapse is considered very important, since it affects TCR signaling [185–190]. Interestingly, CD45 is highly excluded from the TCR regions. Davis and van der Merwe proposed the kinetic segregation model (KSM) [99], which suggested that the T cell receptor can get activated due to the exclusion of phosphatases

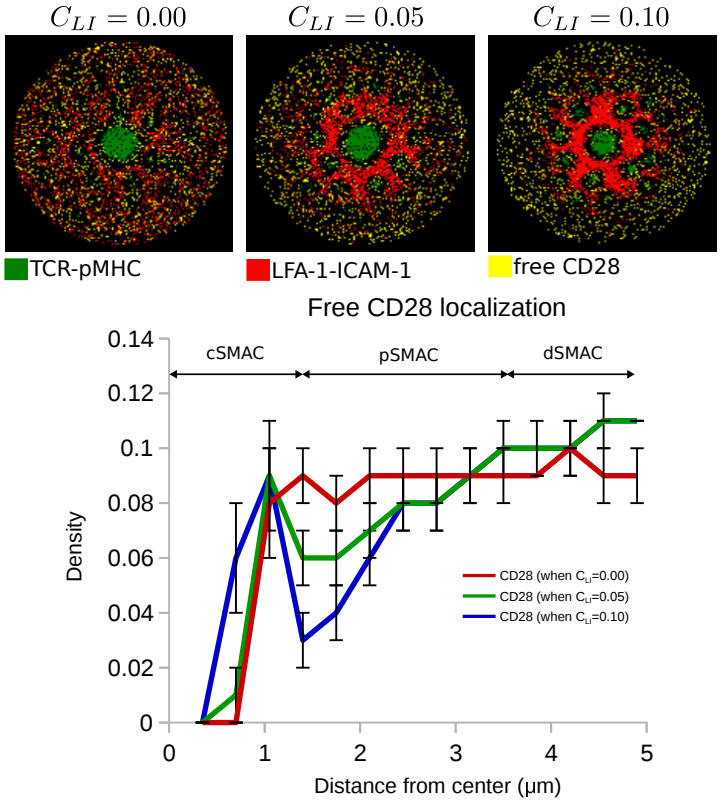

Figure 3.7: Impact of the LFA-1 gradient on free CD28 molecules, in the absence of the CD80 ligand. **(a)** Altering LFA-1 actin coupling strength, (left) $C_{\mathrm{LI}} = 0.00$, (middle) $C_{\mathrm{LI}} = 0.05$ and (right) $C_{\mathrm{LI}} = 0.10$ at 600 seconds. **(b)** Radial density profile of free CD28 molecules along the distance from the center at 600 seconds. Error bars represent the SD of $n = 10$ simulations. TCR-pMHC: green, LFA-1-ICAM-1: red, CD28: yellow.

like CD45, further supported by the observation of higher calcium flux when CD45 molecules are excluded from the centripetally travelling TCR-pMHC microclusters [92, 197]. Hence, the mechanisms of the particular localization and dynamics of CD45 are relevant to understand the regulation of TCR signaling in the synapse [108, 194].

The agent-based model was complemented with freely diffusing CD45 molecules, without any interactions with TCR-pMHC and LFA-1-ICAM-1 taking place. In that case, CD45 was observed to localize uniformly spread throughout the contact interface (Figure 3.8 (first column)). As before, the emergence of the LFA-1 gradient, excluded more and more CD45 molecules towards the dSMAC as the centripetal force, C_{LI}, became larger. Despite the exclusion, the thick CD45 ring in the dSMAC was not reproduced, with a substantial amount remaining trapped in the central-peripheral SMAC border [185, 197]. The proposed KSM as well as the size of the diffusing CD45 molecules, $\approx 45\,\mathrm{nm}$, pointed to the introduction of additional mechanisms [99, 198].

The idea was that since CD45 molecules do not have known ligands, they could possibly bend and fit into close contact regions, such as the TCR-pMHC microclusters. KSM suggested that conformational changes on the intracellular tales of TCR and CD45 molecules during antigen recognition might be responsible for the exclusion of CD45. In order to keep the model as simple as possible, I avoided to introduce complex mechanisms, such as conformational changes or membrane

bending. Instead, the exclusion of CD45 from the TCR microclusters was modelled as a repulsive force, representing the effect of KSM. This force is similar to the repulsive forces due to size-based segregation (SBS). This repulsive force was defined within a radius R_{CD45TCR}, and was weighted by W_{CD45TCR}. The range of CD45-TCR interaction was set to be at maximum equal to the range of TCR-pMHC and LFA-1-ICAM-1 interaction, since the size of LFA-1-ICAM-1 complexes are similar to that of CD45. Therefore, I investigated repulsion radii of $R_{\mathrm{CD45TCR}} = 0.14 - 0.42\,\mu$m, and the forces were weighted with $W_{\mathrm{CD45TCR}} = -1.0$. As the interaction range increased, CD45 were excluded from the TCR regions, and colocalized with LFA-1 in the pSMAC. The additional LFA-1 pSMAC gradient further excluded CD45 toward the dSMAC but still a substantial population remained in the pMSAC region (Figures 3.8a, b). One could argue that the amount of exclusion achieved only by the combined repulsion from TCR-pMHC and the LFA-1-ICAM-1 gradient on CD45, is enough to reproduce the experimental observations, as seen in Figure 3.8a for $R_{\mathrm{CD45TCR}} \geq 0.28\,\mu$m and LFA-1-F-actin interaction strength of $C_{\mathrm{LI}} \geq 0.05$ [185, 197].

However, I still wanted to investigate if an additional repulsion from LFA-1-ICAM-1 to CD45 would affect the observed IS pattern. Similar to the interaction with TCR-pMHC, the repulsion between LFA-1 and CD45 was defined in a range $R_{\mathrm{CD45LFA}} = 0.00 - 0.28\,\mu$m, and weighted with $W_{\mathrm{CD45LFA}} = -1.0$. The LFA-1 centripetal force was set equal to $C_{\mathrm{LI}} = 0.05$, as in most of the cases presented. As seen in Figures 3.9a (bottom row, second column) & b (green dotted line), a very weak repulsion from LFA-1, in the range of $R_{\mathrm{CD45LFA}} = 0.14\,\mu$m, managed to exclude almost 100% of CD45, which formed a dense dMSAC ring structure, provided there was strong exclusion from TCR. Interestingly, stronger repulsion between CD45 and LFA-1-ICAM-1, instead of leading to complete exclusion of CD45, blocked its outward movement and resulted in clusters of CD45 appearing around the cSMAC or even spread in the pSMAC region (Figure 3.9a (bottom right corner)).

These results together suggest that the repulsive interaction between CD45 and TCR-pMHC due to KSM or simply due to size exclusion by SBS, can recapitulate the experimentally observed CD45 dSMAC ring structure. Interestingly, CD45 localization is also affected by interactions with LFA-1-ICAM-1. Weak repulsion can additionally help CD45 reach the dSMAC, whereas stronger repulsion can block its outward flow, suggesting that if this interaction is present in reality, it has to be a weak one.

3.6 Conclusions

In this chapter, I showed that the agent-based model was able to reproduce the observed characteristic IS pattern [68, 79], with very simple mechanisms. SBS was able to segregate long from short complexes, while centrally directed transport of complexes representing coupling to the F-actin arc flow, resulted in the accumulation of TCR-pMHC complexes in the central area of the cell-cell contact interface. The model predicted the emergence of an LFA-1-ICAM-1 gradient in the pSMAC region toward the cSMAC, provided the interaction of these complexes with actin centripetal flow.

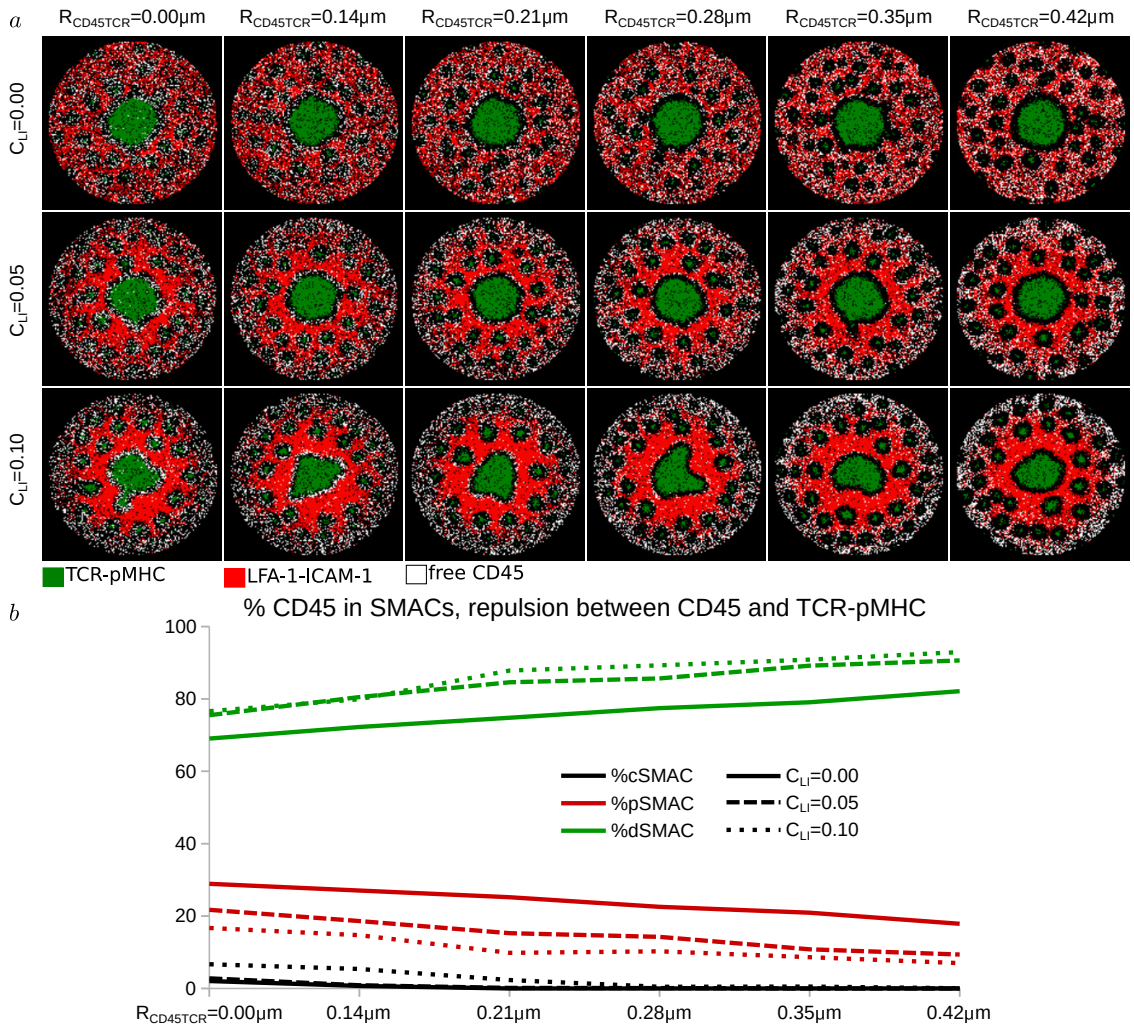

Figure 3.8: CD45 localization during interaction with TCR-pMHC complexes at 10 minutes of IS formation. **(a)** Different centripetal force of LFA-1-ICAM-1 complexes together with different strengths of repulsion, R_{CD45TCR} between CD45 and TCR-pMHC. **(b)** Amount of CD45 in the central, peripheral and distal SMAC. TCR-pMHC: green, LFA-1-ICAM-1: red, CD45: white.

The effect of the LFA-1 gradient was studied in the case of freely diffusing molecules, without ligand. The emergence of the gradient resulted in the separation of these molecules into distinct populations, one in the cSMAC region and another in the outer pSMAC and dSMAC region.

In the following chapter, I will investigate the effect of the LFA-1-ICAM-1 gradient on additional complexes forming by the introduction of new molecules to the model. Further localization mechanisms for the newly introduced complexes will be studied and discussed, based on experimental observations.

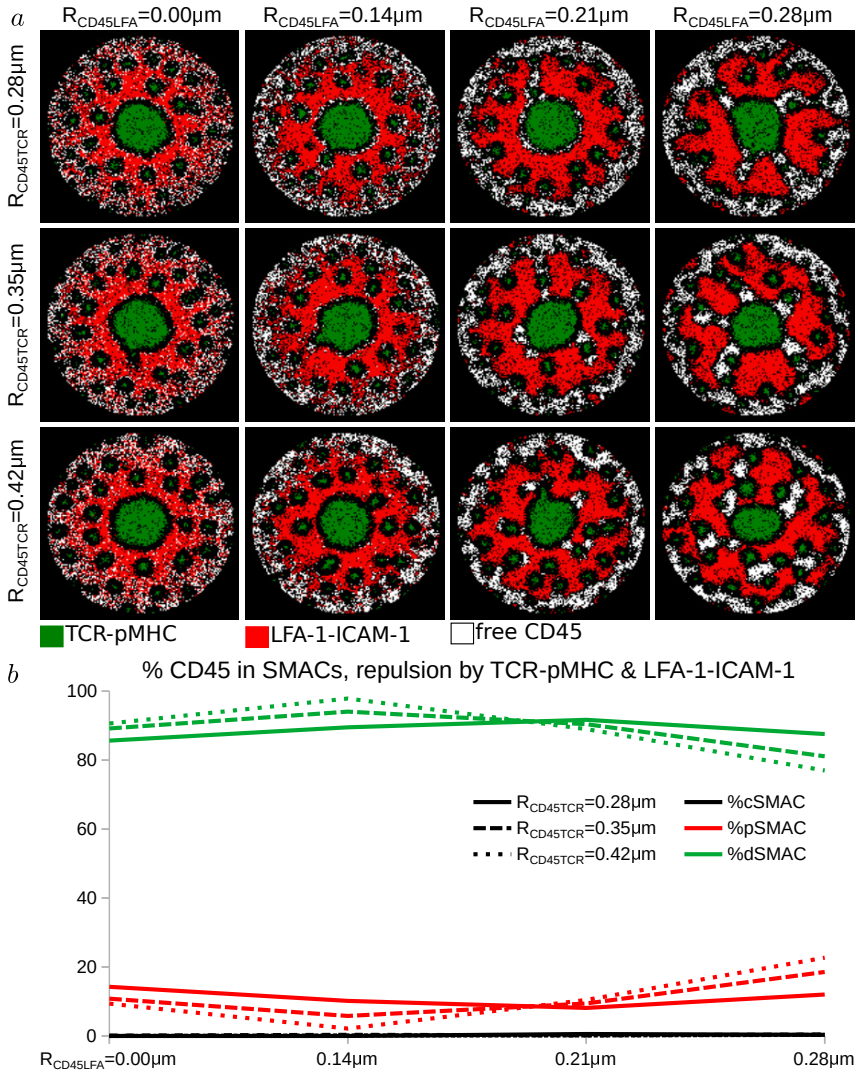

Figure 3.9: Impact of an additional LFA-1-ICAM-1 repulsion toward CD45. **(a)** IS pattern at 10 minutes, in presence of TCR-pMHC and LFA-1-ICAM-1 repulsive force on CD45. **(b)** Amount of CD45 in the central, peripheral and distal SMAC. TCR-pMHC: green, LFA-1-ICAM-1: red, CD28: white.

Chapter 4

F-Actin-Driven CD28-CD80 Localization in the Immune Synapse

4.1 Introduction

T cells require two signals in order to get activated. The first signal is antigen specific, and is provided by the TCR-pMHC engagement. The second signal comes from so called costimulatory molecules. This signal is not antigen-specific and requires the binding of surface molecules on the T cell surface to molecules present on the APC surface. There are many examples of costimulatory molecules, such as CD28, CD2, ICOS and others. The signals received from such costimulatory molecules are essential for T cell proliferation, differentiation and survival.

In this chapter, I will talk about CD28. As already mentioned in the previous chapter, freely diffusing CD28 molecules are relocated by the emergence of the LFA-1 gradient in the pSMAC. Here, I will investigate the behaviour of CD28 in presence of one of its ligands and explore their localization mechanisms. CD28 carries a significant role for regulatory and follicular helper T cell differentiation [199,200]. Binding of CD28 to one of its major ligands, CD80 (B7-1) and CD86 (B7-2), supports TCR signaling [201,202], while a lack of CD28 costimulation leads to an apathetic state of the T cell, known as anergy, where killing or boosting of other cells is impaired [201, 203, 204].

CD28 has been shown to preferentially locate in the cSMAC [196, 205]. This particular localization was attributed to the ligation with CD86 [204], or CD80 [206]. A ring of CD28 around the cSMAC has been described [206], and was further confirmed by the colocalization of CD28 and protein kinase Cθ (PKCθ) that also forms a ring around the cSMAC [196, 207, 208]. The reasons for this characteristic pattern are still poorly understood. The cytoplasmic domain of CD80 was shown to segregate CD28 from TCR complexes whereas the tailless form of CD80 allows colocalization with TCR [206]. CD80 is not sufficient for a proper CD28 localization, since a mutation in

the cytosolic tail of CD28 disrupts the ring-like pattern [207]. There is also evidence that CD28 binds to F-actin, since it is observed to recruit Filamin-A (FLNa), an actin binding protein, upon ligation [209, 210]. Cytoskeleton-driven motion is further supported by a linear motion of CD28 complexes toward the cSMAC [183], raising the question whether actin-driven forces could explain the localization of CD28.

The majority of experimental data available use only CD80 ligands instead of CD86 [196]. The model was therefore extended to include CD80 ligand on the SLB lattice, in order to compare the *in silico* results with experimental work [196]. The size of CD28-CD80 and TCR-pMHC complexes is very similar, $\simeq 11\,\mathrm{nm}$, such that I assume no SBS between them unless stated otherwise, and the same SBS to LFA-1-ICAM-1 as for TCR-pMHC. Physiological parameters for the association and dissociation rates were taken from literature, $k_\mathrm{d} = 4\,\mu\mathrm{M}$, with $k_\mathrm{off} \geq 1.6\,\mathrm{s}^{-1}$ and $k_\mathrm{on} \geq 4 \times 10^5\,\mathrm{M}^{-1}\mathrm{s}^{-1}$ [211, 212] (see Table 2.1).

4.2 CD28 complexes behave as passive followers of TCR-pMHC movement

The *in silico* experiments began with the same setting as in Figure 3.3b. TCR-pMHC segregate from LFA-1-ICAM-1 complexes due to SBS and further centripetal force on TCR-pMHC and LFA-1-ICAM-1 complexes leads to the accumulation of TCR-pMHC in the cSMAC and the emergence of the LFA-1-ICAM-1 gradient in the pSMAC region toward the SMAC. Initially, only SBS between CD28-CD80 and LFA-1-ICAM-1 complexes was introduced into the model. In this way, CD28-CD80 complexes were sterically excluded and pushed into the TCR-pMHC microclusters. The majority of CD28-CD80 did not reach the SMAC as is experimentally observed [196], due to the LFA-1 gradient repelling them from the inner pSMAC region (Figure 4.1a, c (dashed line)). However, a substantial amount passively followed the centripetal movement of TCR-pMHC microclusters, a behavior not appreciated before, resulting in a small CD28-CD80 ring around the cSMAC (Figures 4.1a, 4.2 (dashed line)).

This behavior occurred due to the SBS between CD28-CD80 and LFA-1-ICAM-1 in combination with the TCR-pMHC centripetal flow, which allowed CD28 complexes to follow low tension paths toward the center. The CD28 ring generated by passively following TCR-pMHC movement *in silico* was too weak to explain the experimentally observed CD28 ring around the cSMAC [196]. Hence, there are mechanisms that had to be included in order to *in silico* recapitulate the appropriate CD28-CD80 annular localization.

4.3 Actin-dependent localization of CD28

Several experimental studies suggested a potential actin-driven motion of CD28 complexes [183,209, 210]. The effect of this interaction was analysed in the model (Figure 4.1b). SBS between CD28-CD80 and LFA-1-ICAM-1 as before, together with a CD28-CD80 actin coupling were sufficient to

colocalize CD28-CD80 complexes with TCR-pMHC microclusters and to form a CD28 ring around the cSMAC (Figures 4.1b, c (solid line), 4.2 (solid line)) as in experiment [196].

CD28 coupling to actin did not change colocalization of TCR-pMHC and CD28-CD80 at the early times of IS formation (Figure 4.2a, 60 seconds). However, after 120 and 300 seconds, colocalization of CD28 and TCR complexes was decreased without actin coupling (Figure 4.2a). With actin coupling, it remained stable and increased after 600 seconds when the cSMAC formed. In *in silico* microclusters, CD28 hardly colocalize with TCRs at a distance of less than 210 nm (Figure 4.2b). This reflects the fact that TCRs move faster to the center than CD28. However, actin coupling resulted in a higher colocalization of CD28 and TCR in the ring around the cSMAC.

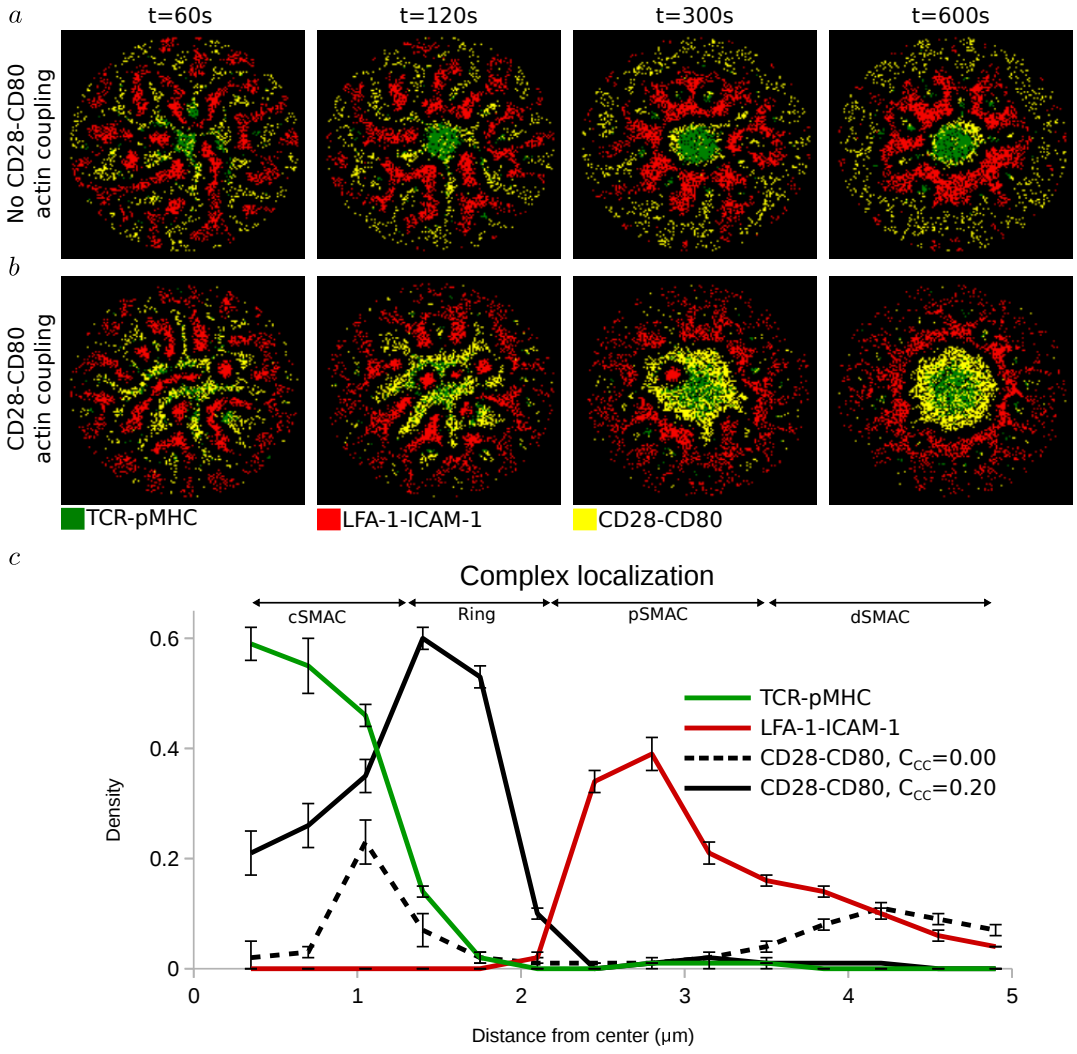

Figure 4.1: Effect of CD28-CD80 actin coupling on the dynamics of the IS. IS formation at 60, 120, 300 and 600 seconds, **(a)** with absence of CD28-CD80 coupling to actin, $C_{CC} = 0.00$ and **(b)** with presence of CD28-CD80 coupling to actin, $C_{CC} = 0.20$, in the presence of a LFA-1 gradient. **(c)** Radial density profile of complexes along the distance from the center at 600 seconds, with or without CD28 coupling to actin. Error bars represent the SD of $n = 10$ simulations. TCR-pMHC: green, LFA-1-ICAM-1: red, CD28-CD80: yellow.

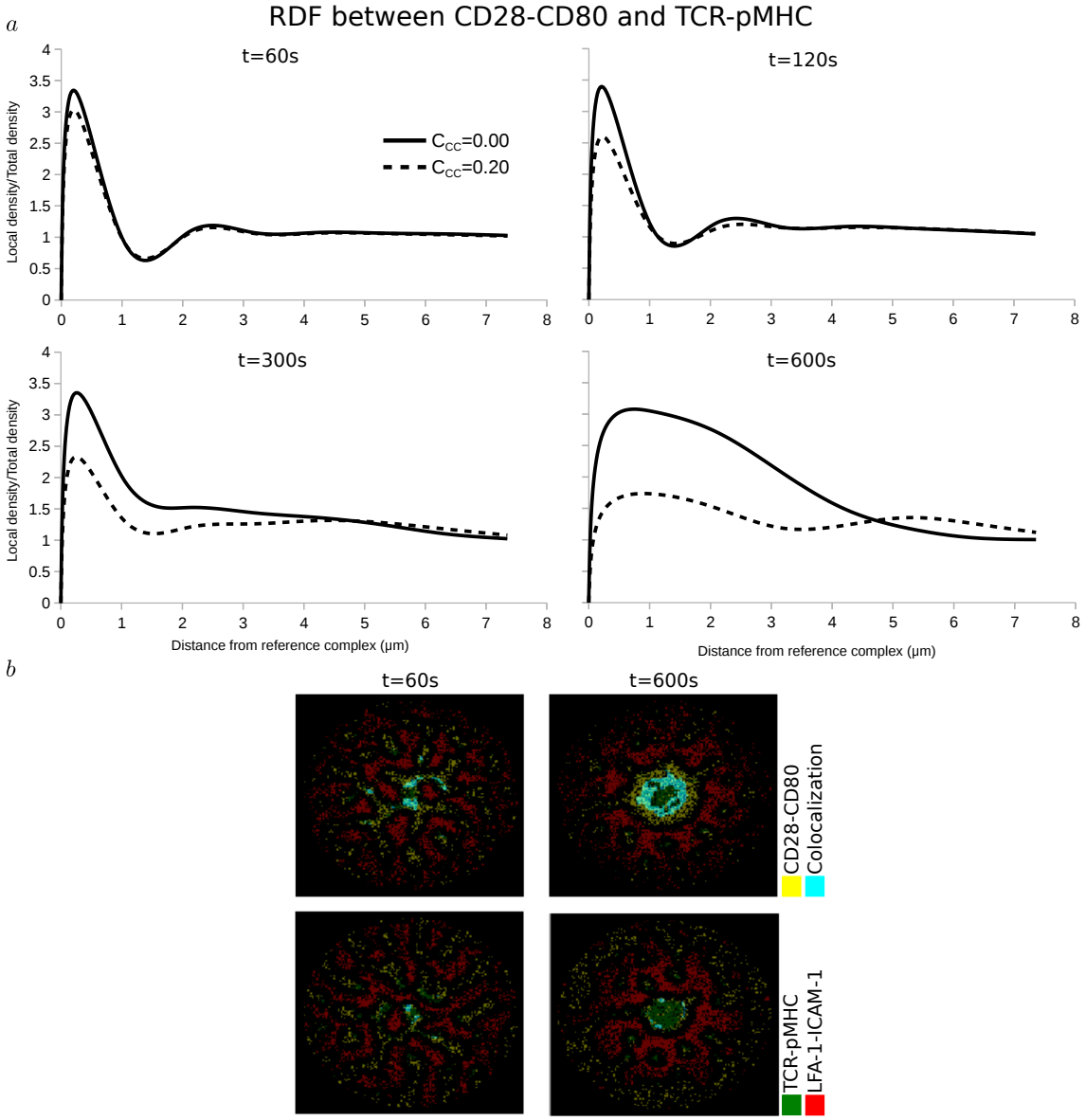

Figure 4.2: CD28-actin coupling impacts on colocalization of CD28-CD80 and TCR-pMHC. **(a)** Radial distribution function of Figure 4.1, at 60, 120, 300, and 600 seconds of IS formation with ($C_{\mathrm{CC}} = 0.20$) or without ($C_{\mathrm{CC}} = 0.00$) CD28 coupling to actin. **(b)** Short distance colocalization at less than 210 nm (blue) of CD28-CD80 and TCR-pMHC, with ($C_{\mathrm{CC}} = 0.20$) or without ($C_{\mathrm{CC}} = 0.00$) CD28 coupling to actin. TCR-pMHC: green, LFA-1-ICAM-1: red, CD28-CD80: yellow, Colocalization: Cyan.

4.4 Model calibration

The use of SLB systems allows biologists to control and quantify the ligand concentrations, which would be almost impossible in the 3D T cell-APC system. For the *in silico* CD28 localization study, I used a variety of CD80 concentrations, ranging between 60−120% of the amount of floating ICAM-1 on the SLB [196]. Similarly to the experiments, I investigated these concentrations of CD80 ligand on the SLB lattice (Figure 4.3). The patterns were recapitulated within the experimental range, and therefore I decided to perform all the *in silico* experiments with CD80 at 60% of ICAM-1.

Similar to the case of TCR-pMHC and LFA-1-ICAM-1 synapse formation, I investigated

possible changes in the emerging patterns, by altering the association and dissociation rates of CD28-CD80 complexes. The dissociation constant for CD28-CD80 complexes is $k_{\mathrm{d}} = 4\,\mu\mathrm{M}$, with $k_{\mathrm{off}} \geq 1.6\,\mathrm{s}^{-1}$ and $k_{\mathrm{on}} \geq 4 \times 10^5\,\mathrm{M}^{-1}\mathrm{s}^{-1}$ (Figure 4.4e) [211]. As seen in Figure 4.4, only the amount but not the localization of CD28-CD80 changes [180].

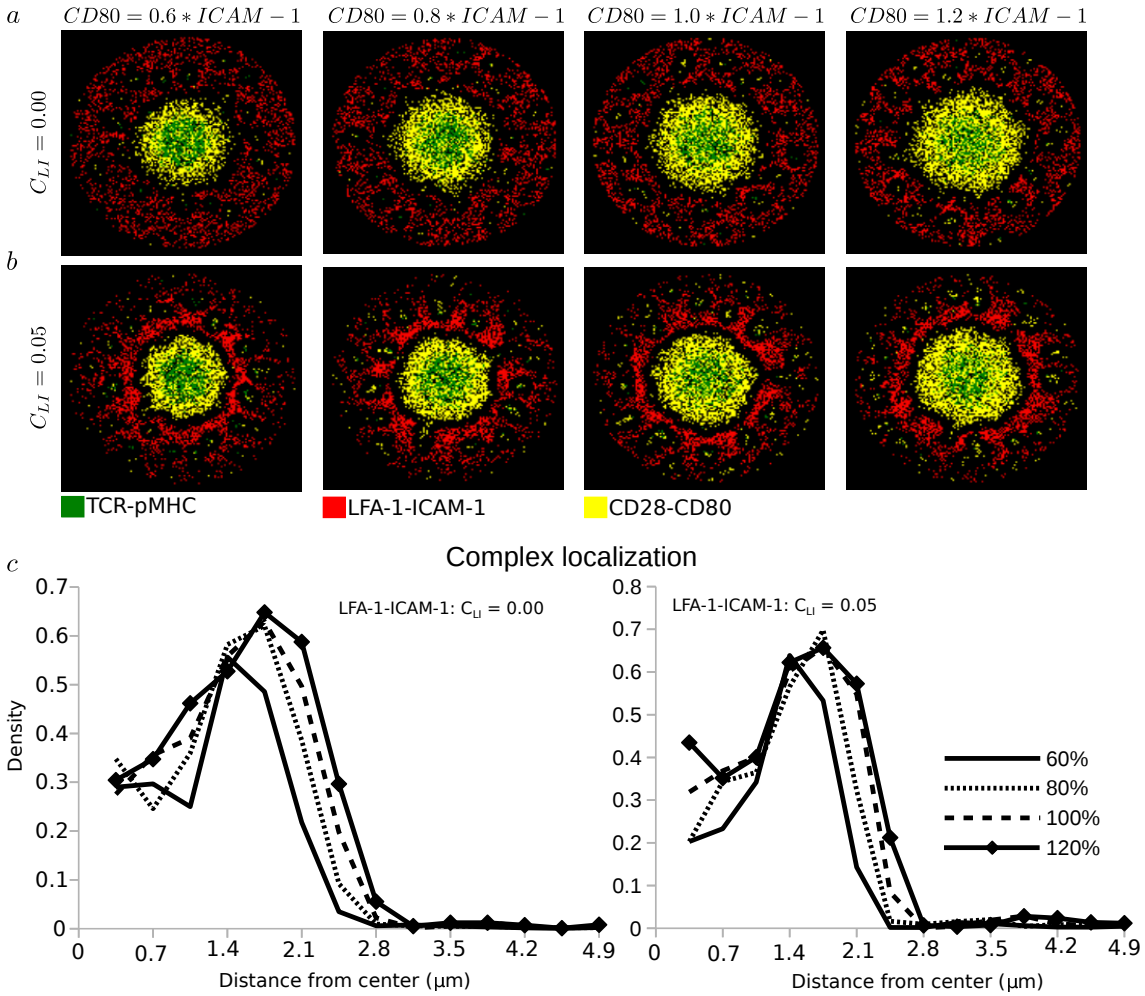

Figure 4.3: Model calibration for the amount of CD80 molecules. Variation between $60 - 120\%$ of ICAM-1 amount, for constant CD28-CD80 coupling to actin strength, $C_{\mathrm{CC}} = 0.20$. **(a)** Absence of LFA-1-ICAM-1 coupling to F-actin, $C_{\mathrm{LI}} = 0.00$. **(b)** Presence of LFA-1-ICAM-1 coupling to F-actin, $C_{\mathrm{LI}} = 0.05$. **(c)** CD28-CD80 localization in the IS, in absence (left graph) or presence (right graph) of LFA-1 coupling to F-actin. TCR-pMHC: green, LFA-1-ICAM-1: red, CD28-CD80: yellow.

4.5 Model Robustness

To investigate the robustness of the results presented, additional *in silico* experiments for molecular crowding were performed. The total density of the molecules in Figure 4.1b was gradually increased from 30% to 60% (Figure 4.5a). As expected, this increased the sizes of the cSMAC and the CD28 ring (Figure 4.5a), and, consequently, pushed the LFA-1 pSMAC further away from the IS center. Despite of size changes, the required mechanisms for the formation of the ring-like structure remained the same.

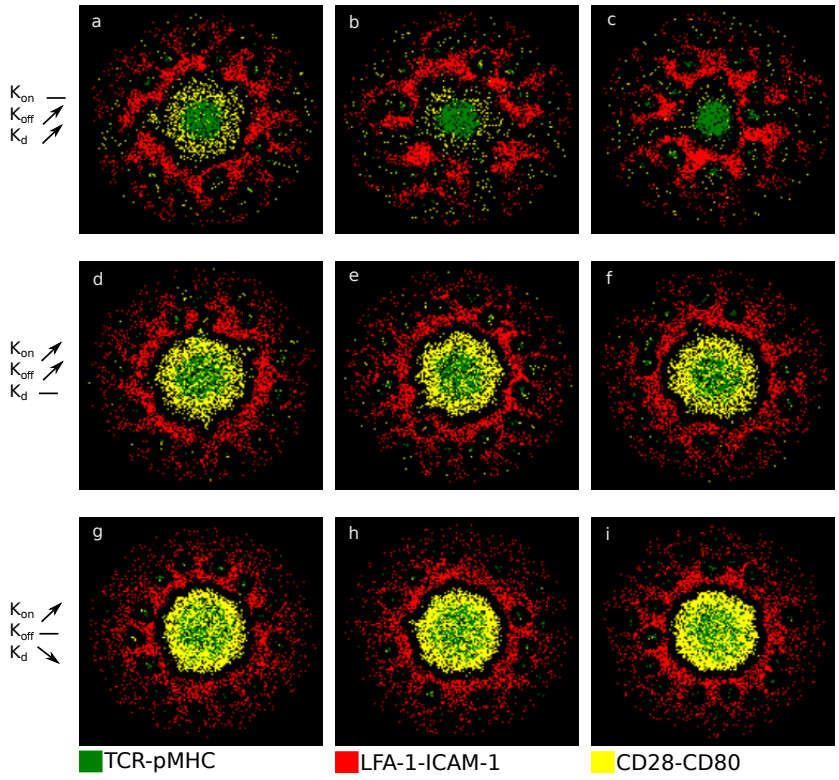

Figure 4.4: Model calibration for the On and Off rates of CD28-CD80. Keeping k_{on} constant and increasing k_{off} (first row), having k_{d} constant and increasing both k_{on} and k_{off} (second row) and finally, k_{off} constant while increasing k_{on} (third row). The values shown in (e), $k_{\text{on}} = 4 \times 10^5\,\text{M}^{-1}\text{s}^{-1}$, $k_{\text{off}} = 1.6\,\text{s}^{-1}$ with $k_{\text{d}} = 4\,\mu\text{M}$, are the ones used throughout this article. When a value is considered constant, it is taken from (e). (a) $k_{\text{off}} = 6\,\text{s}^{-1}$, (b) $k_{\text{off}} = 12\,\text{s}^{-1}$, (c) $k_{\text{off}} = 24\,\text{s}^{-1}$, (d) $k_{\text{on}} = 15 * 10^5\,\text{M}^{-1}\text{s}^{-1}$, $k_{\text{off}} = 6\,\text{s}^{-1}$, (f) $k_{\text{on}} = 30 * 10^5\,\text{M}^{-1}\text{s}^{-1}$, $k_{\text{off}} = 12\,\text{s}^{-1}$, (g) $k_{\text{on}} = 15 * 10^5\,\text{M}^{-1}\text{s}^{-1}$, (h) $k_{\text{on}} = 30 * 10^5\,\text{M}^{-1}\text{s}^{-1}$ and (i) $k_{\text{on}} = 60 * 10^5\,\text{M}^{-1}\text{s}^{-1}$. TCR-pMHC: green, LFA-1-ICAM-1: red, CD28-CD80: yellow.

Starting from Figure 4.1b, we introduced different densities of an extra population of arbitrary molecules (AM) on the T cell lattice without ligands on the SLB. Similar to Figure 3.7, AM are affected by the LFA-1 gradient in the pSMAC and are excluded to the outer region of the IS. With increasing AM density, and based on the same mechanisms for pattern formation, CD28 localization was affected but not to a degree that changed its annular accumulation around the cSMAC (Figure 4.5b, d (left graph)).

In order to exclude that the lattice resolution of $\alpha = 70\,\text{nm}$ would generate artefacts, we replicated the critical simulations with different lattice resolutions, $\alpha = 100$, 50, 35, 17 nm (Figure 4.5c, d (right graph)). The localization of all the complexes, TCR-pMHC, LFA-1-ICAM-1 and CD28-CD80 was not affected as shown in Figure 4.5d (right graph), and can be appreciated from the IS formation snapshots in Figure 4.5c.

Additionally, a swapping algorithm was implemented, which allowed agents moving by active forces, such as repulsion and centrally-directed force, to exchange positions when the two agents wanted to move to the other's position [180,182]. This generated a more realistic fluidity similar to a lattice gas model. Similarly to the previous robust experiments, all the mechanisms and patterns remained in accordance to the reference resolution of $\alpha = 70\,\text{nm}$ (Figure 4.6).

All together, the results show that CD28 coupling to the centripetal actin flow is sufficient for the formation of the ring-like structure and that SBS and passive following alone are not able to generate this pattern.

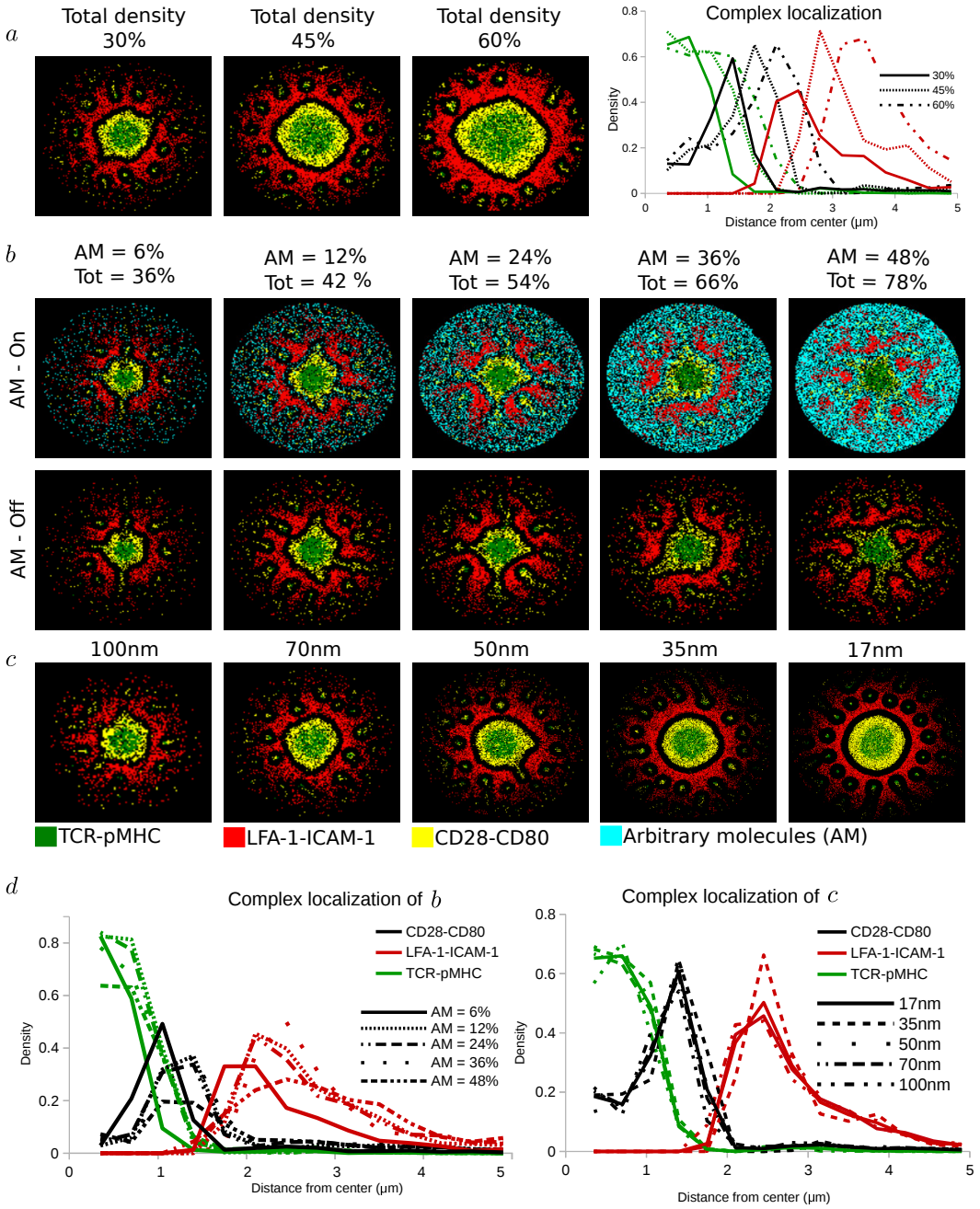

Figure 4.5: Robustness of the results to molecular crowding and resolution changes. **(a)** Increase of the total density on the lattices, Total density = 30%, 45%, 60%. **(b)** Introduction of an arbitrary molecule (AM) without ligand that only diffuses on the T cell lattice. Titration of the amount of AM from 6 to 48% density on the T cell lattice, and total density ranging from 36% to 78%. **(c)** Altering of the resolution of the simulation from $\alpha = 70\,\text{nm}$ to $\alpha = 100$, 50, 35, 17 nm, respectively. $C_{\text{TM}} = 1.00$, $C_{\text{LI}} = 0.05$ and $C_{\text{CC}} = 0.20$. **(d)** Complex localization in the different *in silico* simulations of **(b)** (left graph) and **(c)** (right graph). TCR-pMHC: green, LFA-1-ICAM-1: red, CD28-CD80: yellow, AM: cyan.

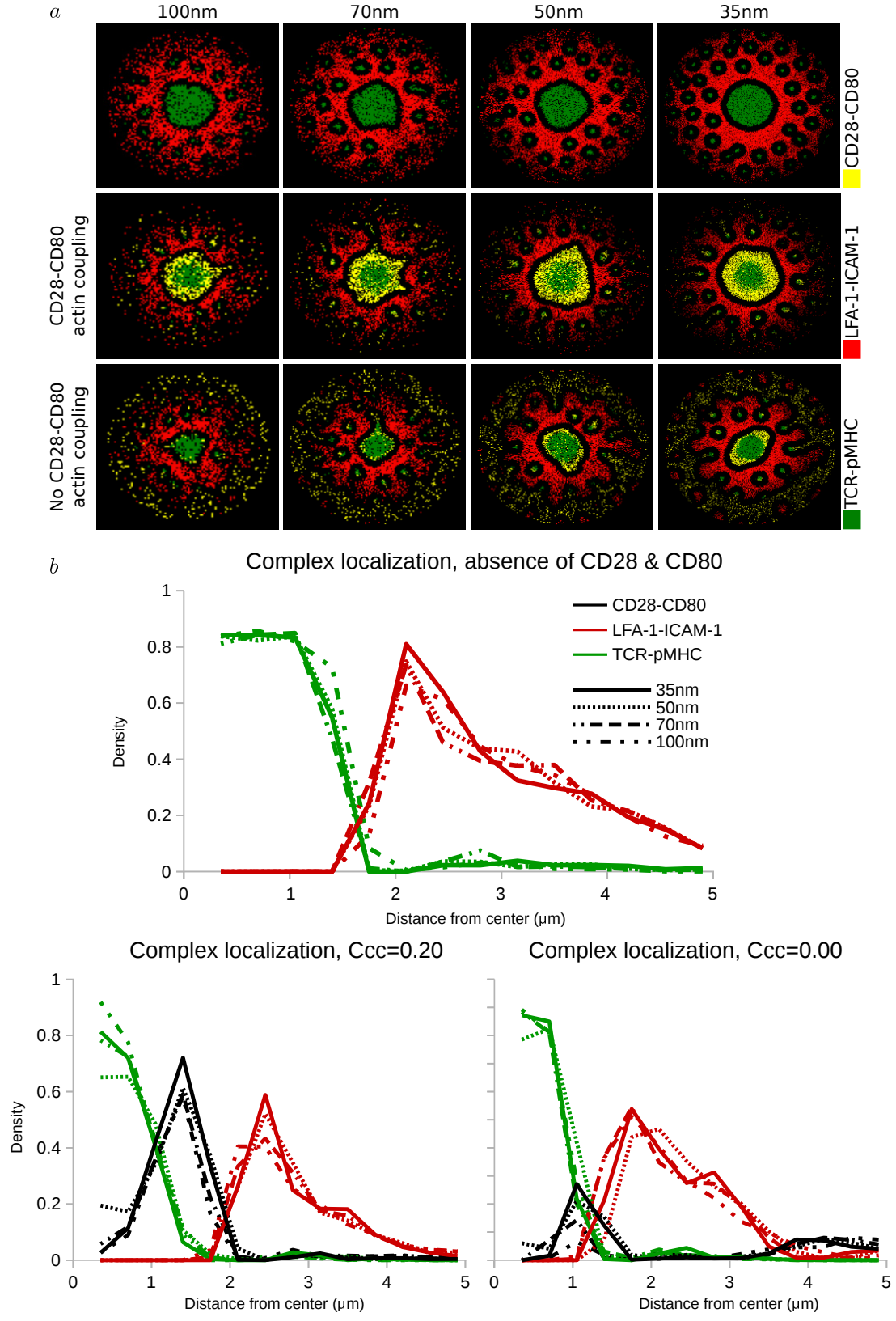

Figure 4.6: Robustness of the results to the exchange algorithm and resolution changes. **(a)** Altering of the resolution of the simulation together with the exchange algorithm from $\alpha = 70\,\text{nm}$ to $\alpha = 100$, 50, 35 nm, respectively. $C_{\text{TM}} = 1.00$, $C_{\text{LI}} = 0.05$, $C_{\text{CC}} = 0.20$ and $C_{\text{CC}} = 0.00$. **(b)** Complex localization of the different resolutions and different CD28 actin coupling, $C_{\text{CC}} = 0.00$ and $C_{\text{CC}} = 0.20$. TCR-pMHC: green, LFA-1-ICAM-1: red, CD28-CD80: yellow.

4.6 Model predictions on CD28-CD80 localization

The strength of the model becomes obvious when it comes to predictions. In Section 3.3, we showed that we can selectively inhibit molecules from F-actin interactions, and predict the cell-cell IS pattern. We showed that LFA-1-ICAM-1 coupling to F-actin in the absence of TCR-pMHC centripetal flow leads to the exclusion of the second to the outer region of the IS (Figure 3.6). Similar predictions were made with CD28, where coupling to F-actin led to the characteristic annular localization, while arrest of F-actin coupling resulted in the staggering behaviour of passive following of the TCR-pMHC molucules (Figure 4.1). What else can the model predict?

4.6.1 Geometrical repatterning of the SLB can distinguish between presence or absence of CD28-CD80 F-actin coupling

A characteristic example of experiment-model-experimental interaction came from some of the first models presented [71, 100, 174]. Mossman et al. showed that TCR signaling was affected by introducing chromium barriers on the SLB that blocked diffusion [71]. Later, Figge and Meyer-Hermann tried to distinguish between TCR centripetal flow *versus* long range attraction between TCR-pMHC complexes using barriers on the *in silico* SLB [174], suggesting that further experiments where needed in order to distinguish between the different forces. These experiments where performed by DeMonde et al., and showed that TCR-pMHC bind to F-actin and are centripetally transported [100]. Therefore, we used the same approach, trying to perform *in silico* experiments, which are easy to be experimentally investigated.

In order to find a criterion that allows to distinguish pure passive following from CD28-CD80 coupling to actin, we investigated how barriers in several shapes that block the diffusion of molecules and complexes on the SLB would influence IS formation (Figure 4.7) [71, 100]. Colocalization of CD28 and TCR was stronger when CD28 coupling to actin was allowed. Without actin coupling, most of CD28 was located in the dSMAC (Figure 4.7a). In the annular and square setting, a structural difference is found: With passive following alone, CD28 accumulates on both sides of the barriers (Figure 4.7a Annular, Square), which are low tension areas due to the accumulation of TCR complexes. Still, a substantial amount manages to reach the cSMAC but less compared to when F-actin coupling is considered. In this case, CD28 accumulates on the outside of the barriers and in the center of the IS (Figure 4.7b Annular, Square) [180]. This is a result of the continuous centripetal flow which is either interrupted by the barrier or guides CD28 into the cSMAC area. Thus, an experiment using such constraints in the SLB would reveal whether CD28 is coupled to actin or not [71, 100].

4.6.2 Existence of an optimal F-actin coupling strength

Next, we asked to which extent actin coupling controls CD28-CD80 localization and varied the coupling strength from complete absence, $C_{\mathrm{CC}} = 0.00$, to strength same as the one on TCR-pMHC complexes, $C_{\mathrm{CC}} = 1.0$ (Figure 4.8). Both, TCR and LFA-1 coupling were kept as in Figure

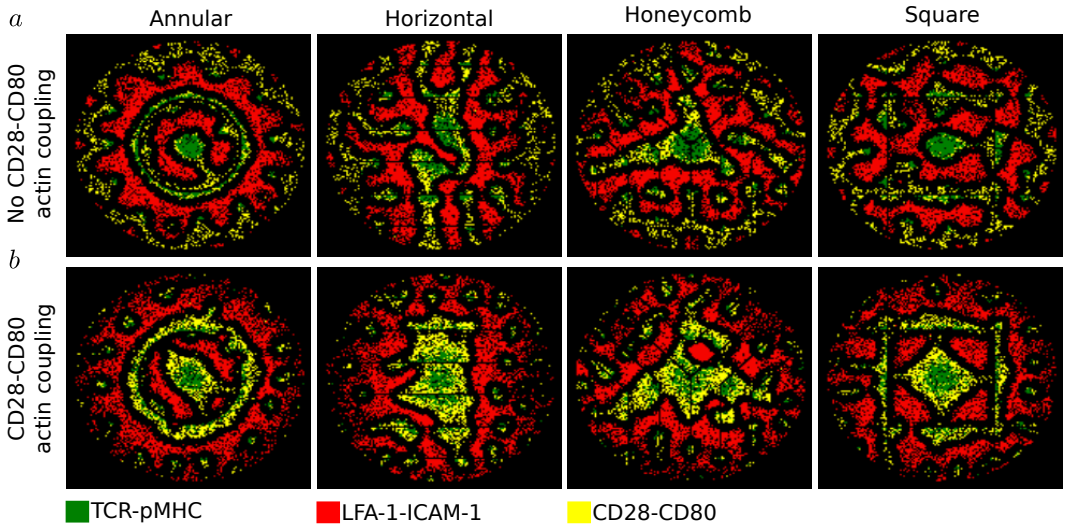

Figure 4.7: Effect of barriers added to the SLB that block the diffusion of CD28-CD80 complexes. **(a)** Absence of CD28-CD80 coupling to actin, $C_{\mathrm{CC}} = 0.00$. **(b)** Presence of CD28-CD80 coupling to actin, $C_{\mathrm{CC}} = 0.20$. TCR-pMHC: green, LFA-1-ICAM-1: red, CD28-CD80: yellow.

4.1b. The amount of CD28 in the cSMAC and in the surrounding ring increased with increasing coupling strength (Figure 4.8b), while the dSMAC population was decreased. The time of pattern formation and the coupling strength were not clearly correlated and for weak actin coupling, the ring pattern never developed, even at later simulation times. Our analysis suggested that the ring-like structure is a result of the complex combination of (i) SBS between CD28 and LFA-1 complexes, (ii) CD28 passively following TCRs, and (iii) the centripetal force on CD28 due to actin coupling. We identified an optimal coupling strength of CD28 to actin, which best reproduces the experimentally observed pattern [196]. Weaker actin coupling led to the separation of CD28 into two distinct populations in the cSMAC and the dSMAC (Figure 4.8a ($C_{\mathrm{CC}} = 0.00 - 0.10$)), in contrast to [196]. Stronger actin coupling led to an unrealistically high colocalization of CD28 and TCR complexes in the cSMAC and the microclusters (Figure 4.8a ($C_{\mathrm{CC}} = 1.00$)), and to the absence of the ring-like pattern of CD28.

This shows that the relative localization of CD28-CD80 in the cSMAC *versus* dSMAC can be tightly regulated by actin forces, and that the experimentally observed CD28 ring suggests a substantial, actin-driven motion of CD28. Note that the existence of an optimal CD28 coupling strength to actin does not rely on the LFA-1 gradient in the pSMAC and is also evident in simulations where we inhibited the LFA-1-ICAM-1 coupling to actin (Figure 4.9).

4.6.3 Could a CD28-TCR interaction alter F-actin coupling strength?

Despite of the similar sizes between TCR-pMHC and CD28-CD80 complexes, there are experimental observations showing that even a tiny difference in the range of $2 - 3\,\mathrm{nm}$, could induce steric exclusion. Therefore, SBS between CD28-CD80 and TCR-pMHC complexes was introduced to the model. Then we hypothesized that if CD28-CD80 coupling to actin is stronger than the optimal value obtained in Figure 4.8, a repulsive force from TCR-pMHC should still lead to the

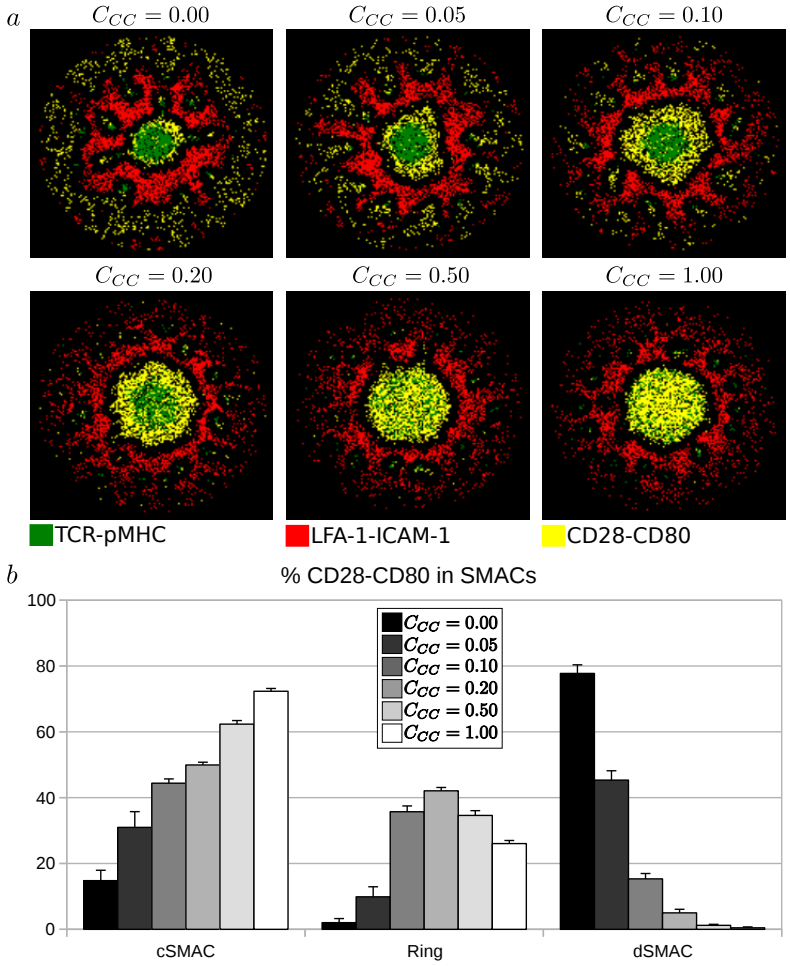

Figure 4.8: Variation of the strength of CD28 coupling to actin. **(a)** C_{CC} = 0.00, 0.05, 0.10, 0.20, 0.50 and 1.00 = C_{TM}. TCR-pMHC: green, LFA-1-ICAM-1: red, CD28-CD80: yellow. **(b)** Amount of CD28-CD80 complexes in the different regions of the IS, cSMAC, ring around cSMAC and dSMAC. Error bars represent the SD of $n = 10$ simulations.

experimentally observed annular pattern.

Therefore, we performed *in silico* experiments in the limit of strong coupling of CD28 to actin for the intermixed pattern observed in the cSMAC (Figure 4.8 ($C_{\mathrm{CC}} \geq 0.50$)). SBS in different radii, $R_{\mathrm{SBS,CC-TM}} = 0.14 - 021\,\mu$m, and strengths, $W_{\mathrm{SBS,CC-TM}} \in (-1.0, -0.2)$, was then applied between TCR-pMHC and CD28-CD80 complexes. Initially, the effect of SBS was investigated for the case of optimal CD28-F-actin coupling strength (Figure 4.10). SBS was unable to affect the ring structure in the IS with the optimal CD28 coupling to actin (Figure 4.10c). For higher CD28 F-actin coupling strengths, $C_{\mathrm{CC}} \geq 0.50$, the intermixed cSMAC pattern could not be resolved. SBS led to TCR clustering in, and even exclusion from the cSMAC (Figure 4.10b, c). Thus, the model predicts that the optimal CD28-CD80 coupling to actin is weaker than for TCR-pMHC. Furthermore, the actin force acts as the regulator of CD28-CD80 distal to central SMAC ratio (Figure 4.8).

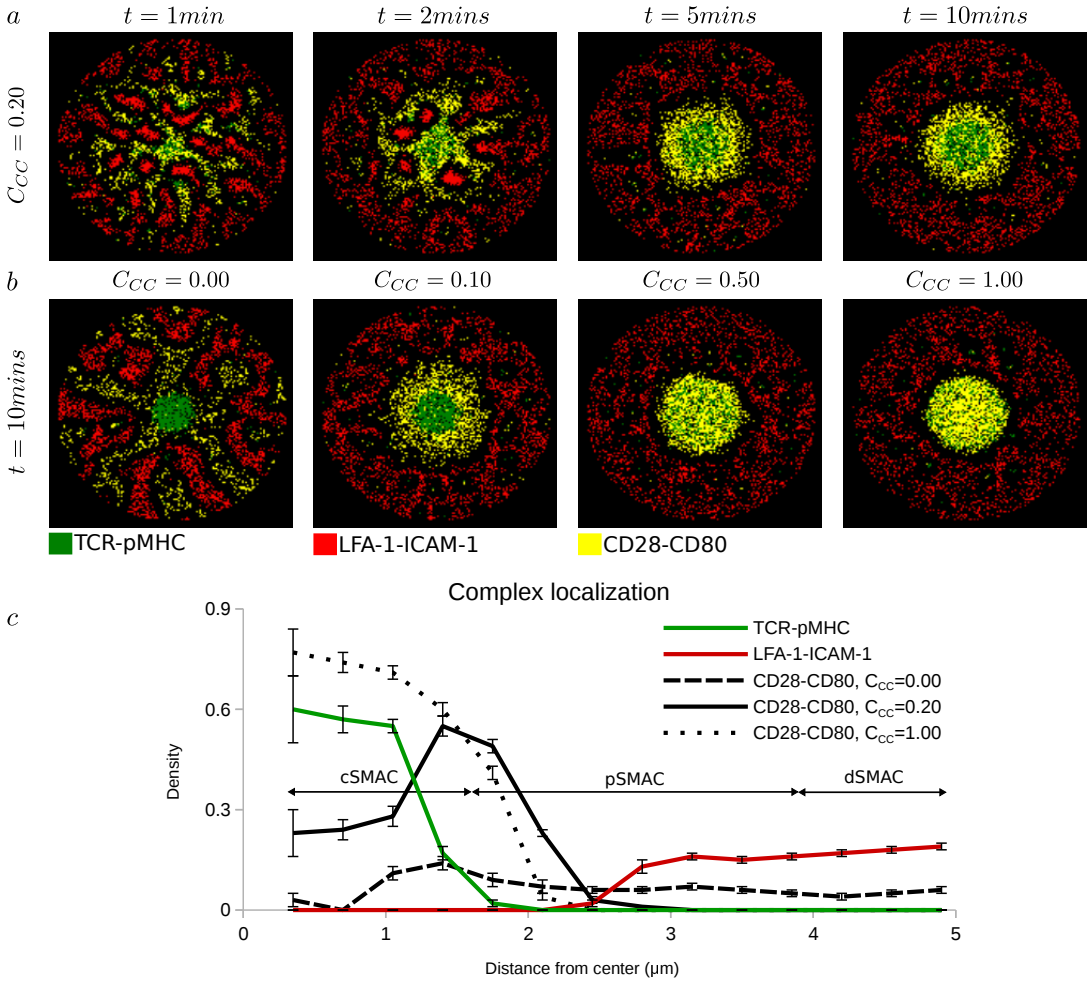

Figure 4.9: Blocking of LFA-1 actin coupling. **(a)** Step-by-step IS formation at 1, 2, 5 and 10 minutes, respectively, with CD28-CD80 coupling to actin, $C_{\mathrm{CC}} = 0.20$. **(b)** CD28 binding to actin with different strengths, $C_{\mathrm{CC}} = 0.00, 0.10, 0.50, = 1.00 = C_{\mathrm{TM}}$, respectively. TCR-pMHC: green, LFA-1-ICAM-1: red, CD28-CD80: yellow. **(c)** Density of complexes as a function of the distance from the center at 10 minutes. Error bars represent the SD of $n = 10$ simulations.

4.7 Conclusions

The working model was complemented with CD28 and CD80 molecules on the T cell and SLB lattice respectively. The localization of CD28-CD80 complexes was achieved with a combination of three mechanisms. First, SBS with LFA-1 leading to their segregation and the colocalization of CD28 and TCR complexes in the microclusters at the initial stages of IS formation. Second, CD28-CD80 pairs *passively following* the TCR-pMHC movement toward the cSMAC, a behaviour not appreciated before, and third, CD28-CD80 actively moving toward the center due to interaction with the F-actin network, modeled as a centrally directed force.

The robustness of the mechanisms was tested in different settings, such as increased concentration of all molecules in the IS region, introduction of freely diffusing molecules and, finally, different resolutions of the lattices.

Finally, the predictive power of the model was then presented. *In silico* experiments with barriers that block the diffusion on the SLB, similar to experiments performed by [71,100], showed

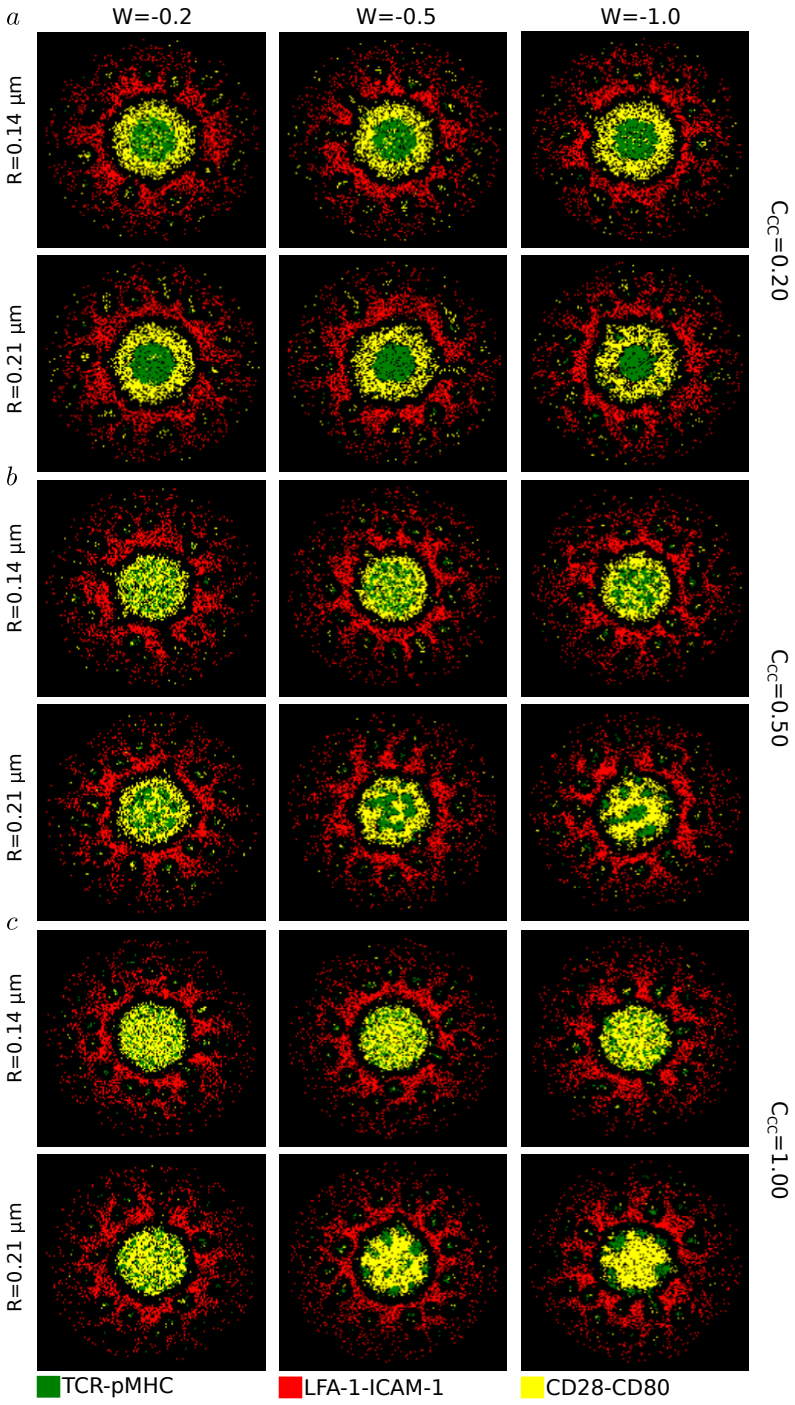

Figure 4.10: SBS between TCR-pMHC and CD28-CD80. **(a)** $C_{\mathrm{CC}} = 0.20$, **(b)** $C_{\mathrm{CC}} = 0.50$ and **(c)** $C_{\mathrm{CC}} = 1.00$, for different radii of interaction, $R = 0.14 - 0.21\,\mu$m, as well as different strengths of the repulsive forces, $W = (-1.0, -0.2)$. $C_{\mathrm{LI}} = 0.05$. TCR-pMHC: green, LFA-1-ICAM-1: red, CD28-CD80: yellow.

that we can distinguish between CD28 complexes coupling to actin or not, just by observing the emerging IS patterns. Furthermore, the optimal CD28-actin interaction strength was studied, which is impossible with currently published experimental techniques.

The importance of CD28-CD80 in T cell activation drove the presented study of the mechanisms of their localization. The model not only managed to recapitulate the experimentally observed patterns with simple mechanisms, but also shed light onto unknown behaviours of these molecules.

In the following chapter, another costimulatory molecule, namely CD2, with a completely different localization is discussed.

Chapter 5

CD2 *corolla* pattern formation

5.1 Introduction

As was discussed so far, TCR signaling needs the costimulatory support of other molecules, such as CD2 [212–215] and the previously discussed CD28 [196, 199, 200]. These two costimulatory molecules have very similar size, with CD2-CD58 being around $\simeq 13\,\text{nm}$ [214] while CD28-CD80 being around $\simeq 11\,\text{nm}$, and therefore I would expect them to locate at the same regions of the IS, around the cSMAC as I was discussing in the previous chapter. Interestingly though, they reside in completely different regions of the IS, with CD2 forming a flower petal-like pattern in the distal SMAC (dSMAC), called *corolla* pattern, according to unpublished data by [216].

CD2 interacts with CD58 in humans and CD48 in rodents. Early studies measured the affinity between CD2 and its ligands in different species, and observed that the interacting molecules affect the adhesion between the two interacting cells [212, 217–221]. CD2 is considered to be one of the most important costimulatory molecules. CD2-CD58 complex formation supports T cell polarization [222]: CD2 is redistributed in the uropod and its compartmentalization with the TCR prearranges the cellular activation machinery in a kind of *presynapse*. Espagnolle et al [223] found that CD2-CD58 augments and sustains antigen-induced Ca^{2+} increase in interacting cells, and that impeding interactions between CD2 and CD58 leads to impaired recruitment of PLCγ1. Interestingly, CD2 and TCR synergize in order to activate PLCγ1 [223]. Therefore, the unique spatial *corolla* pattern of CD2 in the synapse seems very important for the regulation of TCR signaling in space and consequently the function of T cells.

In this chapter I will try to shed light into the mechanisms leading to the staggering CD2 localization. I will further investigate how a synapse with both the costimulatory molecules would develop based on experimental observations [216].

5.2 CD2-CD58 passive followers and exclusion from the IS

In order to understand the mechanisms driving the spatial organization of CD2-CD58 in the IS, the model was put into test one more time [180]. In this case, I took into account TCR, LFA-1 and CD2 on the T cell and their respective ligands, pMHC, ICAM-1 and CD58 molecules on the supported lipid bilayer (SLB) lattice, respectively. Steric exclusion between TCR-pMHC and LFA-1-ICAM-1 complexes due to size-based segregation (SBS) as well as F-actin driven centripetal transport of complexes - which leads to the accumulation of TCR-pMHC in the central area of the IS [104, 105, 180], and also to the development of an LFA-1-ICAM-1 gradient toward the center of the IS in the pSMAC - are considered the standard mechanisms [116, 180].

Next, CD2 and CD58 molecules were introduced, on the T cell and SLB lattice, respectively. CD2 and CD58 bind and unbind according to association and dissociation constants taken from literature [212, 217–221]. The size of a formed CD2-CD58 complex is around 13 nm [214, 224], and very similar to that of a TCR-pMHC complex. Therefore, the model was complemented with SBS between CD2-CD58 and LFA-1-ICAM-1, but no interaction between CD2-CD58 and TCR-pMHC was introduced.

The *in silico* experiments showed that CD2-CD58 and TCR-pMHC complexes initially colocalize in the microclusters (Figure 5.1). Interestingly, similar to what I observed for CD28 (Figure 4.1a), a small population of CD2-CD58 complexes passively followed the TCR-pMHC movement toward the center of the IS (Figure 5.1a). This population is called *passive followers*. Further, the emergence of the LFA-1-ICAM-1 gradient in the pSMAC, excluded the rest of the CD2-CD58 complexes to the outer region of the IS (dSMAC). In these *in silico* experiments, the separation of CD2-CD58 complexes into two distinct populations was observed. The *passive followers* resided in an annular structure around the cSMAC, while the excluded population formed a ring in the dSMAC region.

From Figure 5.1b, it was obvious that the excluded CD2-CD58 population is larger than the passive followers. Further, observation of the localization dynamics (Figure 5.1c) showed that initially (1-2 minutes) CD2-CD58 are dispersed throughout the forming IS, whereas at the later stages (10 minutes) of IS formation, CD2 is separated into two populations. The initial *in silico* experiments though, could not reproduce the reported flower like *corolla* pattern [216]. Thus, additional simulations were necessary in order to reproduce the observed pattern.

5.3 CD2 titration leads to a solid annular dSMAC

Experimental observations suggested that one factor behind the *corolla* pattern appearance could be the expression level of CD2 on the T cell surface [216], since for example memory T cells appear to express more CD2 than naive T cells [225]. As a result, I decided to perform *in silico* experiments where I titrated the amount of CD2.

The question I then asked, was if the amount of CD2 in the IS region could lead to the characteristic pattern, since there are observations that high expression of CD2 in T cells alters their

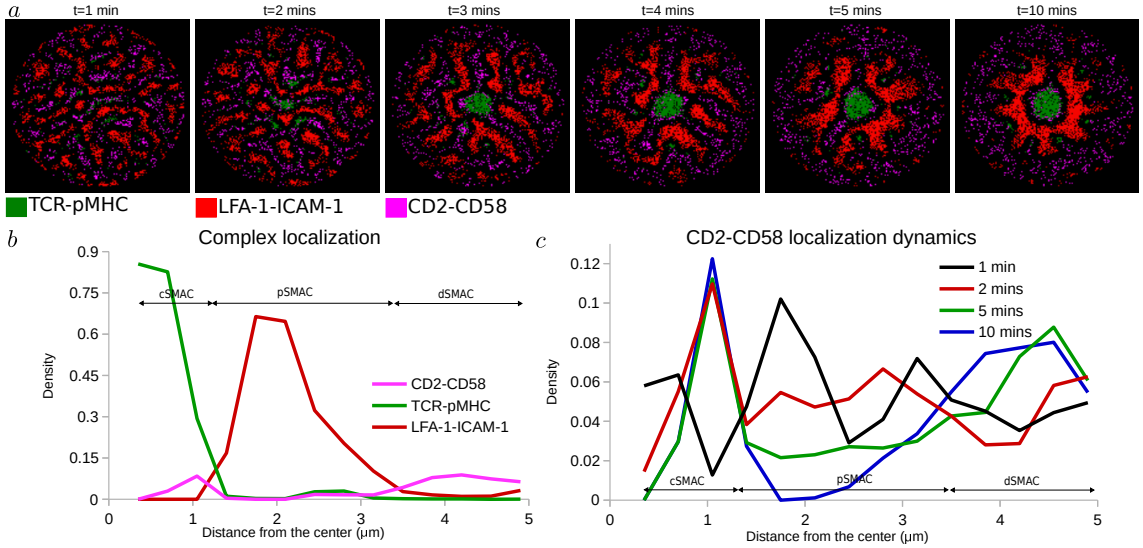

Figure 5.1: CD2-CD58 is separated into two populations. **(a)** IS Formation dynamics between 1 and 10 minutes. **(b)** Radial density profiles of all the complexes (TCR-pMHC, LFA-1-ICAM-1, CD2-CD58) along the distance from the center at 10 minutes. **(c)** Dynamics of the radial density profiles of CD2-CD58 complexes along the distance from the center at 1, 2, 5 and 10 minutes. TCR-pMHC: green, LFA-1-ICAM-1: red, CD2-CD58: magenta.

localization [216]. The amount of CD58 in the SLB lattice was adequate, 100 CD58 molecules/μm^2, so that it didn't act as a limiting factor for CD2 binding. I then studied the localization of CD2-CD58, starting with a population of as low as 1 and reaching up to 73 CD2 molecules/μm^2, where for the sake of simplicity only concentrations between 9 and 55 CD2 molecules/μm^2 are shown.

As the initial CD2 population increased, the CD2-CD58 ring in the dSMAC became more prominent (Figure 5.2a, b). Further, the increased CD2 amount led to increased population size in the dSMAC (Figure 5.2b). Interestingly, as a result of steric exclusion between CD2-CD58 and LFA-1-ICAM-1, the *passive follower* population in the ring around the cSMAC saturated at a maximum capacity (Figure 5.2b). Once again though, no clustering in the dSMAC ring appeared. The absence of the CD2-CD58 *corolla* pattern led to investigating additional mechanisms, which could lead to the clustering of CD2 in the dSMAC.

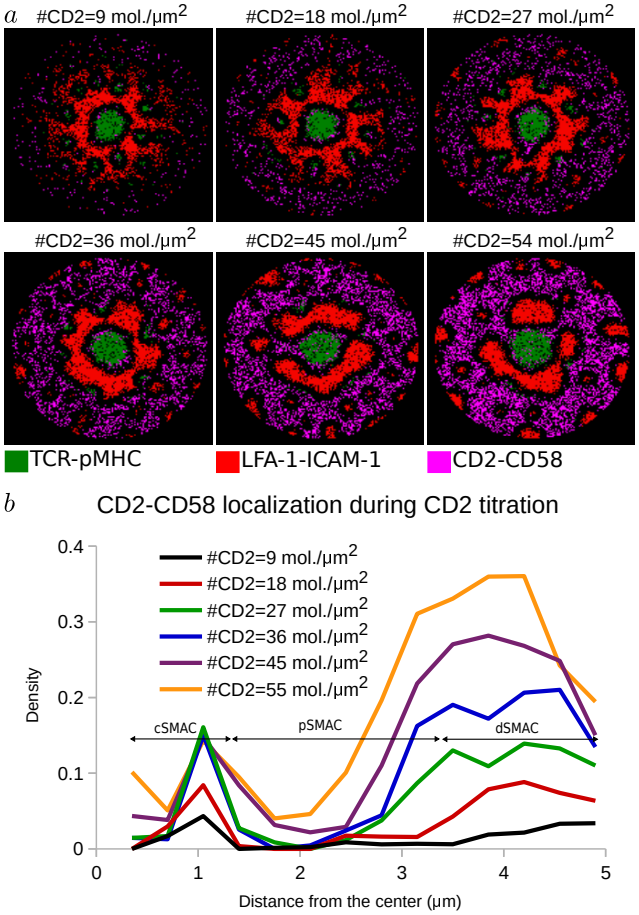

Figure 5.2: CD2 initial amount titration with constant CD58 amount. **(a)** Titration of the initial CD2 amount. **(b)** Radial density profiles of CD2-CD58 complexes along the distance from the center for different initial CD2 amounts. TCR-pMHC: green, LFA-1-ICAM-1: red, CD2-CD58: magenta.

5.4 CD2-CD58 self attraction results in the *corolla* pattern

Despite the exclusion of the majority of CD2-CD58 from the IS, the *corolla* pattern failed to form. In an attempt to achieve this characteristic pattern, an attractive interaction between CD2-CD58 complexes was included in the model. This interaction has a strength $W_{\mathrm{Att,\,Self}} > 0$ and the complexes interact within a radius $R_{\mathrm{Att,\,Self}}$. The radius defines the number of interacting neighbors, here shown between 3 and 6 neighbors, $R_{\mathrm{Att,\,Self}} = 0.21 - 0.42\,\mu$m.

As the initial CD2 amount increased, together with increased radius of interaction, CD2-CD58 clustering appeared in the dSMAC, at least after considering more than four interacting neighbors, $R_{\mathrm{Att,\,Self}} \geq 0.28\,\mu$m (Figure 5.3). This added mechanism resulted in the desired *corolla* pattern [216]. The model not only reproduced the experimental results, but close observation of the formation dynamics of Figure 5.5 showed the same behaviour of CD2-CD58 movement in the forming IS. Initially, CD2-CD58 colocalized with TCR-pMHC in microclusters and moved inwards as passive followers (Figure 5.1 & CD2localizationTitration, 1-2 minutes). Between 2 and 5 minutes, they localized in the pSMAC while being excluded toward the dSMAC from the LFA-1-ICAM-1 gradient (Figure 5.1, 5.2 & 5.5). Finally, the CD2-CD58 clusters formed the *corolla* pattern, which

remained stable after 10 minutes (Figure 5.5). Interestingly, examination between 10 and 30 minutes showed that CD2 clusters around the cSMAC eventually travelled toward the dSMAC *corolla*. The clustering was lost at the highest CD2 concentrations, > 45 CD2 molecules/μm^2, suggesting that space is also an important factor.

I then went back to the experiments and investigated if indeed the concentration of CD2 on the T cell and thereby within the contact interface affects the *corolla* pattern. Interestingly, for very low amounts of expressed CD2, up to 4 CD2 molecules/μm^2, the CD2-CD58 population is split in $\approx 50\%$ passive followers and $\approx 50\%$ excluded into the dSMAC (Figure 5.4). At concentration greater than 7 CD2 molecules/μm^2, I observed a clear cut change in the localization of CD2-CD58 complexes. Around 90% of all the CD2-CD58 complexes are excluded to the dSMAC where they form the *corolla* pattern, whereas only around 10% remains trapped around the cSMAC (Figure 5.4). This observation was in accordance with experimental findings [216], and suggested that the expression level of CD2 can lead to the *corolla* pattern.

Eventually, I investigated how the strength of the attractive interaction affects the clustering, starting from very low strength, $W_{\mathrm{Att,\,Self}} = 0.2$ and went up to $W_{\mathrm{Att,\,Self}} = 1.0$. On the one hand, in the cases of $R_{\mathrm{Att,\,Self}} = 0.21{-}0.28\,\mu$m, the higher strength resulted in more prominent CD2-CD58 clusters. On the other hand, radii bigger than $R_{\mathrm{Att,\,Self}} > 0.35\,\mu$m, already managed to clearly cluster CD2-CD58, and therefore the increased strength did not have any obvious effect (Figure fig:CD2corollaAttraction), while in some cases, higher attractive strength resulted in reduced CD2-CD58 amount around the cSMAC (Figure 5.6b, c, d & e).

5.5 CD2 presence in the synapse alters CD28 localization

So far I showed that two very similar in size costimulatory molecules, CD2 and CD28, localized very differently in the mature synapse (Figures 4.1 & 5.3). But in reality, these two might coexist in a forming IS. It is experimentally shown that when both CD2 and CD28 were present in the synapse and interacted with their respective ligands, CD28 complexes relocated in the *corolla* [216]! Hence I investigated how the localization of these two costimulatory molecules is affected when they coexist and what are the possible mechanisms that could lead to the eventual exclusion of CD28-CD80 toward the *corolla*.

Initially, both CD2 and CD28, as well as their ligands CD58 and CD80 respectively, where included in the model. As shown before, CD28-CD80 localize in an annular pattern around the cSMAC (Figure 5.7a). The introduction of CD2 and the consequent formation of CD2-CD58 complexes that moved to form the *corolla* pattern did not affect the localization of CD28 significantly. As seen in Figure 5.7b, there was a minor reduction in the CD28 population around the cSMAC region. This population then resided together with CD2-CD58 in the *corolla*. A possible explanation is that the appearance of low tension regions in and around the *corolla* could help CD28 passive followers reside in these regions instead of following the TCR centripetal transport. However, the experimentally observed transport of the majority CD28-CD80 to the *corolla* did not appear.

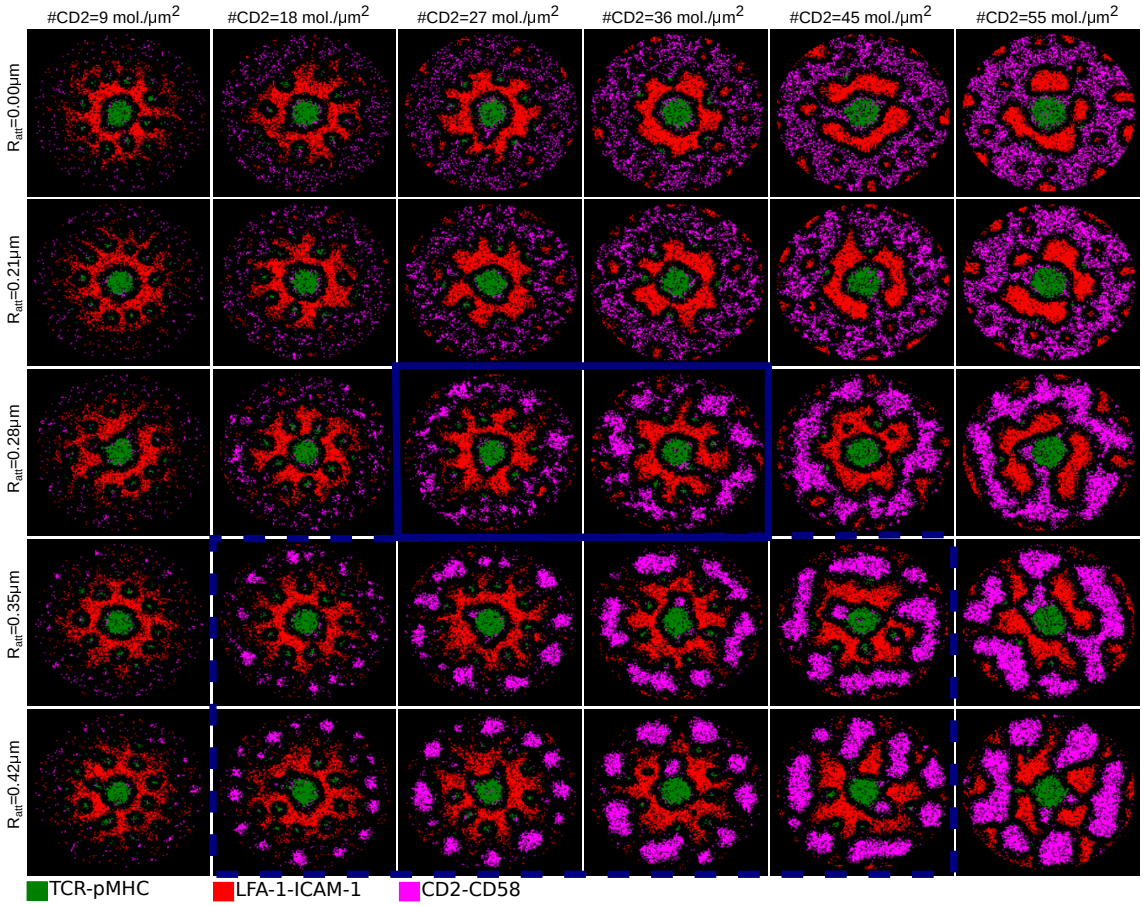

Figure 5.3: Appearance of the CD2-CD58 *corolla* pattern. **(Rows)** Different radii of attractive interaction, $R_{\mathrm{Att,\,Self}}$, between CD2-CD58 complexes. **(Columns)** Different initial concentration of CD2 molecules. **(Blue rectangle)** First appearance of the CD2-CD58 *corolla* pattern. **(Blue dashed rectangle)** Presence of the CD2-CD28 *corolla* pattern. TCR-pMHC: green, LFA-1-ICAM-1: red, CD2-CD58: magenta.

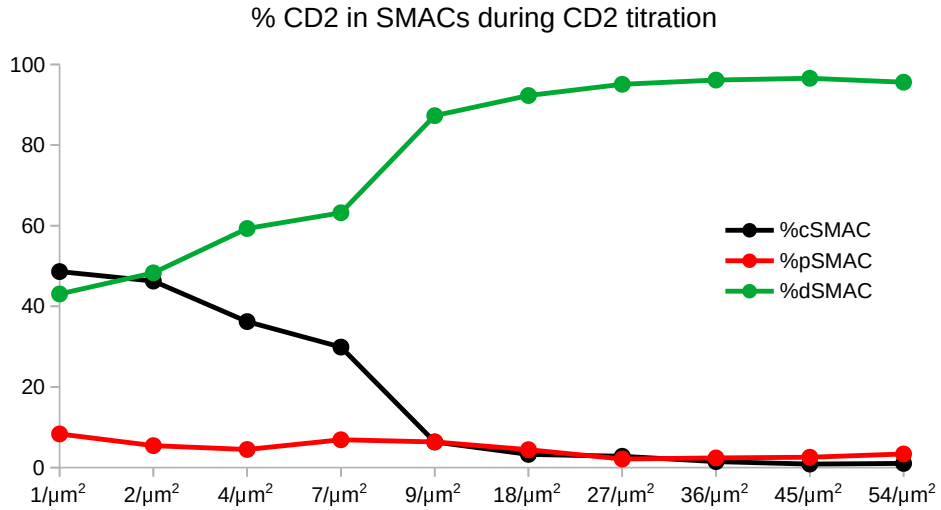

Figure 5.4: Amount of CD2-CD58 during titration of initial CD2 concentration in the three different regions of the IS, central, peripheral and distal SMACs.

The similar size as well as the similar function of the two costimulatory molecules might suggest that some type of interaction keeps them together. One such interaction could be an attractive

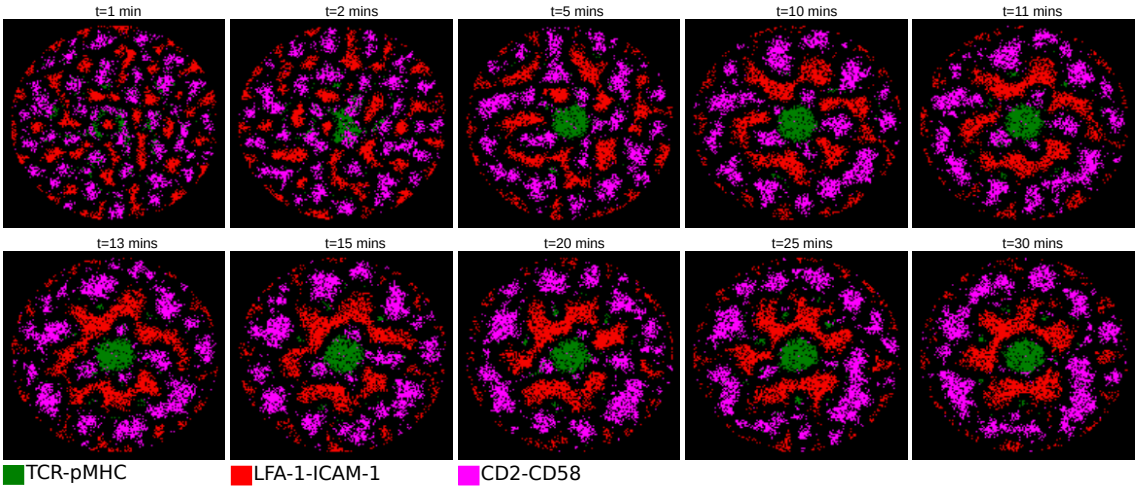

Figure 5.5: Dynamics of the CD2-CD58 *corolla* pattern formation (t = 1-30 minutes). TCR-pMHC: green, LFA-1-ICAM-1: red, CD2-CD58: magenta.

force between CD2 and CD28 complexes. Thus, I introduced an attractive force between the two kinds of complexes. The interaction radius was defined by $R_{\mathrm{CD2CD28}} = 0.14 - 0.35\,\mu\mathrm{m}$) and was weighted with $W_{\mathrm{CD2CD28}} = 1.0$. A weak attraction then led to higher exclusion of CD28 toward the corolla, $R_{\mathrm{CD2CD28}} = 0.14\,\mu\mathrm{m}$, whereas an even stronger interaction, $R_{\mathrm{CD2CD28}} \geq 0.21\,\mu\mathrm{m}$, led to more than 90% of CD28-CD80 in the corolla (Figure 5.7a, b).

In order to visualize the findings of Figure 5.7, I used the colocalization of the two kinds of complexes. When at least two complexes of both CD2 and CD28 pairs are within a distance of 210 nm, the *in silico* experiments show that there is colocalization. As can be seen from Figure 5.8, the increasing attraction radius, R_{CD2CD28}, results in higher colocalization in the outer IS region, where the CD2 *corolla* pattern is present. This result made clear that indeed an attractive interaction between the two kinds of complexes, CD2-CD58 and CD28-CD80, can relocate the second, and that the result is a high colocalization in the dSMAC. The reason for the relocation of CD28-CD80 could be to support signaling at the periphery, where TCR microclusters form continuously [108, 109, 112, 201, 216, 226, 227], but this has to be experimentally tested.

Since the experimentally discussed pattern emerged, I then investigated whether the amount of CD2 on the T cell surface played a role in the emergence of this pattern. The initial amount of CD2 was titrated between 1 and 54 molecules/$\mu\mathrm{m}^2$, together with the variation of the attraction range, R_{CD2CD28}. In Figure 5.9a (top and bottom graphs), the mean localization of CD2 is shown in grey and the deviation from the mean in black. Interestingly, at very small CD2 concentrations, $1 - 4$ molecules/$\mu\mathrm{m}^2$, the majority of CD28 resided in the cSMAC region despite the attractive interaction. Moreover, at these low CD2 concentrations, CD2 was not managing to form the *corolla*, but instead was pulled toward the annular CD28 pattern (Figure 5.9b). Irrespective of that, and since these very low CD2 concentrations are unrealistic, the attraction strength between CD2 and CD28 and not the CD2 concentration appeared as the driving factor behind CD28's displacement in the *corolla*.

Finally, to further highlight the importance of the LFA-1 gradient, and the strength of the

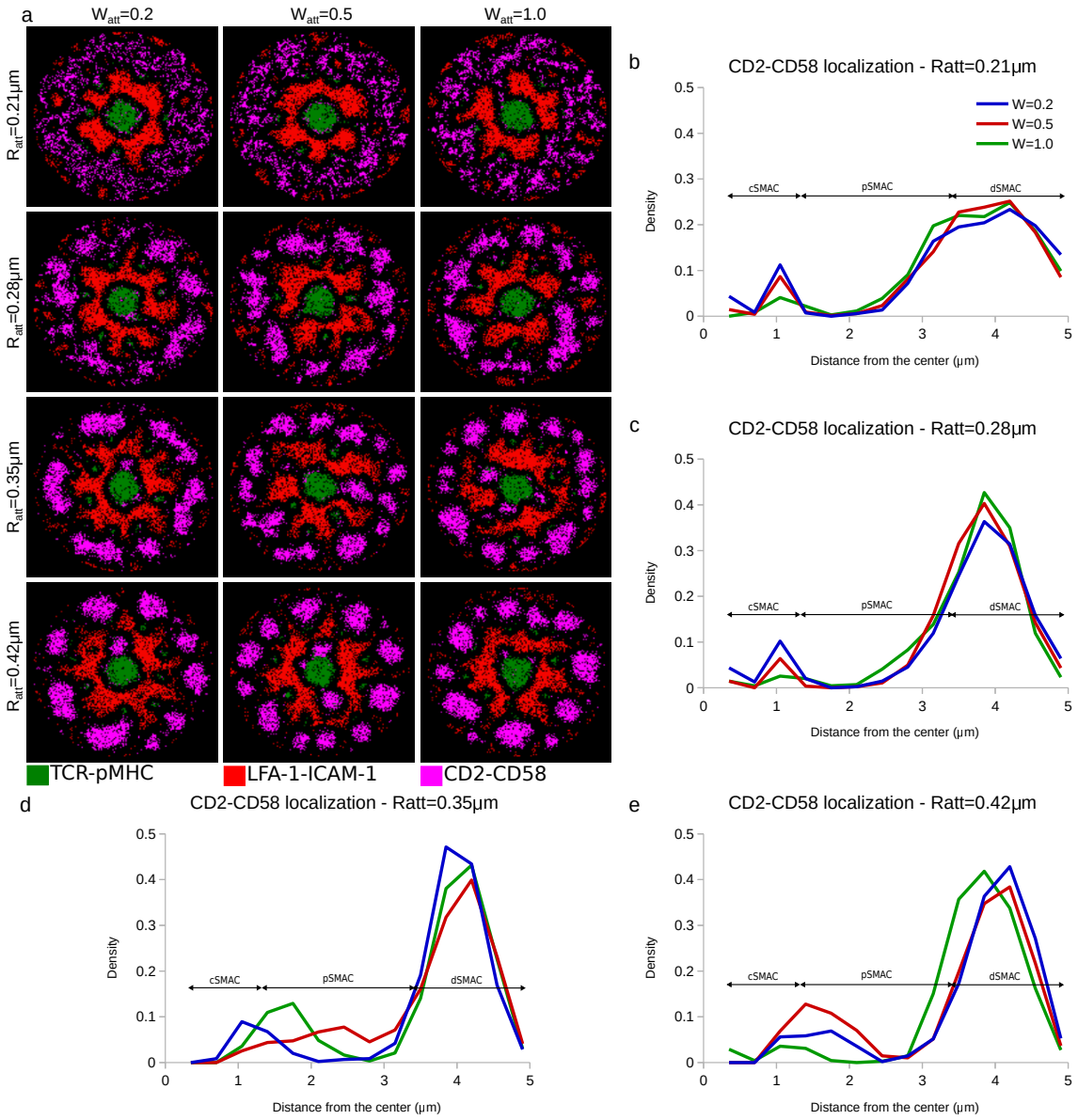

Figure 5.6: Alterations in strength, $W_{\mathrm{Att,\,Self}}$, and radii, $R_{\mathrm{Att,\,Self}}$, of the attractive force, with initial CD2 concentration $CD2 = 36$ molecules/μm^2. **(a Rows)** Different radii of attractive interaction, $R_{\mathrm{Att,\,Self}}$, between CD2-CD58 complexes. **(a Columns)** Different strengths of attractive interaction, $W_{\mathrm{Att,\,Self}}$, between CD2-CD58 complexes. **(b, c, d & e)** Radial density profiles of CD2-CD58 complexes along the distance from the center of each row of (a). TCR-pMHC: green, LFA-1-ICAM-1: red, CD2-CD58: magenta.

model, I performed *in silico* simulations for different coupling strengths of LFA-1-ICAM-1 to the centrally directed flow of F-actin. As was mentioned so far, the emergence of the LFA-1 gradient acts as an exclusion mechanism both for free molecules (Figure 3.7) as well as for complexes (Figures 4.1, 5.3). Therefore, as seen in Figure 5.10a, absence of LFA-1 centripetal transport, $C_{\mathrm{LI}} = 0.00$, does not result in the CD2 *corolla* but rather in clusters around the cSMAC of CD2 and CD28 complexes. Gradually increasing the strength of the LFA-1 coupling to F-actin resulted in incomplete exclusion of the CD2 clusters, $C_{\mathrm{LI}} = 0.03$, whereas very strong LFA-1 centripetal transport led to significant exclusion of CD2 and CD28 complexes. Additionally, the stronger the coupling of LFA-1 to F-actin, the denser the LFA-1 ring is in the pSMAC (Figure 5.10a). Moreover,

the strength of CD2-CD28 attraction again resulted in CD28 displacement from the cSMAC region toward the dSMAC *corolla*, where around 90% of all CD28-CD80 complexes accumulated (Figure 5.10b).

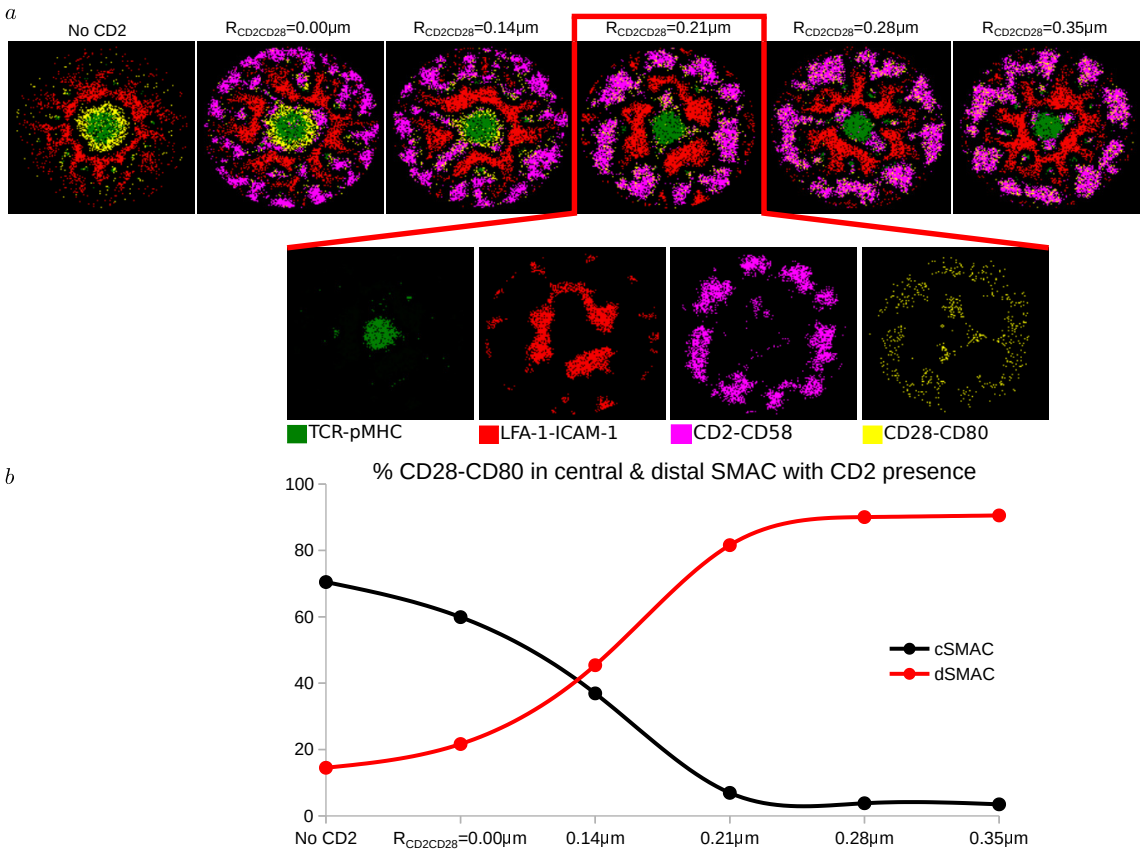

Figure 5.7: CD28 relocates to the CD2 *corolla* provided there is a weak attraction between CD2 and CD28 complexes. **(a)** IS pattern formation, within various attraction radii, R_{CD2CD28}. **(b)** Amount of CD28 in the central and distal SMAC for the various attraction ranges, R_{CD2CD28}. TCR-pMHC: green, LFA-1-ICAM-1: red, CD2-CD58: magenta, CD28-CD80: yellow.

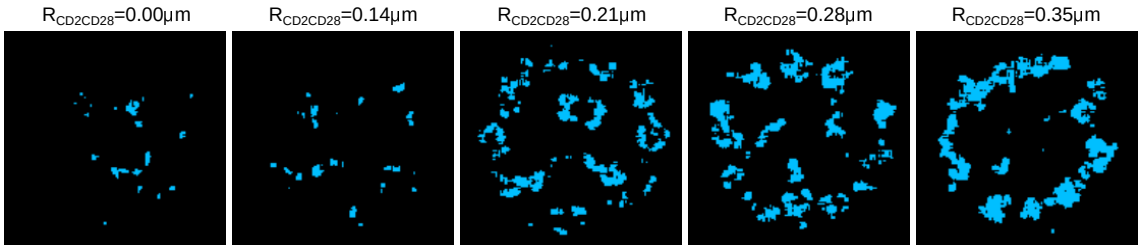

Figure 5.8: Colocalization of CD2-CD58 and CD28-CD80 complexes for different attraction radii between them. Colocalization: cyan

5.6 Conclusions

The localization mechanisms of the costimulatory molecule CD2 was subject of investigation in this chapter. The model showed that the *corolla* pattern requires the exclusion of CD2 by LFA-1 complexes due to SBS and an additional attractive force between CD2-CD58 complexes. The amount

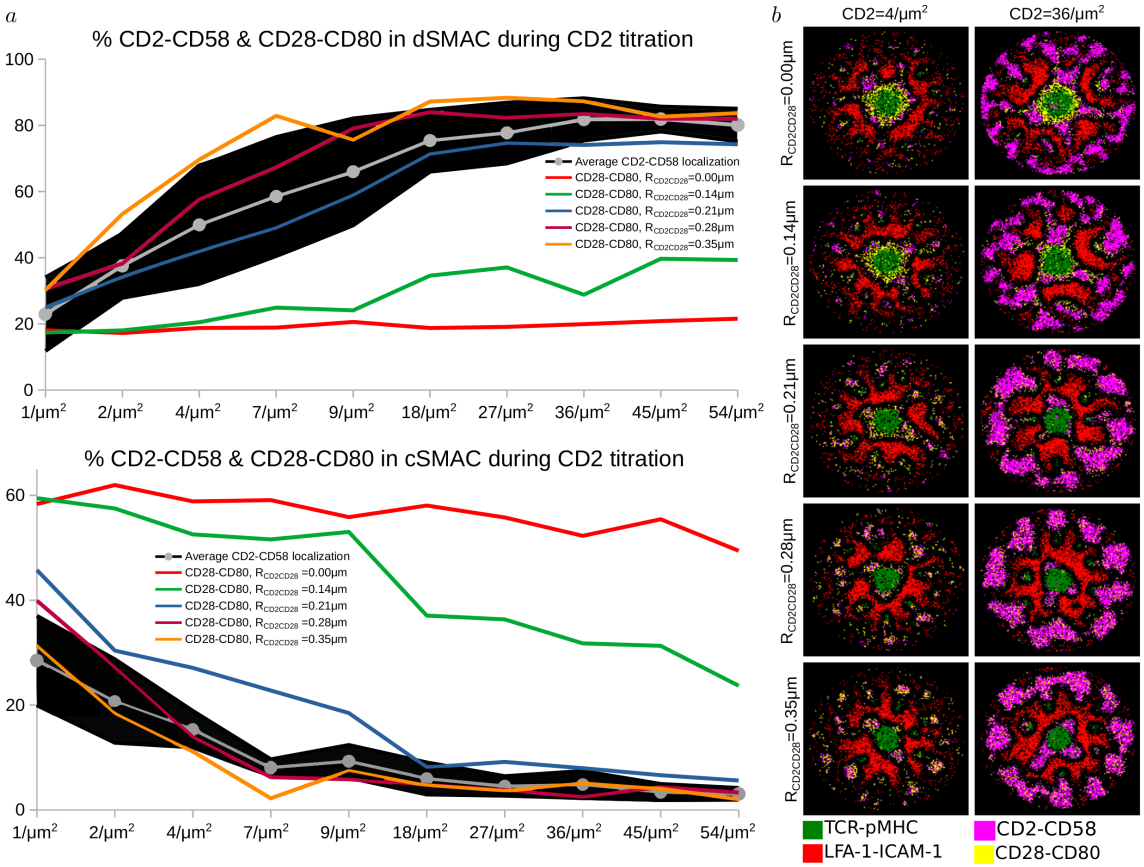

Figure 5.9: CD2 and CD28 localization during CD2 titration and CD2-CD28 attractive force range variation, R_{CD2CD28}. **(a)** Average CD2 population size and CD28 localization for different attractive force strength, in distal (top) and central (bottom) SMAC. **(b)** IS pattern formation for different R_{CD2CD28} for low (left) and high (right) CD2 concentrations. TCR-pMHC: green, LFA-1-ICAM-1: red, CD2-CD58: magenta, CD28-CD80: yellow.

of CD2 showed a switch-like behaviour, with low concentrations resulting in central localization, whereas an increased amount showed that around 90% of the CD2 molecules present in the IS went to the dSMAC where they formed the *corolla* pattern.

The experimental observation of CD28-CD80 relocation to the corolla in presence of CD2-CD58 was recapitulated by the introduction of an attractive force between CD2-CD58 and CD28-CD80 complexes. Finally, the importance of the LFA-1 gradient was shown once again. In absence of the LFA-1 gradient, the *corolla* pattern was not formed, while the stronger the centripetal LFA-1 force, the higher the exclusion of CD2 from the central IS region.

In the next chapter, the model will be utilized in order to investigate the proposed TCR-pMHC affinity modulation during pMHC titration and discuss possible mechanisms that result in this TCR behaviour.

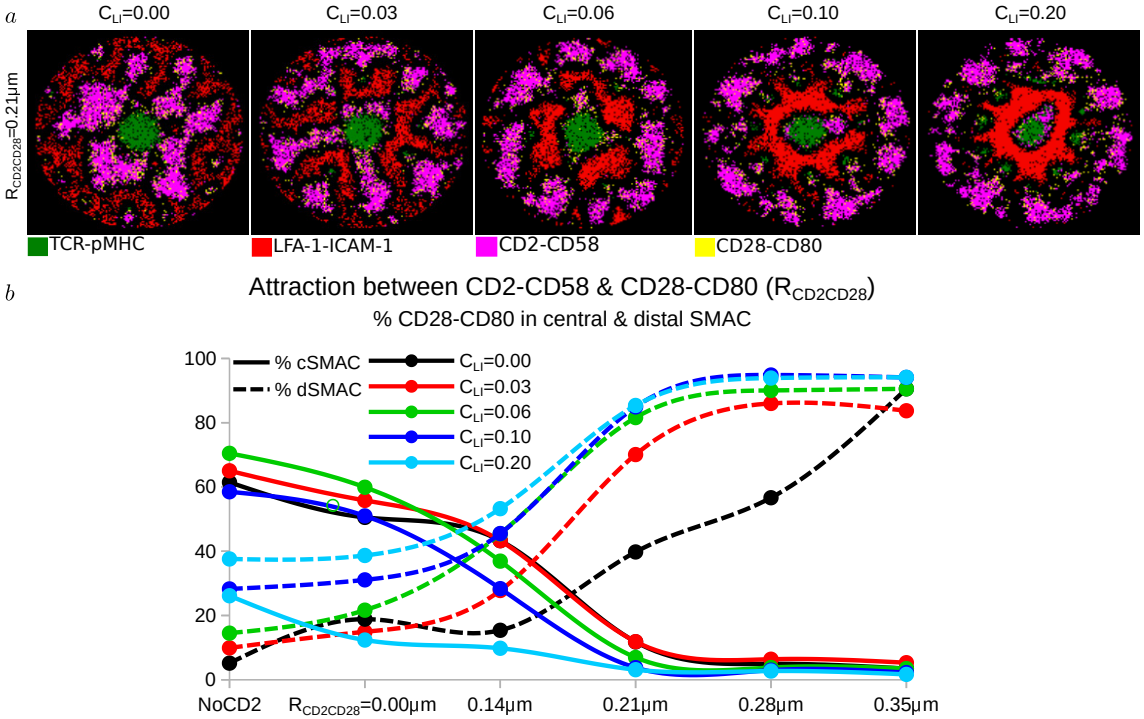

Figure 5.10: Alterations in strength of LFA-1 coupling to the F-actin flow, C_{LI}. **(a)** IS pattern formation for different C_{LI}. **(b)** Amount of CD28-CD80 complexes in the central and distal SMAC during LFA-1-F-actin coupling strength variation. TCR-pMHC: green, LFA-1-ICAM-1: red, CD2-CD58: magenta, CD28-CD80: yellow.

Chapter 6

T cell receptor cooperativity

6.1 Introduction

TCR binding to the presented pMHC is shown to be a low affinity interaction [140, 228, 229], although T cells are so sensitive to this interaction that even a single pMHC can trigger cytokine production [230]. Stone et al. also showed that TCRs can discriminate between different pMHC molecules based on their association rates, k_{on}, during sampling of the APC surface [231]. Furthermore, recent experimental evidence suggested that the observed TCR affinity toward antigen is actively modulated during the early steps of TCR signaling, i.e. TCR-pMHC microcluster formation [183, 232].

It is observed that the avidity of microclusters is dependent on pMHC density, and that at low doses, an increase of pMHC density increases the avidity of the interaction. This was interpreted as cooperativity between TCRs to increase their affinity toward pMHC, during the accumulation of TCR-pMHC complexes [183]. This behaviour was shown to operate on a narrow time window, where the initial TCR-pMHC ligations favor further binding events [232]. Pielak et al. detected that the dwell time, τ_{off}, and consequently the dissociation rate, k_{off}, of individual TCR-pMHC complexes remains unchanged. This led to the assumption of active modulation of the association rate, k_{on}. This could be a result of a pMHC seeing multiple TCRs, since the latter have been observed to be pre-organized in nanoclusters [94, 142, 233–235]. It was also shown that TCR-pMHC accumulation in the central supramolecular activation cluster (cSMAC) at the later stages of IS formation results in signal termination [108], suggesting that the earlier antigen recognition could result in better TCR signaling.

It is unclear how the association rate, k_{on}, is modulated. Is there a feedback on the association rate, k_{on}? And if this feedback exists, where does it come form? These important questions remain unanswered. Is it a result of the changes of the cortical actin cytoskeleton [71, 109]? Is the generation and transmission of *inside-out* signals from the T cell cytoplasm toward the adhesion molecules (LFA-1) able to stabilize the T cell on the APC surface, which can consequently lead to easier APC surface scanning by TCRs [236, 237]? Could it be allostery that affects the way

a ligand binds in presence or absence of other binding events [238, 239], or eventually a feedback from the F-actin foci [121]?

F-actin foci are dynamically polymerized structures resulting from local nucleation of F-actin, and appear at TCR-pMHC sites [112,121]. There is evidence that F-actin can bind to phospholipase C-γ1 (PLCγ1), a key regulator of calcium flux downstream of TCR activation [39, 240]. Interestingly, F-actin foci depletion does not alter the IS pattern, it does manage though to reduce the degree of PLCγ1 phosphorylation [121], suggesting that F-actin foci may locally upregulate PLCγ1 phosphorylation [241], and consequently alter the observed association rate, k_{on}, of TCR-pMHC complexes, as suggested by Pielak et al [183].

I show that, without specific active mechanism, the observed avidity between the receptor and ligands is evolving over time. These changes depend on the density of pMHC and TCR molecules on the respective cells. Comparison of centrally directed flow of TCR-pMHC pairs due to F-actin coupling or absence of it suggested centripetal transport as a possible mechanism for the affinity modulation. The model further suggested that time of affinity measurement is critical, resulting from the higher affinities obtained at the later time points of synapse formation. This result was further supported by the experimental observation that the cooperative TCR behaviour peaks between 4 and 8 minutes after IS formation initiation. Finally, a mathematical model of F-actin foci formation was incorporated in the agent-based model. *In silico* experiments showed that TCR affinity toward pMHC could potentially be actively modulated by a positive/negative feedback on the association rate k_{on}, when TCRs colocalize with F-actin foci.

6.2 TCR affinity modulation during antigen recognition

Pielak et al [183] observed that the density of pMHC molecules impacts on the observed affinity of the interaction between microclusters of TCR and pMHC molecules. In order to discriminate which kind of mechanisms could explain this property, I utilize the agent-based model of immunological synapse formation [180]. The model takes into account the diffusion of molecules and complexes, chemical kinetics for binding and unbinding, steric exclusion of different sized complexes, called size-based segregation (SBS), which is modeled as a repulsive force, and finally, a centrally-directed flow of the complexes present in the IS, TCR-pMHC and LFA-1-ICAM-1, due to F-actin coupling [179, 180]. According to experiments, the readout under investigation is the in situ dissociation rate defined by Pielak et al. [183] as:

$$^{\text{cell}}K_{\text{D}} = \frac{[TCR_{free}][pMHC_{free}]}{[TCR\text{-}pMHC]}.$$

This value represents the inverse of the affinity between TCR and pMHC molecules. The dwell time between TCR-pMHC complexes has been observed to remain constant [183], suggesting that the dissociation rate, k_{off}, is not changing, but rather that the association rate, k_{on} of TCR microclusters toward pMHC molecules is modulated over time.

In order to remain in accordance with the experimental procedure, simulations were performed using a constant density of TCR molecules, and the pMHC amount was titrated between 0.07 and 100 molecules/μm^2. The $^{\text{cell}}K_{\text{D}}$ observed in the simulations is shown at different pMHC densities, without altering the association or dissociation rates, k_{on} and k_{off} respectively, of TCR-pMHC complex formation (Figure 6.1). Interestingly the pMHC titration resulted in a behaviour, qualitatively similar to the experiments, as seen in Figure 6.1a, while the observed IS patterns were different for the different pMHC concentration (Figure 6.1b), due to moderate or excessive pMHC expression. The $^{\text{cell}}K_{\text{D}}$ was systematically decreasing as the pMHC density was increasing until a minimum value was reached, after which the $^{\text{cell}}K_{\text{D}}$ value increased again. The minimum value reached represents the optimum affinity between TCR and pMHC molecules. According to experiments, this optimum coincides with the activation threshold for the T cell. By comparison with the experimental setting, the absolute pMHC number required to reach a minimum of $^{\text{cell}}K_{\text{D}}$, i.e. maximum affinity, is higher in the *in silico* experiments, probably due to the absence of T cell activation in the model. These results suggest that the pMHC density plays an important role for the observed TCR-pMHC affinity.

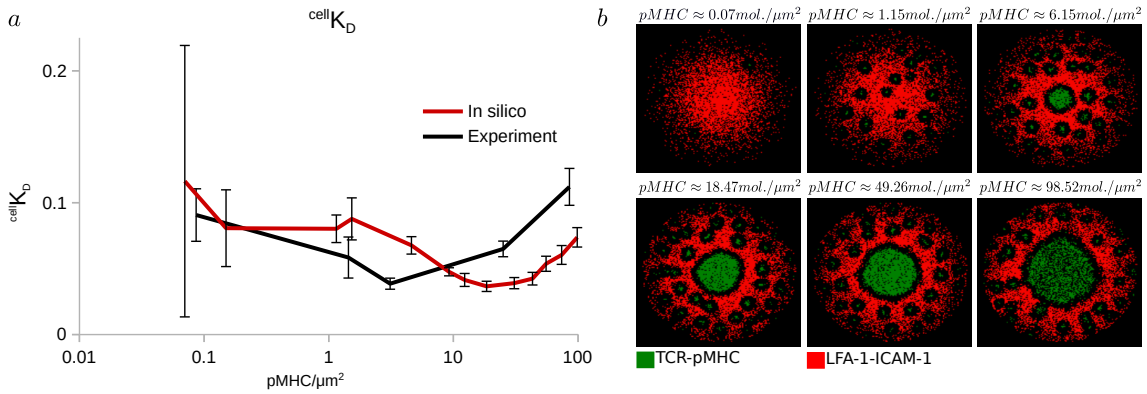

Figure 6.1: TCR affinity modulation during IS formation. **(a)** In situ dissociation constant, $^{\text{cell}}K_{\text{D}}$, for different pMHC densities. Error bars represent the SD of $n = 10$ simulations. **(b)** Immunological synapse snapshots after 10 minutes of contact initiation, for different pMHC densities. Data taken from Pielak et al. [183]. TCR-pMHC: green, LFA-1-ICAM-1: red.

6.3 TCR-pMHC affinity is also affected by the TCR density

I then asked whether the TCR density may play a role in regulating $^{\text{cell}}K_{\text{D}}$. The model predicted that by varying the density of TCR in the synapse area from 4.5 to 55.5 molecules/μm^2 while repeating pMHC titration (Figure 6.2a), $^{\text{cell}}K_{\text{D}}$ qualitatively followed the same behaviour for all the TCR densities checked. In all cases, $^{\text{cell}}K_{\text{D}}$ initially decreased, reached a minimum value and then increased again.

Interestingly, not only the value of pMHC molecules to reach a minimum changed, but also the minimum was achieved at different points depending on the TCR concentration on the synapse area (Figure 6.2b). The minimum $^{\text{cell}}K_{\text{D}}$ was shifting toward higher pMHC densities as the TCR density increased. This suggests that the density of TCRs present in the synapse plays an important role

for antigen recognition. The results for very low pMHC concentrations, $\leq 1/\mu m^2$, showed very high ${}^{cell}K_D$ deviation from the mean, making them hard to interpret. This happens because pMHC are so few that TCRs fail to find them while scanning the APC surface. Therefore, results with pMHC concentrations $> 1/\mu m^2$ will only be shown.

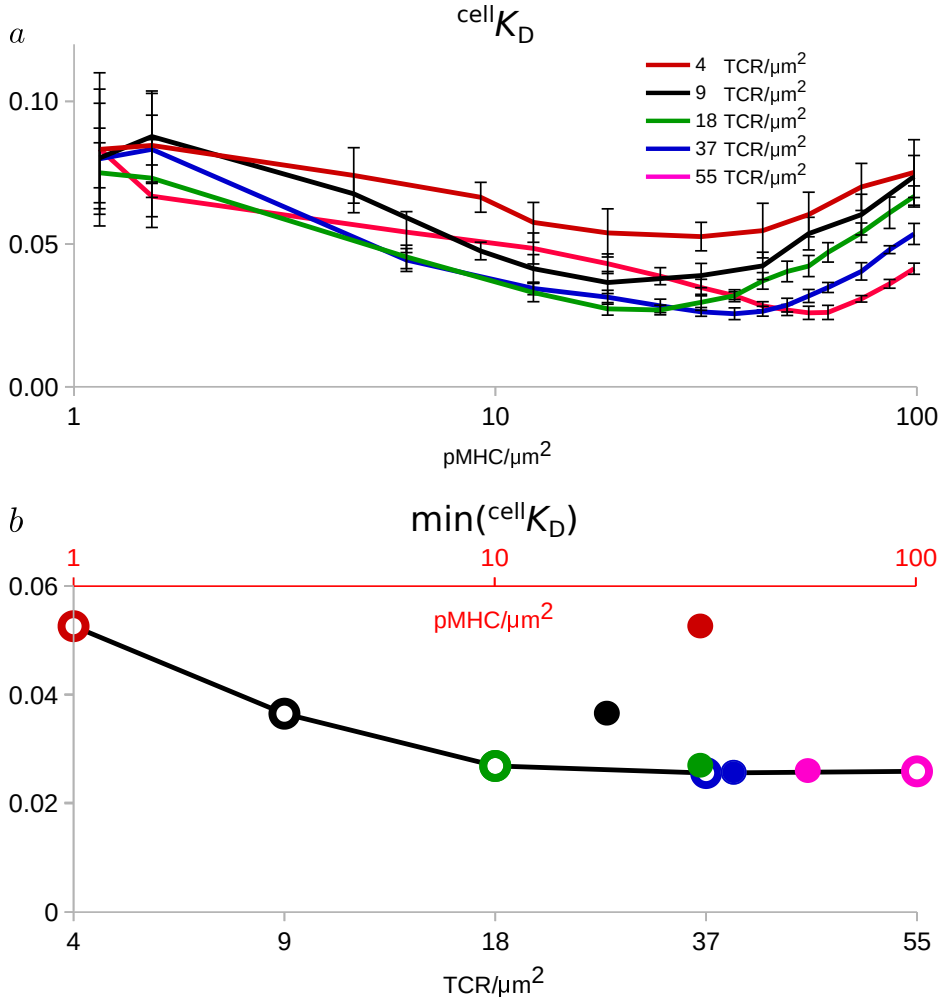

Figure 6.2: Affinity modulation during TCR amount titration. **(a)** In situ dissociation constant, ${}^{cell}K_D$, changes during TCR amount titration. Error bars represent the SD of $n = 10$ simulations. **(b)** Minimum ${}^{cell}K_D$ values for each TCR density (grey axis) during TCR amount titration and pMHC density (red axis) for which the minimum ${}^{cell}K_D$ values are achieved.

6.4 A possible mechanism for TCR affinity modulation

Interestingly, the previous results were obtained without active modulation of the association, k_{on}, or dissociation, k_{off} rates. All the changes resulted only from the pMHC or TCR density titration. But the question why that happens is still not answered. Is there a mechanism in the model that allows for this behaviour that was not appreciated so far? In an attempt to shed light on why ${}^{cell}K_D$ is actively modulated during synapse formation, I decided to check mechanisms which have a direct impact on synapse formation. One such mechanism suggested both experimentally and theoretically, is the coupling of molecules to the centripetal flow of the

F-actin arcs [104,105,116,180]. The strength of the model is that it can be used to perform further *in silico* experiments with targeted inhibition of mechanisms. Therefore, the centrally directed transport of the complexes present in the IS was inhibited. The same experiments are easy to perform, since there are known F-actin inhibitors [242–244].

Interestingly, arrest of F-actin coupling resulted in a qualitatively different behaviour (Figure 6.3) than before (Figure 6.2). pMHC as well as TCR titration, resulted in constant or in some cases, TCR$\geq 37/\mu m^2$, slowly decreasing ${}^{\text{cell}}K_{\text{D}}$. Even in the cases of decreasing ${}^{\text{cell}}K_{\text{D}}$, the minimum was not reached and consequently the value failed to increase again. Therefore, as the model predicts, further experiments should be performed with F-actin actin depletion [242–244], to investigate whether the centrally directed motion of TCR-pMHC complexes indeed supports TCR cooperativity and also assists in the transition from decreasing to increasing ${}^{\text{cell}}K_{\text{D}}$. This behaviour can be considered as a transition from positive to negative feedback on TCR affinity [183]. All together, the centripetal transport of complexes due to interactions with the F-actin flow could be the mechanism behind TCR affinity modulation.

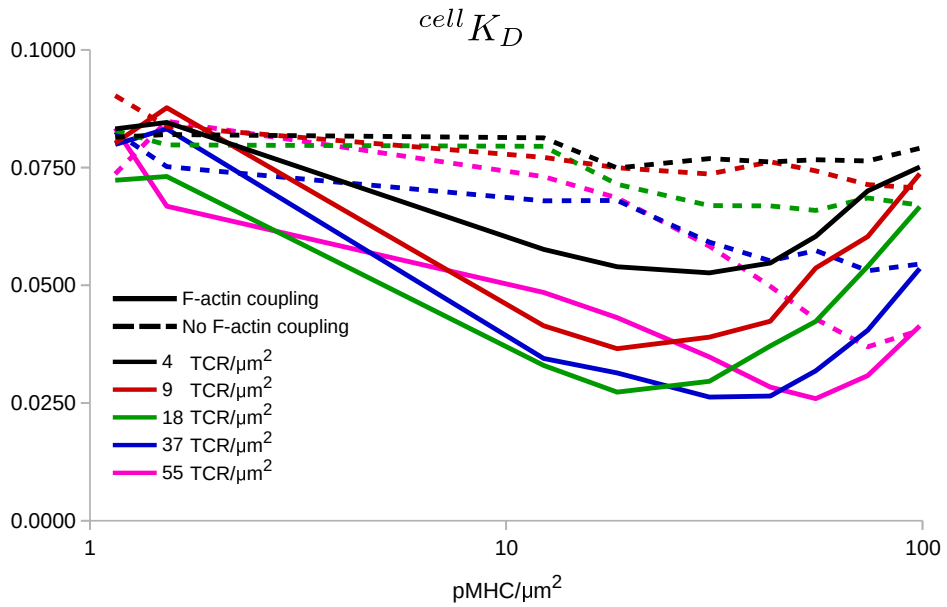

Figure 6.3: Affinity modulation during TCR and pMHC amount titration, in presence (solid lines) or absence (dashed lines) of complexes coupling to F-actin.

6.5 Affinity dynamics suggest time of measurement

I then investigated the time evolution of the affinity changes with and without interactions of complexes with F-actin (Figure 6.4). During the first minute of the *in silico* experiments, both centrally directed movement or absence of it, resulted in constant or slowly decreasing ${}^{\text{cell}}K_{\text{D}}$ (Figure 6.4), in contrast to what was observed in Figure 6.2.

At later times points though, 2-10 minutes, as the pMHC density increased, ${}^{\text{cell}}K_{\text{D}}$ initially decreased, reached a minimum value and then increased again, similar to Figure 6.2. As also shown in Figure 6.3, this behaviour is not observed when actin coupling of molecules is arrested.

Furthermore, the minimum value of ${}^{\text{cell}}K_{\text{D}}$ kept on decreasing as the measurement was performed at later time points (i.e. 10 minutes) (Figure 6.5). In case of F-actin arrest, ${}^{\text{cell}}K_{\text{D}}$ remained at constant levels throughout the *in silico* experiments. Together, these results showed that the time point of the observed affinity measurement is important, allowing for clear indication of TCR affinity modulation around 5 minutes after the initiation of immune synapse formation. The model is in accordance with experimental findings, which suggest that the peak of cooperativity is achieved between 4-8 minutes after the first observed binding event [232].

So far I showed that TCR and pMHC densities are important for the changes in ${}^{\text{cell}}K_{\text{D}}$. Therefore, I decided to investigate whether the in situ dissociation constant is affected when the total TCR and pMHC population is kept constant (TCR+pMHC=constant) while titrating the amount of both, i.e. changing the ratio TCR/pMHC (Figure 6.6). As in every case investigated so far, the first minute of ${}^{\text{cell}}K_{\text{D}}$ measurement showed similar values with or without F-actin coupling for the complexes present in the IS. This behaviour again changed as the measurement was performed at later time points, 2-10 minutes. For low TCR and high pMHC, and *vice versa*, high TCR and low pMHC densities, ${}^{\text{cell}}K_{\text{D}}$ values remained high. But this changed when the amounts of TCR and pMHC were similar, and the minimum value of ${}^{\text{cell}}K_{\text{D}}$ was achieved. Interestingly, the maximum affinity was found at pMHC densities, similar to Figures 6.2 and 6.3.

6.6 An F-actin foci model

Although the results already suggested that the centrally directed motion of TCR-pMHC pairs is a possible mechanism for the TCR affinity modulation, I further investigated if active modulation of the association rate, k_{on}, could produce the same results. According to experimental findings, the dissociation rate, k_{off} was not affected. A possible mechanism suggested in the literature is the F-actin foci, which assist in TCR activation and signaling [121]. F-actin foci are dynamically polymerized structures resulting from local nucleation of F-actin, and appear at TCR-pMHC sites [112, 121].

In this model, TCR-pMHC binding leads to nucleation of F-actin molecules, which are called nucleation points. In presence of LFA-1-ICAM-1, these nucleation points get polymerized, labelled nucleation polymerized points (Figure 6.7a). Additionally, presence of LFA-1-ICAM-1 in this neighborhood, $R_{\text{neighborhood}}$, leads to polymerization of F-actin molecules around nucleation or polymerized nucleation points. These polymerization points form clusters, which correspond to the experimentally observed F-actin foci (Figure 6.7b).

When TCRs colocalize with these clusters, their probability to bind to pMHC is actively modulated by a parameter called *Binding coefficient (BC)*. *BC* enters the model as a coefficient multiplied with the probability of a complex to form,

$$p_{\text{on}} = BC \times \frac{\tau \times k_{\text{on}}}{V \times N_{\text{A}}},$$

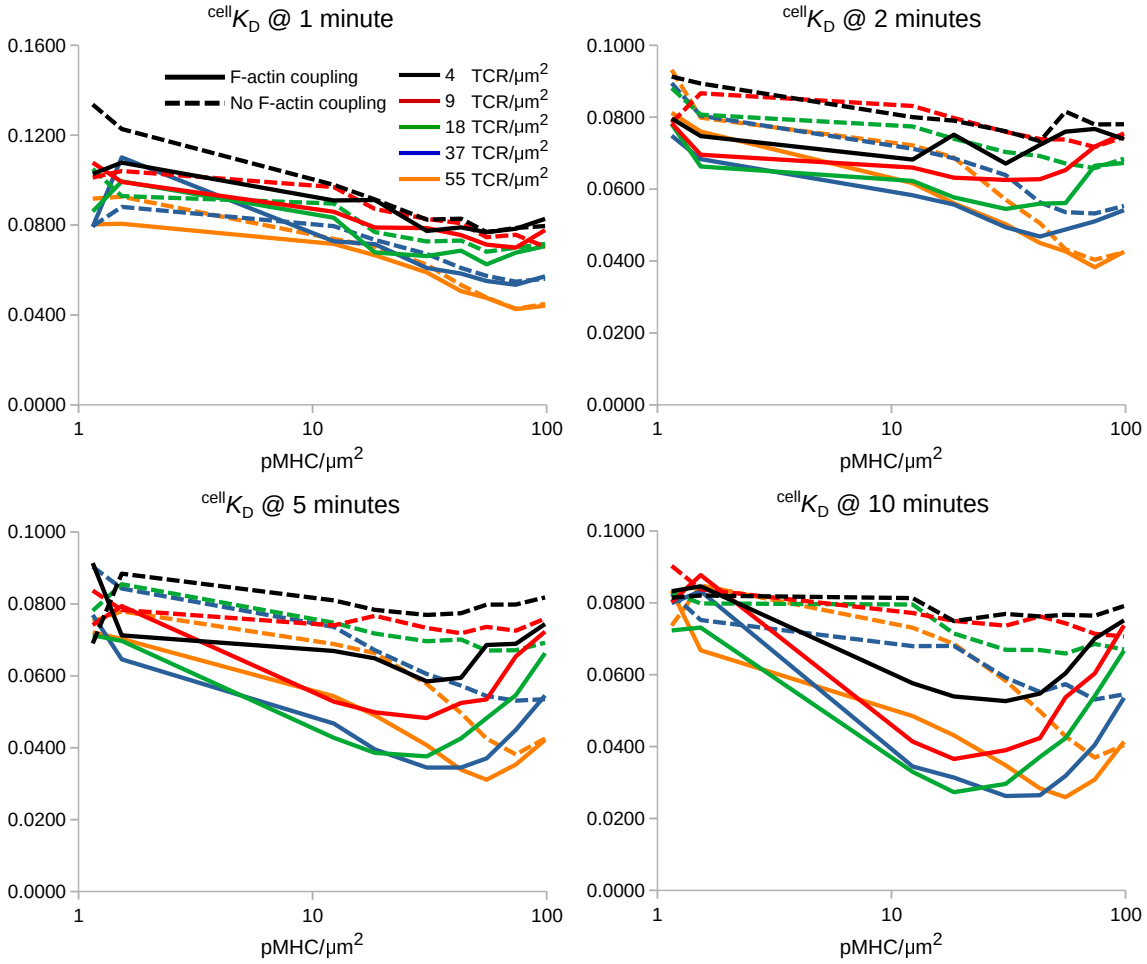

Figure 6.4: Time evolution of ${}^{\text{cell}}K_{\text{D}}$ during TCR and pMHC titration, in presence (solid lines) or absence (dashed lines) of F-actin centripetal transport, at 1, 2, 5 and 10 minutes respectively.

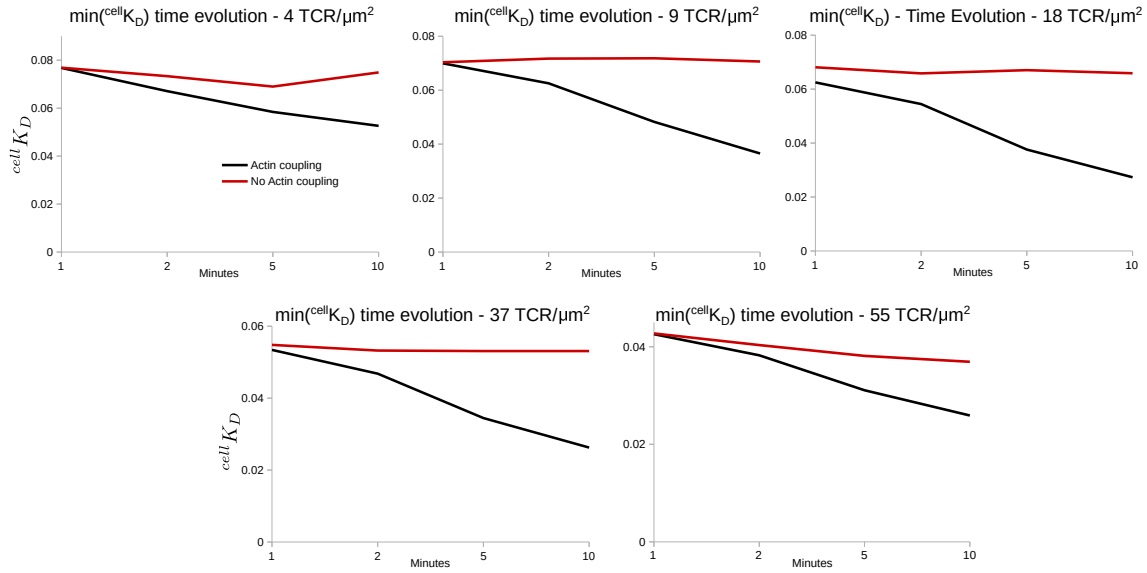

Figure 6.5: Time evolution of $\min({}^{\text{cell}}K_{\text{D}})$ during TCR and pMHC titration, in presence (solid lines) or absence (dashed lines) of F-actin centripetal transport.

where τ is the time step, V is the volume, N_{A} is Avogadro's number and k_{on} the association rate of the forming complex. The model allows to investigate both positive and negative feedbacks from

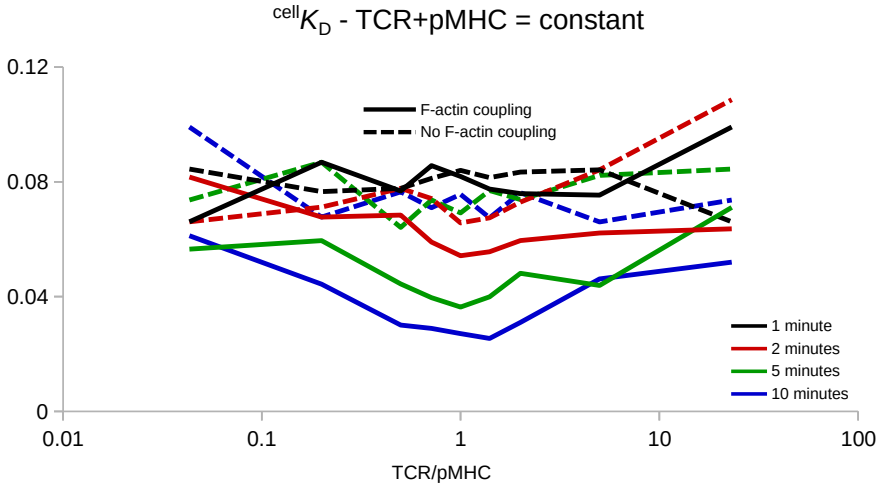

Figure 6.6: Time evolution of $^{\text{cell}}K_{\text{D}}$ during TCR and pMHC titration, in presence (solid lines) or absence (dashed lines) of F-actin centripetal transport. The total amount of TCR and pMHC molecules remains constant during titration.

F-actin foci to TCR binding, either by having $BC > 1$ or $BC < 1$, respectively.

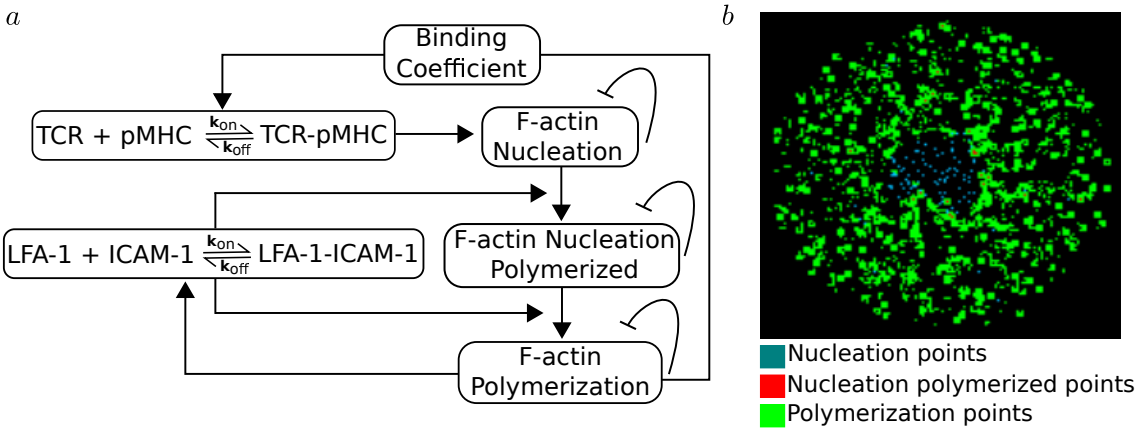

Figure 6.7: F-actin foci modeling. **a** Model for F-actin foci formation. **b** Formed F-actin foci during IS formation. Nucleation points: cyan, nucleation polymerized points: red, polymerization points: green.

6.7 Modulation of TCR-pMHC association rate by positive/negative feedback from the F-actin foci

Now that F-actin foci have been implemented into the model I initially had to investigate whether the observed changes in $^{\text{cell}}K_{\text{D}}$ remained as before (Figures 6.2 & 6.3). To do this, the control *in silico* experiments were performed with BC set to 1, $BC = 1$. In this case, the measured $^{\text{cell}}K_{\text{D}}$ values obtained in Figure 6.8 (top row) were similar to Figure 6.4.

As seen before, at later time points, coupling to actin resulted in decreasing $^{\text{cell}}K_{\text{D}}$ for low pMHC densities, which eventually reached a minimum value and then increased again with increasing pMHC densities. Interestingly, the affinity saturated after 10 minutes of synapse formation, as

seen at 30 minutes in Figure 6.8 (solid magenta line).

I then investigated how BC can affect this behavior. Initially, I increased from $BC = 1$ to $BC = 2$ and 10. On the one hand, the minimum ${}^{\text{cell}}K_{\text{D}}$ value reached kept on decreasing as BC increased (Figures 6.8 (middle row), 6.9 (middle row)). These results showed that affinity can increase if there is a positive feedback on the probability of TCR binding. On the other hand, decreasing the binding coefficient, $BC = 0.5$ and 0.1, therefore having a negative feedback from the F-actin foci, did not alter the minimum ${}^{\text{cell}}K_{\text{D}}$ value significantly compared to the case of $BC = 1$ (Figures 6.8 (bottom row), 6.9 (bottom row)). The reason for this behaviour is a direct outcome of the model (Figure 6.7). Foci formation already requires TCR-pMHC binding. When overlapping with foci, TCR-pMHC binding is impaired, but everywhere else on the T cell surface the binding is happening normally, with the association and dissociation rates, k_{on} and k_{off}, shown in Table 2.1. Therefore, the small overlapping foci and TCR regions are not able to affect the observed affinity values compared to the case without feedback.

Finally, Figure 6.10 shows how the ${}^{\text{cell}}K_{\text{D}}$ valued is affected in presence (positive and negative) or absence of TCR binding feedback. Starting from the case of absence of feedback (black line), and as Figures 6.8 and 6.9 suggested, positive feedback (red and blue lines) reduced ${}^{\text{cell}}K_{\text{D}}$ and therefore the affinity was increasing, while negative feedback (green and orange lines) did not alter the ${}^{\text{cell}}K_{\text{D}}$ significantly compared to the case of $BC = 1$.

All together, these results suggested that TCR-pMHC affinity can be positively modulated by interaction with the F-actin foci, which in turn can act as positive regulators of the binding probability. The feedback alone in the absence of centripetal flow of complexes though failed to reproduce the characteristic trend of decreasing, reaching a minimum and then increasing again the ${}^{\text{cell}}K_{\text{D}}$ value. This suggested that the centripetal transport of the complexes is more important than even a strong feedback ($BC = 10$). This analysis could be experimentally confirmed by inhibition of F-actin arc and F-actin foci formation [121, 242–244], and comparison of obtained ${}^{\text{cell}}K_{\text{D}}$ values.

6.8 Conclusions

In this chapter, the developed agent-based model was not used in order to understand mechanisms of pattern formation, but to investigate how TCR molecules react to different pMHC concentrations during the process of antigen recognition. The model suggested that the experimentally observed ${}^{\text{cell}}K_{\text{D}}$ changes can be recapitulated by the centrally directed flow of TCR-pMHC complexes, without including additional mechanisms. Blockade of the centripetal movement showed only minor increase in the affinity over time, instead of the switch-like behavior from positive to negative regulation of the affinity during pMHC titration.

The implemented F-actin foci model acted as an active positive regulator of the association rate of TCR-pMHC complexes, k_{on}. This positive feedback from the foci, resulted in increased TCR and pMHC affinity and was observed for all the different pMHC concentrations investigated.

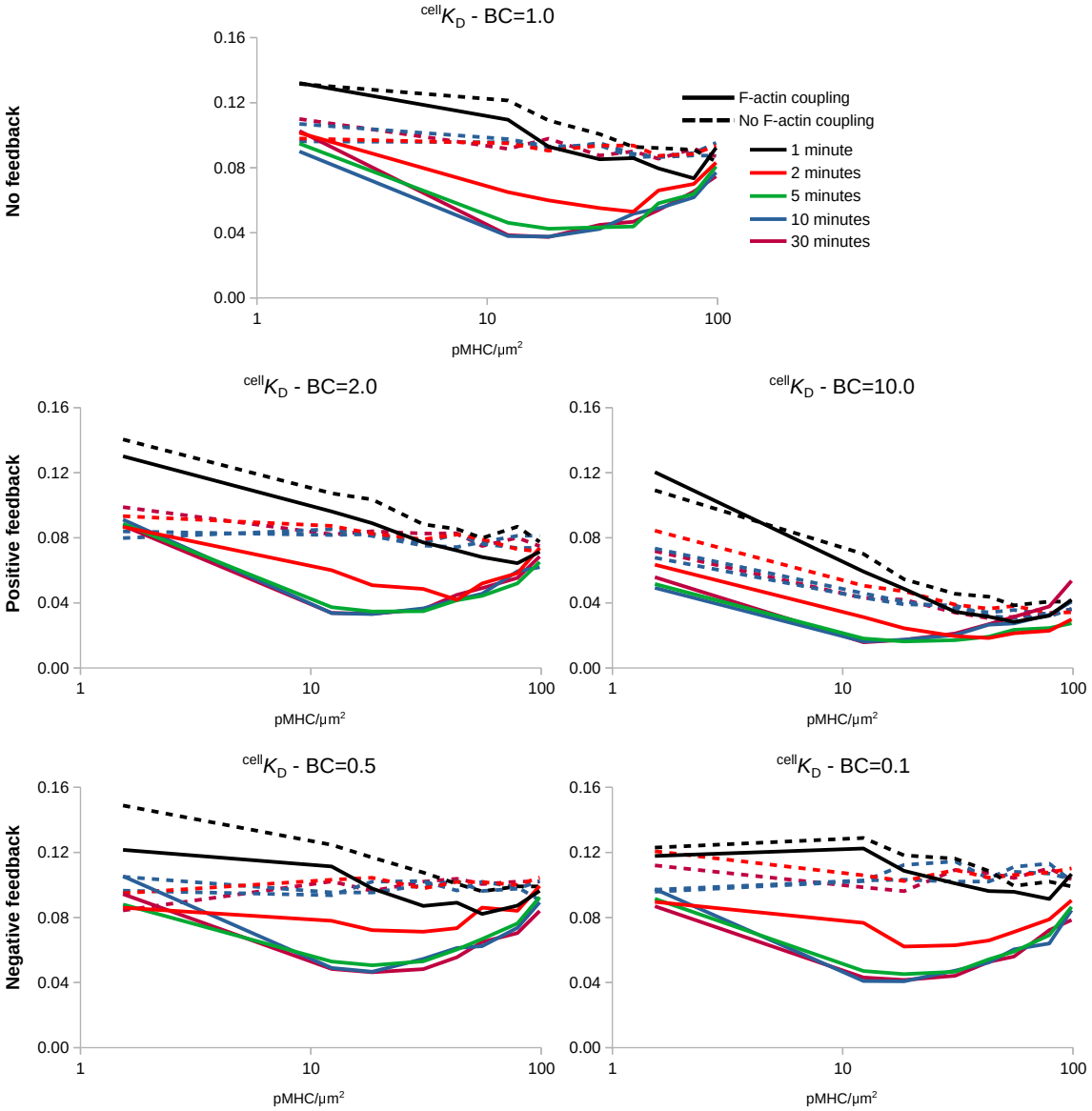

Figure 6.8: Time evolution of the effect of the binding coefficient, BC, on ${}^{\text{cell}}K_{\text{D}}$, with presence or absence of centripetal transport of complexes.

This mechanism though was not able to act alone, since the centripetal transport was still needed to obtain the cooperative behaviour.

These two mechanisms, centripetal flow of TCR-pMHC complexes and active modulation of the association rate by the F-actin foci, can be experimentally investigated, by either blocking the centripetal F-actin transport with F-actin or myosin II inhibitors, or by inhibiting the F-actin foci formation [121], and monitoring possible changes on the ${}^{\text{cell}}K_{\text{D}}$ values.

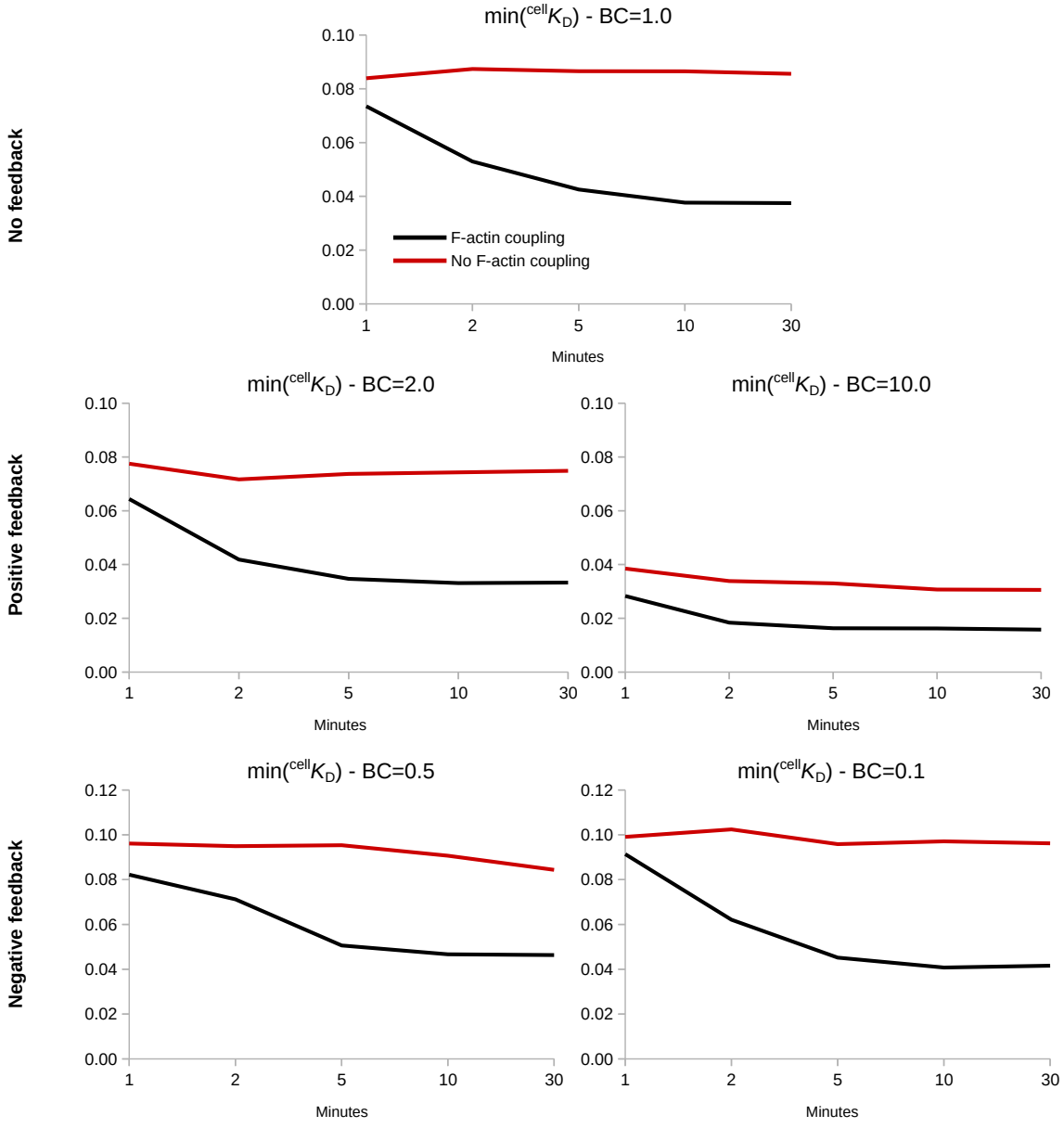

Figure 6.9: $\min(^{\text{cell}}K_{\text{D}})$ dynamics during feedback from the binding coefficient, BC, in the presence or absence of centripetal transport of complexes.

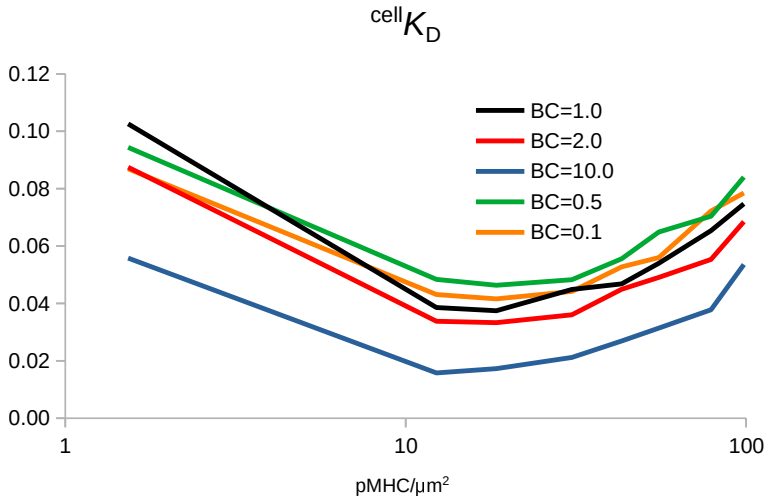

Figure 6.10: ${}^{\text{cell}}K_{\text{D}}$ changes during pMHC concentration titration and positive or negative feedback from the binding coefficient, BC, in presence of centripetal transport of complexes.

Chapter 7

Discussion

7.1 Mechanisms of IS pattern formation in the presence of a costimulatory molecule

I developed a phenomenological agent-based model for the investigation of the localization mechanisms of different molecules present in the cell-cell contact interface. The model focused on the abstract IS formation, where TCR, pMHC, LFA-1 and ICAM-1 molecules were considered. This basic model was complemented with molecules important for TCR signaling, such as the phosphatase CD45 and the costimulatory molecules CD28 and CD2, with their respective ligands, CD80 and CD58.

TCR-pMHC centripetal flow together with the SBS between TCR-pMHC and LFA-1-ICAM-1, led to the formation of microclusters that traveled toward the center, merged into bigger clusters, and finally formed the cSMAC, confirming previous experiments [68,79], and models [166,171]. The model predicts that the coupling of LFA-1-ICAM-1 to F-actin induces a gradient of these complexes within the pSMAC with a higher density toward the cSMAC. The formation of the gradient relies on the combination of diffusion and actin-coupling. The predicted gradient is confirmed in experimental settings [104, 116, 196], however, its relevance for other molecules in the IS has not been appreciated so far. The model showed that freely diffusing molecules are excluded toward the dSMAC by the forming gradient, as was also experimentally observed [196]. The strength of the LFA-1 coupling to the actin flow eventually resulted in the separation of the freely diffusing molecules into two populations, one in the cSMAC region and the other in the dSMAC. In the case of CD45 molecules, repulsive interactions with TCR-pMHC, combined with the emergence of the LFA-1 gradient, resulted in the formation of a ring of CD45 molecules in the dSMAC, recapitulating experimental observations [185, 197].

The halo of free space devoid of LFA-1, generated by the SBS between LFA-1 and TCR complexes, allowed TCR to move through the dense pSMAC. Interestingly, complexes with similar sizes to TCR were also located in these open areas, allowing them to move through the pSMAC by passively following the TCR centripetal flow (Figure 4.1a). Despite that, the LFA-1 gradient

acted as an exclusion mechanism for complexes too, pushing them away from the pSMAC, either toward the central or the distal SMAC (Figures 3.7, 4.5b). This suggests that the LFA-1 gradient impedes molecules and complexes from escaping or entering the cSMAC. The stronger the coupling of LFA-1 to actin, the more it affected the localization of other molecules and complexes (Figures 3.7).

The model predicts that a substantial amount of CD28 complexes behave as passive followers of the TCR-pMHC microcluster movement and localize around the cSMAC (Figure 4.1a). This is a result of two mechanisms: SBS of LFA-1-ICAM-1 and CD28-CD80 complexes in the pSMAC, which pushes CD28 complexes into the microclusters, plus actin-driven transport of TCR-pMHC complexes toward the cSMAC, which opens up low tension paths for CD28 complexes toward the IS center. The model results show that the previously undescribed mechanism of *passive following* is in part responsible for the localization of CD28 in a ring around the cSMAC. Similar was the behaviour of CD2 complexes, due to the similar size with CD28 complexes. The higher concentration of CD2 though resulted in a more pronounced exclusion toward the dSMAC.

Coupling of CD28 to actin was sufficient to guide CD28-CD80 complexes together with the TCR-pMHC microclusters to the cSMAC (Figures 4.1, 4.2) [196]. The ring-like positioning of CD28 around TCRs was best achieved with an optimal strength of the centripetal flow of CD28-CD80. In the limit of strong coupling of CD28 to actin, the intermixed pattern in the cSMAC (Figures 4.8a) could not be resolved by SBS between CD28-CD80 and TCR-pMHC complexes and restore the ring structure (Figures 4.10b, c). SBS was even unable to affect the ring structure in the IS with optimal CD28 coupling to actin (Figure 4.10a). Thus, the model predicts that the optimal CD28-CD80 coupling to actin is weaker than for TCR-pMHC. The actin force acts as the regulator of CD28 distal to central SMAC ratio (Figure 4.8).

In the *in silico* experiments, TCR-pMHC led the way toward the center of the IS, while CD28-CD80 followed (Figures 4.1a (a-d), 4.2b). This suggests an early separation of TCR and CD28 during IS formation. The CD28 ring forms because TCRs reach the center faster. The spatial resolution of the model between 17 and 100 nm allowed for a more detailed insight of surface molecule movement than currently available experimental data, based e.g. on TIRF (total internal reflection fluorescence) microscopy ($\simeq$ 100 nm resolution). Therefore, experiments with higher resolution imaging would be needed to confirm the early segregation of CD28 and TCR, such as STORM (stochastic optical reconstruction microscopy) imaging ($\simeq$ 20 nm resolution) [93].

By showing that actin has a critical role in the relative positioning of molecules inside the IS, especially signaling molecules such as TCR, LFA-1 and CD28, this work further suggests that actin is important for bringing signaling molecules together and structuring signaling pathways in time and space. It has been suggested that TCR signaling is more potent in the microclusters compared to the cSMAC, likely related to the exhaustion of TCR signaling complexes [112,226,227]. The model reveals that actin coupling increases the amount of CD28-CD80 complexes in the vicinity of TCR-pMHC microclusters (Figure 4.2) and strengthens costimulation in microclusters, as also suggested experimentally [196,209,210,245]. In contrast, in the outer cSMAC, there is high

colocalization of CD28-CD80 and TCR-pMHC when the CD28 ring forms, but a low colocalization in the inner cSMAC. Together with the presence of phosphorylated PKCθ around the cSMAC [196], this suggests that there is still signaling in that area, but the degree of colocalization deep in the cSMAC decreases and reduces signaling [72, 108].

The analysis and implications of transmembrane molecules coupling to actin was in the focus of the developed model. Actin coupling was modeled as a phenomenological centripetal force acting on molecules. While this representation is justified for the analysis of IS pattern formation, the mechanisms behind the actin re-orientation and transport toward the center of the IS were not considered [105]. A more explicit representation of the actin dynamics would allow going deeper into the coupling mechanisms and investigate complex interactions governing the binding to actin such as the suggested frictional coupling [100]. This work shows that the strength of coupling to centripetal forces is critical for the organization of the IS, and opens the question whether coupling to actin is a regulated process or could be manipulated by chemical compounds. It could be interesting to assess *in silico* whether this process impacts on the speed or coupling of molecules to the actin flow.

This work led to the creation of a very powerful agent-based model [180], which I used as a tool to investigate additional characteristics of the forming IS, including not only the localization of other molecules, but also properties such as TCR cooperativity.

7.2 The interesting case of CD2 molecules

The case of CD2 complexes is also interesting, since their comparable sizes to TCR-pMHC and CD28-CD80 complexes would suggest a similar ring-like pattern with CD28 or even an intermixed cSMAC with TCR. Nonetheless, CD2 complexes are not only excluded to the dSMAC region, but also form clusters in a flower petal-like structure known as *corolla* pattern. Similar to the CD28 case, CD2 molecules behaved as passive followers of the centrally-directed flow of TCR, due to mutual repulsion with LFA-1-ICAM-1 as a result of SBS. The majority of CD2 complexes was excluded to the outer region of the contact interface but required self attraction, i.e. CD2-CD2 attraction, for clustering (Figure 5.3). The model showed that the amount of CD2 played an important role in its localization. The *in silico* CD2 titration led to a step-like behaviour, where at low CD2 concentrations, passive following of TCR-pMHC transported the majority of CD2 to the cSMAC region, whereas at higher concentrations, around 90% of the CD2 complexes were excluded to the dSMAC where the *corolla* pattern appeared (Figure 5.4), also complying with experimental observations showing that the CD2 amount controls the *corolla* formation [216]. In this case, interaction of CD2 with actin was not needed. One could argue that the attractive forces required by the model to cluster CD2 complexes can be a result of CD2-actin interactions. The proof of such a mechanism would require additional experiments.

The exclusion of CD2 might also have evolved in order to enhance TCR signaling. CD2-CD58 complexes are shown to synergize with TCR, resulting in enhanced PLCγ1 phosphorylation [223].

The exclusion of CD2 could act in a way to increase TCR calcium flux in the peripheral region of the IS, further supporting the idea of signaling in microclusters instead of the cSMAC [112, 226, 227].

Looking at the completely different locations of two similar - at least size-wise - complexes, it is clear that T cell signaling gets even more complicated. Apart from the very complex signaling cascades presented in Figure 1.10, the different costimulatory molecule localizations seem to be important too. The questions that remain to be answered are where exactly does signaling take place during IS formation and how the costimulatory molecules affect it.

Interestingly though, when both CD28 and CD2 find their ligands, the localization of CD28 changes from the ring-like structure around the cSMAC to colocalization with CD2 in the *corolla* [216]. The model was able to recapitulate this strange behaviour, by a phenomenological, attractive force between CD2 and CD28 complexes (Figure 5.7). In the absence of such a force, the localization of the two kinds of complexes was not affected. The translocation of CD28 to the *corolla* might also be a way to enhance signaling during the early stages of antigen recognition and TCR activation.

7.3 TCR cooperativity and active affinity modulation

In this study I additionally developed an actin nucleation model, simulating the dynamics of F-actin foci formation and feedback on the association rate of TCR molecules. This model was implemented in the already developed agent-based model of IS formation dynamics [180]. The new model was used to investigate the mechanisms behind the suggested active modulation of the association rate of the T cell receptor during antigen discrimination [183, 232].

The in situ dissociation rate, ${}^{\text{cell}}K_{\text{D}}$, was calculated as the fraction of the density of unbound TCR and pMHC molecules over the density of TCR-pMHC complexes: $\frac{[TCR_{\text{free}}][pMHC_{\text{free}}]}{[TCR\text{-}pMHC]}$. The model showed that during IS formation, pMHC titration leads to a qualitatively similar behaviour to experiments [183], but required a 10-fold higher pMHC density to achieve the maximum affinity (Figures 6.1 &,6.2). Experimentally, the maximum affinity coincided with NFAT translocation, and therefore T cell activation [183]. Afterwards, cooperativity becomes negative (${}^{\text{cell}}K_{\text{D}}$ is increasing), with a possible explanation being the exhaustion of bigger TCR-pMHC clusters in which signaling is terminated as they reach the cSMAC [108]. Earlier studies showed that during T cell activation, conformational changes and avidity increase of TCR towards pMHC are leading to improved sensing of low antigen amounts [140, 141, 246, 247]. TCR cross-linking though can be excluded form the possible mechanisms [141,248–250], at least for the lower pMHC densities, since no physical contact, between TCR-pMHC complexes was observed during the phase of positive cooperativity. Instead, during the formation of bigger clusters the TCR behaviour changed to being anti-cooperative [183]. Additionally, the finding that even a single pMHC triggers multiple TCRs and cytokine production [230], suggested that there is a missing mechanism in the model, which might be essential for reducing the densities to the levels predicted experimentally. Nonetheless, the qualitative behaviour is similar between *in silico* and experimental observations.

The model qualitatively reproduced the results without active modulation of the association

rate of TCR and pMHC molecules, k_{on}. Therefore, I looked deeper into the *in silico* experiments trying to understand how the cooperative behaviour emerges. A first step was to inhibit IS formation and measure affinities. The motivation came from the finding that a certain small amount of TCR-pMHC binding events was needed in order to initiate their retrograde flow and eventually their accumulation in the cSMAC [183]. These simple simulations were performed by inhibiting the centripetal movement of the complexes and causing therefore the accumulation of TCR-pMHC in the cSMAC. Surprisingly, these straightforward simulations showed major differences in cooperativity, with titration of pMHC not effectively altering the observed ${}^{\text{cell}}K_{\text{D}}$, and the two stages of positive and negative cooperativity not being observed (Figure 6.3). Together, these results suggested that cooperativity can simply be a side effect of IS formation. As the initial TCR-pMHC binding events happen, they start forming clusters and move towards the center of the contact region. In this way, free TCRs trapped inside these clusters can find more pMHC on the way, or free pMHC trapped in these clusters can sequentially bind to multiple TCRs resulting in the observed increase in affinity [94, 234, 235]. These experiments can be performed by inhibition of F-actin arc formation [104, 105].

The model also showed that the time of affinity measurement is crucial. The affinity modulation could be clearly observed around 5 minutes after initiation of IS formation, in accordance with experimental findings [232].

The active modulation of the association rate, k_{on}, of TCR towards pMHC was the subject of further investigations, since the dissociation rate, k_{off}, was observed to remain unchanged [183]. If this was true, would allostery affect the affinity by modulating only k_{on} [232, 238]? In order to investigate if and how active modulation of k_{on} affects the affinity, an F-actin foci model was implemented (Figure 6.7). This allowed the model to actively modulate the association probability based on a parameter dependent on the colocalization of foci and free TCRs, namely the binding coefficient (BC). This parameter altered the binding probability and acted as a positive ($BC > 1$) or negative ($BC < 1$) feedback.

On the one hand, the extra positive feedback resulted in more pronounced affinity changes, by achieving lower ${}^{\text{cell}}K_{\text{D}}$ values, suggesting higher cooperativity between TCRs. On the other hand, the negative feedback did not show significant changes of TCR-pMHC affinities (Figure 6.10). Interestingly, the characteristic IS pattern is still appearing by inhibition of F-actin foci formation [121], but not by inhibition of the formation of F-actin arcs [104, 105]. The model showed the centripetal transport of complexes is more important than the active modulation by the foci, since arrest of centripetal movement even with strong positive feedback from the foci did not reproduce the two phases of TCR cooperativity (Figure 6.8), from increasing to decreasing affinity. Even in the case of positive feedback, the maximum affinity obtained by the model required higher pMHC densities than observed in experiments [183]. The reason behind it might be the ability of a single pMHC to activate multiple TCRs, which are residing in nanoclusters even before the initiation of antigen recognition [94, 142, 233–235], which is a mechanism not implemented in the model, but would require extensive changes in the current implementation.

7.4 General remarks and model limitations

It has to be noted that the physiological interaction between two immune cells harbors more complex mechanisms not studied here. The interacting cells build a complex 3D interface with undulating membranes [84–88]. The cytoskeleton of the APC dynamically changes during IS formation [95], and different APCs can generate IS patterns with different properties [96]. Actin protrusions in the form of microvilli push parts of the membrane toward the opposite cell, which increases the interaction surface [251,252]. Endo- and exocytosis, or recruitment of molecules from the rest of the cell surface to the IS [150] further increase the complexity of trafficking dynamics.

The presented work was designed to reproduce experimental systems relying on SLBs, where molecules on the "virtual APC" side move freely (Figure 2.1). In this simplified system, actin forces on the T cell side can be studied separately under controlled conditions. High resolution data of the IS were mostly performed on SLBs and those imaging data were used to validate the model. For instance, the observed size of microclusters [195, 226], the speed of microcluster movement [100], and the speed of cSMAC formation [79], are consistent with the dynamics of the model. Despite the lack of more complex mechanisms, the simplified *in silico* IS model contains the critical ingredients to recapitulate IS formation and to be in close agreement with experimental observations on SLBs [71, 79]. But as the results of the model were derived from SLB data, it remains to be proven that the identified mechanisms apply to real life 3D IS patterns, which harbor many more complexes with different sizes, such as CTLA-4-CD80/86 and PD-1-PD-L1. Further, it has been suggested that F-actin transport occurs within membrane extensions [253], which would correspond to a space-dependent actin coupling in the model [114, 254].

Data from 3D T cell-APC interfaces will allow to optimize the model.Finally, despite the absence of an explicit signaling model, the *in silico* experiments already pointed to some possible mechanisms for the observed affinity modulation during antigen recognition. Such a model should be implemented as a next step toward the direction of investigating TCR signaling in the forming synapse.

7.5 Future work and model extensions

The model has been able to reproduce many different experimental observations based on very simple mechanisms. Its ability to do so while studying a very complex system makes it a powerful tool, which could be used in different ways to improve and assist biological results and also predict mechanisms that are not foreseen, hard to interpret or even impossible to investigate by the biological community. Nonetheless, the model remains phenomenological. In order to understand the effect of membrane bending and undulations, the model could be reformulated in 3D. In this way, additional data from experiments using cell-cell conjugates would help to parametrize the model. Consequently, the model could help experimentalists by suggesting and discussing mechanisms that lead to IS patterns.

A quicker step forward would be to introduce other important molecules to the model. CTLA-4

is competing with CD28 for the same ligands, i.e. CD80 and CD86, which in turn reduces TCR signaling [206, 255, 256]. CTLA-4 molecules are localized in an intracellular pool in T cells and their recruitment to the IS region depends on the strength of TCR signaling [257] and the ligation to one of its ligands [204]. For this part, modeling of internalization and recycling of molecules can be introduced, since CTLA-4 trafficking is an important checkpoint regulating autoimmunity and responses to tumours [258, 259]. Additionally, the model will be implemented with trans-endocytosis, a mechanism by which CTLA-4 binds to CD80 and/or CD86 on the APC surface and gets internalized with it [259, 260].

Another important checkpoint in tumour immunology as well as autoimmunity is a molecule known as programmed cell death protein 1, or simply PD-1. PD-1 is not only structurally similar to CTLA-4, but also can inhibit the function of CD28 and consequently T cell activation [261], just like CTLA-4. PD-1 has also two ligands presented on APCs, namely PD-L1 and PD-L2 [262, 263]. Blockade of PD-1 interaction with its ligands is shown to inhibit immune resistance [264] and this technique is used for treatment of Hodgkin's lymphoma [265], melanoma [266, 267] and lung cancer [268, 269]. It would be interesting to model the localization mechanisms of PD-1 in the IS [216], as well as possible interactions with the molecules already present in the model, such as CD28 and CD2.

As explained in Chapter 2, the F-actin flow was modeled as a centrally directed force. A more analytical representation of the F-actin network would allow understanding F-actin bundle formation in the dSMAC region, their re-orientation into concentric arcs by interacting with myosin IIa molecules in the pSMAC, and of course their depolymerization in the cSMAC. Such a model would help us understand how molecules are transported by coupling to F-actin arcs, an interaction where experimentalists don't have answers, at least until now.

Of course, I should not overlook the purpose of IS formation, which is T cell activation driven by TCR signaling. A signaling model should be introduced into the presented model, such as the one described by Schmeitz and colleagues [270]. In this case, calcium channels could be spatially localized on the forming synapse and we could study how TCR signaling is affected by presence of costimulatory molecules, such as CD28 and CD2 or exclusion of CD45 from TCR-pMHC sites [134, 271–274].

7.6 Conclusions

This work brings new insights into the mechanistic foundations of a mature IS. Understanding the mechanisms leading to the different characteristic patterns can help biologists understand why the reorganization of all surface molecules takes place, and more importantly how T cells get activated because of these emerging patterns. It is known that the formation of stable ISs is an important step of the body's defence against pathogens. In autoimmune diseases though, such as type-1 diabetes and multiple sclerosis [160], as well as in breast cancer [161–164], the synapses observed are not stable and the T cells fail to get activated and eradicate the danger. Therefore,

the development of new drugs against the aforementioned diseases can be possibly assisted by a proper mechanistic understanding of synapse formation. Adding to this equation the vast amount of signaling molecules present on the T cell-APC interface, we can eventually help in preventing and eliminating such diseases. The predictions made by the model suggested easy to test experiments that would help further understand the suggested mechanisms. Hopefully, this work and potential extensions of it will contribute to the significant increase of our understanding of Immunological Synapse formation.

Bibliography

[1] G. Beck and G. S. Habicht, "Immunity and the invertebrates," *Scientific American*, vol. 275, no. 5, pp. 60–66, 1996.

[2] R. Medzhitov and C. A. Janeway Jr, "Innate immunity: impact on the adaptive immune response," *Current opinion in immunology*, vol. 9, no. 1, pp. 4–9, 1997.

[3] K. Murphy and C. Weaver, *Janeway's immunobiology*. Garland Science, 2016.

[4] C. A. Janeway Jr and R. Medzhitov, "Innate immune recognition," *Annual review of immunology*, vol. 20, no. 1, pp. 197–216, 2002.

[5] J. D. Capra, C. A. Janeway, P. Travers, and M. Walport, *Inmunobiology: the inmune system in health and disease*. Garland Publishing,, 1999.

[6] A. Aderem and R. J. Ulevitch, "Toll-like receptors in the induction of the innate immune response," *Nature*, vol. 406, no. 6797, p. 782, 2000.

[7] S. Gordon, "Pattern recognition receptors: doubling up for the innate immune response," *Cell*, vol. 111, no. 7, pp. 927–930, 2002.

[8] C. A. Janeway, P. Travers, M. Walport, and M. J. Shlomchik, "Immunobiology: the immune system in health and disease," 2005.

[9] M. K. Slifka, R. Antia, J. K. Whitmire, and R. Ahmed, "Humoral immunity due to long-lived plasma cells," *Immunity*, vol. 8, no. 3, pp. 363–372, 1998.

[10] B. R. Bloom and P. R. Glade, *In vitro methods in cell-mediated immunity*. Academic Press, 2014.

[11] A. Ballesteros-Tato, T. D. Randall, F. E. Lund, R. Spolski, W. J. Leonard, and B. León, "T follicular helper cell plasticity shapes pathogenic t helper 2 cell-mediated immunity to inhaled house dust mite," *Immunity*, vol. 44, no. 2, pp. 259–273, 2016.

[12] F. Wan, C.-b. Hu, J.-x. Ma, K. Gao, L.-x. Xiang, and J.-z. Shao, "Characterization of $\gamma\delta$ t cells from zebrafish provides insights into their important role in adaptive humoral immunity," *Frontiers in immunology*, vol. 7, p. 675, 2017.

[13] R. A. Zander, R. Vijay, A. D. Pack, J. J. Guthmiller, A. C. Graham, S. E. Lindner, A. M. Vaughan, S. H. Kappe, and N. S. Butler, "Th1-like plasmodium-specific memory cd4+ t cells support humoral immunity," *Cell reports*, vol. 21, no. 7, pp. 1839–1852, 2017.

[14] L. S. Walker and A. K. Abbas, "Regulation of cell-mediated immunity: The biology of checkpoints and regulatory t cells," *Cancer Immunotherapy Principles and Practice*, p. 95, 2017.

[15] J. M. Scott, T. J. Lebratti, J. M. Richner, X. Jiang, E. Fernandez, H. Zhao, D. H. Fremont, M. S. Diamond, and H. Shin, "Cellular and humoral immunity protect against vaginal zika virus infection in mice," *Journal of virology*, pp. JVI–00038, 2018.

[16] H. S. Lillehoj, "Cell-mediated immunity in parasitic and bacterial d iseases," in *Avian cellular immunology*, pp. 163–190, Routledge, 2018.

[17] A. García-Ortiz and J. M. Serrador, "Nitric oxide signaling in t cell-mediated immunity," *Trends in molecular medicine*, 2018.

[18] K. Curzytek, M. Kubera, E. Trojan, K. Wójcik, A. Basta-Kaim, J. Detka, M. Maes, and R. Rygula, "The effects of pessimism on cell-mediated immunity in rats," *Progress in Neuro-Psychopharmacology and Biological Psychiatry*, vol. 80, pp. 295–303, 2018.

[19] A. Lanzavecchia, "Antigen-specific interaction between t and b cells," *Nature*, vol. 314, no. 6011, p. 537, 1985.

[20] P. S. Linsley, W. Brady, L. Grosmaire, A. Aruffo, N. K. Damle, and J. A. Ledbetter, "Binding of the b cell activation antigen b7 to cd28 costimulates t cell proliferation and interleukin 2 mrna accumulation.," *Journal of Experimental Medicine*, vol. 173, no. 3, pp. 721–730, 1991.

[21] R. J. Armitage, B. Macduff, M. Spriggs, and W. Fanslow, "Human b cell proliferation and ig secretion induced by recombinant cd40 ligand are modulated by soluble cytokines.," *The Journal of Immunology*, vol. 150, no. 9, pp. 3671–3680, 1993.

[22] D. Paus, T. G. Phan, T. D. Chan, S. Gardam, A. Basten, and R. Brink, "Antigen recognition strength regulates the choice between extrafollicular plasma cell and germinal center b cell differentiation," *Journal of Experimental Medicine*, vol. 203, no. 4, pp. 1081–1091, 2006.

[23] D. Zotos, J. M. Coquet, Y. Zhang, A. Light, K. D'Costa, A. Kallies, L. M. Corcoran, D. I. Godfrey, K.-M. Toellner, M. J. Smyth, *et al.*, "Il-21 regulates germinal center b cell differentiation and proliferation through a b cell–intrinsic mechanism," *Journal of Experimental Medicine*, vol. 207, no. 2, pp. 365–378, 2010.

[24] R. Shinnakasu and T. Kurosaki, "Regulation of memory b and plasma cell differentiation," *Current opinion in immunology*, vol. 45, pp. 126–131, 2017.

[25] D. Suan, C. Sundling, and R. Brink, "Plasma cell and memory b cell differentiation from the germinal center," *Current opinion in immunology*, vol. 45, pp. 97–102, 2017.

[26] E. Hammarlund, A. Thomas, I. J. Amanna, L. A. Holden, O. D. Slayden, B. Park, L. Gao, and M. K. Slifka, "Plasma cell survival in the absence of b cell memory," *Nature communications*, vol. 8, no. 1, p. 1781, 2017.

[27] G. B. Pier, J. B. Lyczak, L. M. Wetzler, and M. J. Ruebush, *Immunology, infection, and immunity*. ASM press Washington, DC, 2004.

[28] A. H. Ellebedy, K. J. Jackson, H. T. Kissick, H. I. Nakaya, C. W. Davis, K. M. Roskin, A. K. McElroy, C. M. Oshansky, R. Elbein, S. Thomas, *et al.*, "Defining antigen-specific plasmablast and memory b cell subsets in human blood after viral infection or vaccination," *Nature immunology*, vol. 17, no. 10, p. 1226, 2016.

[29] M. Tian, Z. Hua, S. Hong, Z. Zhang, C. Liu, L. Lin, J. Chen, W. Zhang, X. Zhou, F. Zhang, *et al.*, "B cell–intrinsic myd88 signaling promotes initial cell proliferation and differentiation to enhance the germinal center response to a virus-like particle," *The Journal of Immunology*, vol. 200, no. 3, pp. 937–948, 2018.

[30] W. Ise, K. Fujii, K. Shiroguchi, A. Ito, K. Kometani, K. Takeda, E. Kawakami, K. Yamashita, K. Suzuki, T. Okada, *et al.*, "T follicular helper cell-germinal center b cell interaction strength regulates entry into plasma cell or recycling germinal center cell fate," *Immunity*, vol. 48, no. 4, pp. 702–715, 2018.

[31] T. Inoue, R. Shinnakasu, W. Ise, C. Kawai, T. Egawa, and T. Kurosaki, "The transcription factor foxo1 controls germinal center b cell proliferation in response to t cell help," *Journal of Experimental Medicine*, vol. 214, no. 4, pp. 1181–1198, 2017.

[32] D. L. Hamilos, "Antigen presenting cells," *Immunologic research*, vol. 8, no. 2, pp. 98–117, 1989.

[33] A. Wollenberg and T. Bieber, "Antigen presenting cells," *Atopic dermatitis. Marcel Dekker, New York*, pp. 267–283, 2002.

[34] S. W. Kashem, M. Haniffa, and D. H. Kaplan, "Antigen-presenting cells in the skin," *Annual review of immunology*, vol. 35, pp. 469–499, 2017.

[35] N. Collins, K. Hochheiser, F. R. Carbone, and T. Gebhardt, "Sustained accumulation of antigen-presenting cells after infection promotes local t-cell immunity," *Immunology and cell biology*, vol. 95, no. 10, p. 878, 2017.

[36] M. F. Lindenbergh and W. Stoorvogel, "Antigen presentation by extracellular vesicles from professional antigen-presenting cells," *Annual review of immunology*, vol. 36, pp. 435–459, 2018.

[37] F. S. Lichtenegger, M. Rothe, F. M. Schnorfeil, K. Deiser, C. Krupka, C. Augsberger, M. Schlüter, J. Neitz, and M. Subklewe, "Targeting lag-3 and pd-1 to enhance t cell activation by antigen-presenting cells," *Frontiers in immunology*, vol. 9, p. 385, 2018.

[38] R. M. Steinman and H. Hemmi, "Dendritic cells: translating innate to adaptive immunity," in *From Innate Immunity to Immunological Memory*, pp. 17–58, Springer, 2006.

[39] J. E. Smith-Garvin, G. A. Koretzky, and M. S. Jordan, "T cell activation," *Annual review of immunology*, vol. 27, pp. 591–619, 2009.

[40] J. L. Hukelmann, K. E. Anderson, L. V. Sinclair, K. M. Grzes, A. B. Murillo, P. T. Hawkins, L. R. Stephens, A. I. Lamond, and D. A. Cantrell, "The cytotoxic t cell proteome and its shaping by the kinase mtor," *Nature immunology*, vol. 17, no. 1, p. 104, 2016.

[41] Y. Li, K. To, P. Kanellakis, H. Hosseini, V. Deswaerte, P. Tipping, M. J. Smyth, B.-H. Toh, A. Bobik, and T. Kyaw, "Cd4+ natural killer t cells potently augment aortic root atherosclerosis by perforin-and granzyme b-dependent cytotoxicity," *Circulation research*, vol. 116, no. 2, pp. 245–254, 2015.

[42] F. A. Ververs, E. Kalkhoven, B. van't Land, M. Boes, and H. S. Schipper, "Immunometabolic activation of invariant natural killer t cells," *Frontiers in Immunology*, vol. 9, 2018.

[43] R. Basu, B. M. Whitlock, J. Husson, A. Le Floc'h, W. Jin, A. Oyler-Yaniv, F. Dotiwala, G. Giannone, C. Hivroz, N. Biais, *et al.*, "Cytotoxic t cells use mechanical force to potentiate target cell killing," *Cell*, vol. 165, no. 1, pp. 100–110, 2016.

[44] S. Halle, K. A. Keyser, F. R. Stahl, A. Busche, A. Marquardt, X. Zheng, M. Galla, V. Heissmeyer, K. Heller, J. Boelter, *et al.*, "In vivo killing capacity of cytotoxic t cells is limited and involves dynamic interactions and t cell cooperativity," *Immunity*, vol. 44, no. 2, pp. 233–245, 2016.

[45] D. L. León, I. Fellay, P.-Y. Mantel, and M. Walch, "Killing bacteria with cytotoxic effector proteins of human killer immune cells: Granzymes, granulysin, and perforin," in *Bacterial Pathogenesis*, pp. 275–284, Springer, 2017.

[46] G. Napolitani, P. Kurupati, K. W. W. Teng, M. M. Gibani, M. Rei, A. Aulicino, L. Preciado-Llanes, M. T. Wong, E. Becht, L. Howson, *et al.*, "Clonal analysis of salmonella-specific effector t cells reveals serovar-specific and cross-reactive t cell responses," *Nature immunology*, p. 1, 2018.

[47] E. Vivier, E. Tomasello, M. Baratin, T. Walzer, and S. Ugolini, "Functions of natural killer cells," *Nature immunology*, vol. 9, no. 5, p. 503, 2008.

[48] E. Vivier, D. H. Raulet, A. Moretta, M. A. Caligiuri, L. Zitvogel, L. L. Lanier, W. M. Yokoyama, and S. Ugolini, "Innate or adaptive immunity? the example of natural killer cells," *science*, vol. 331, no. 6013, pp. 44–49, 2011.

[49] N. J. Wilson, K. Boniface, J. R. Chan, B. S. McKenzie, W. M. Blumenschein, J. D. Mattson, B. Basham, K. Smith, T. Chen, F. Morel, *et al.*, "Development, cytokine profile and function

of human interleukin 17–producing helper t cells," *Nature immunology*, vol. 8, no. 9, p. 950, 2007.

[50] P. Miossec, T. Korn, and V. K. Kuchroo, "Interleukin-17 and type 17 helper t cells," *New England Journal of Medicine*, vol. 361, no. 9, pp. 888–898, 2009.

[51] N. Martin-Orozco, P. Muranski, Y. Chung, X. O. Yang, T. Yamazaki, S. Lu, P. Hwu, N. P. Restifo, W. W. Overwijk, and C. Dong, "T helper 17 cells promote cytotoxic t cell activation in tumor immunity," *Immunity*, vol. 31, no. 5, pp. 787–798, 2009.

[52] Y. Wang, J. Shi, J. Yan, Z. Xiao, X. Hou, P. Lu, S. Hou, T. Mao, W. Liu, Y. Ma, *et al.*, "Germinal-center development of memory b cells driven by il-9 from follicular helper t cells," *Nature immunology*, vol. 18, no. 8, p. 921, 2017.

[53] C. Thompson and F. Powrie, "Regulatory t cells," *Current opinion in pharmacology*, vol. 4, no. 4, pp. 408–414, 2004.

[54] S. Beissert, A. Schwarz, and T. Schwarz, "Regulatory t cells," *Journal of investigative dermatology*, vol. 126, no. 1, pp. 15–24, 2006.

[55] N. S. Joshi, E. H. Akama-Garren, Y. Lu, D.-Y. Lee, G. P. Chang, A. Li, M. DuPage, T. Tammela, N. R. Kerper, A. F. Farago, *et al.*, "Regulatory t cells in tumor-associated tertiary lymphoid structures suppress anti-tumor t cell responses," *Immunity*, vol. 43, no. 3, pp. 579–590, 2015.

[56] H. Onishi, T. Morisaki, and M. Katano, "Regulatory t cells," in *Immunotherapy of Cancer*, pp. 309–322, Springer, 2016.

[57] D. Burzyn, W. Kuswanto, D. Kolodin, J. L. Shadrach, M. Cerletti, Y. Jang, E. Sefik, T. G. Tan, A. J. Wagers, C. Benoist, *et al.*, "A special population of regulatory t cells potentiates muscle repair," *Cell*, vol. 155, no. 6, pp. 1282–1295, 2013.

[58] H. Lei, K. Schmidt-Bleek, A. Dienelt, P. Reinke, and H.-D. Volk, "Regulatory t cell-mediated anti-inflammatory effects promote successful tissue repair in both indirect and direct manners," *Frontiers in pharmacology*, vol. 6, p. 184, 2015.

[59] L. L. Lanier, "Nk cell recognition," *Annu. Rev. Immunol.*, vol. 23, pp. 225–274, 2005.

[60] S. I. Khakoo, S. Cassidy, and K. Cheent, "Effects of peptide on nk cell-mediated mhc i recognition," *Frontiers in immunology*, vol. 5, p. 133, 2014.

[61] S. Regis, F. Caliendo, A. Dondero, F. Bellora, B. Casu, C. Bottino, and R. Castriconi, "Main nk cell receptors and their ligands: regulation by micrornas," 2018.

[62] T. Pradeu and E. Vivier, "The discontinuity theory of immunity," *Science immunology*, vol. 1, no. 1, 2016.

[63] G. Eberl and T. Pradeu, "Towards a general theory of immunity?," *Trends in immunology*, vol. 39, no. 4, pp. 261–263, 2018.

[64] N. A. Campbell, J. Reece, L. Urry, M. Cain, S. Wasserman, P. Minorsky, and R. Jackson, *Biology, Vol. 8.* San Francisco, USA: Pearson International Edition, 2008.

[65] S. D. Marlin and T. A. Springer, "Purified intercellular adhesion molecule-1 (icam-1) is a ligand for lymphocyte function-associated antigen 1 (lfa-1)," *Cell*, vol. 51, no. 5, pp. 813–819, 1987.

[66] T. A. Springer, M. L. Dustin, T. K. Kishimoto, and S. D. Marlin, "The lymphocyte function associated lfa-1, cd2, and lfa-3 molecules: cell adhesion receptors of the immune system," *Annual review of immunology*, vol. 5, no. 1, pp. 223–252, 1987.

[67] J. R. James and R. D. Vale, "Biophysical mechanism of t-cell receptor triggering in a reconstituted system," *Nature*, vol. 487, no. 7405, p. 64, 2012.

[68] C. R. Monks, B. A. Freiberg, H. Kupfer, N. Sciaky, and A. Kupfer, "Three-dimensional segregation of supramolecular activation clusters in t cells," *Nature*, vol. 395, no. 6697, p. 82, 1998.

[69] M. L. Dustin, M. W. Olszowy, A. D. Holdorf, J. Li, S. Bromley, N. Desai, P. Widder, F. Rosenberger, P. A. van der Merwe, P. M. Allen, *et al.*, "A novel adaptor protein orchestrates receptor patterning and cytoskeletal polarity in t-cell contacts," *Cell*, vol. 94, no. 5, pp. 667–677, 1998.

[70] J. B. Huppa and M. M. Davis, "T-cell-antigen recognition and the immunological synapse," *Nature Reviews Immunology*, vol. 3, no. 12, p. 973, 2003.

[71] K. D. Mossman, G. Campi, J. T. Groves, and M. L. Dustin, "Altered tcr signaling from geometrically repatterned immunological synapses," *Science*, vol. 310, no. 5751, pp. 1191–1193, 2005.

[72] B. Alarcón, D. Mestre, and N. Martínez-Martín, "The immunological synapse: a cause or consequence of t-cell receptor triggering?," *Immunology*, vol. 133, no. 4, pp. 420–425, 2011.

[73] B. N. Manz, B. L. Jackson, R. S. Petit, M. L. Dustin, and J. Groves, "T-cell triggering thresholds are modulated by the number of antigen within individual t-cell receptor clusters," *Proceedings of the National Academy of Sciences*, vol. 108, no. 22, pp. 9089–9094, 2011.

[74] K.-H. Lee, A. D. Holdorf, M. L. Dustin, A. C. Chan, P. M. Allen, and A. S. Shaw, "T cell receptor signaling precedes immunological synapse formation," *Science*, vol. 295, no. 5559, pp. 1539–1542, 2002.

[75] K.-H. Lee, A. R. Dinner, C. Tu, G. Campi, S. Raychaudhuri, R. Varma, T. N. Sims, W. R. Burack, H. Wu, J. Wang, *et al.*, "The immunological synapse balances t cell receptor signaling and degradation," *science*, vol. 302, no. 5648, pp. 1218–1222, 2003.

[76] P. T. Sage, L. M. Varghese, R. Martinelli, T. E. Sciuto, M. Kamei, A. M. Dvorak, T. A. Springer, A. H. Sharpe, and C. V. Carman, "Antigen recognition is facilitated by invadosome-like protrusions formed by memory/effector t cells," *The Journal of Immunology*, vol. 188, no. 8, pp. 3686–3699, 2012.

[77] E. Tabdanov, S. Gondarenko, S. Kumari, A. Liapis, M. L. Dustin, M. P. Sheetz, L. C. Kam, and T. Iskratsch, "Micropatterning of tcr and lfa-1 ligands reveals complementary effects on cytoskeleton mechanics in t cells," *Integrative Biology*, vol. 7, no. 10, pp. 1272–1284, 2015.

[78] A. Ortega-Carrion and M. Vicente-Manzanares, "Concerning immune synapses: a spatiotemporal timeline," *F1000Research*, vol. 5, 2016.

[79] A. Grakoui, S. K. Bromley, C. Sumen, M. M. Davis, A. S. Shaw, P. M. Allen, and M. L. Dustin, "The immunological synapse: a molecular machine controlling t cell activation," *Science*, vol. 285, no. 5425, pp. 221–227, 1999.

[80] M. L. Dustin, "What counts in the immunological synapse?," *Molecular cell*, vol. 54, no. 2, pp. 255–262, 2014.

[81] M. L. Dustin and D. Depoil, "New insights into the t cell synapse from single molecule techniques," *Nature Reviews Immunology*, vol. 11, no. 10, pp. 672–684, 2011.

[82] T. A. Springer, "Adhesion receptors of the immune system," *Nature*, vol. 346, no. 6283, pp. 425–434, 1990.

[83] C. T. Baldari, M. L. Dustin, and Baldari, *Immune Synapse*. Springer, 2017.

[84] A. N. Cartwright, J. Griggs, and D. M. Davis, "The immune synapse clears and excludes molecules above a size threshold," *Nature communications*, vol. 5, p. 5479, 2014.

[85] A. Oszmiana, D. J. Williamson, S.-P. Cordoba, D. J. Morgan, P. R. Kennedy, K. Stacey, and D. M. Davis, "The size of activating and inhibitory killer ig-like receptor nanoclusters is controlled by the transmembrane sequence and affects signaling," *Cell reports*, vol. 15, no. 9, pp. 1957–1972, 2016.

[86] J. Huang, X. Zeng, N. Sigal, P. J. Lund, L. F. Su, H. Huang, Y.-h. Chien, and M. M. Davis, "Detection, phenotyping, and quantification of antigen-specific t cells using a peptide-mhc dodecamer," *Proceedings of the National Academy of Sciences*, vol. 113, no. 13, pp. E1890–E1897, 2016.

[87] A. F. Carisey, E. M. Mace, M. B. Saeed, D. M. Davis, and J. S. Orange, "Nanoscale dynamism of actin enables secretory function in cytolytic cells," *Current Biology*, vol. 28, no. 4, pp. 489–502, 2018.

[88] R. Ambler, X. Ruan, R. F. Murphy, and C. Wülfing, "Systems imaging of the immune synapse," in *The Immune Synapse: Methods and Protocols* (C. T. Baldari and M. L. Dustin, eds.), pp. 409–421, Springer, 2017.

[89] J. T. Groves and M. L. Dustin, "Supported planar bilayers in studies on immune cell adhesion and communication," *Journal of immunological methods*, vol. 278, no. 1-2, pp. 19–32, 2003.

[90] V. Kiessling, M. K. Domanska, D. Murray, C. Wan, and L. K. Tamm, "Supported lipid bilayers," *Wiley encyclopedia of chemical biology*, pp. 1–12, 2007.

[91] G. D. Rak, E. M. Mace, P. P. Banerjee, T. Svitkina, and J. S. Orange, "Natural killer cell lytic granule secretion occurs through a pervasive actin network at the immune synapse," *PLoS biology*, vol. 9, no. 9, p. e1001151, 2011.

[92] M. L. Dustin and J. T. Groves, "Receptor signaling clusters in the immune synapse," *Annual review of biophysics*, vol. 41, pp. 543–556, 2012.

[93] M. J. Rust, M. Bates, and X. Zhuang, "Stochastic optical reconstruction microscopy (storm) provides sub-diffraction-limit image resolution," *Nature methods*, vol. 3, no. 10, p. 793, 2006.

[94] S. V. Pageon, T. Tabarin, Y. Yamamoto, Y. Ma, P. R. Nicovich, J. S. Bridgeman, A. Cohnen, C. Benzing, Y. Gao, M. D. Crowther, *et al.*, "Functional role of t-cell receptor nanoclusters in signal initiation and antigen discrimination," *Proceedings of the National Academy of Sciences*, vol. 113, no. 37, pp. E5454–E5463, 2016.

[95] F. Benvenuti, "The dendritic cell synapse: a life dedicated to t cell activation," *Frontiers in immunology*, vol. 7, p. 70, 2016.

[96] C. R. Nowosad, K. M. Spillane, and P. Tolar, "Germinal center b cells recognize antigen through a specialized immune synapse architecture," *Nature immunology*, vol. 17, no. 7, p. 870, 2016.

[97] M. K. Wild, A. Cambiaggi, M. H. Brown, E. A. Davies, H. Ohno, T. Saito, and P. A. Van Der Merwe, "Dependence of t cell antigen recognition on the dimensions of an accessory receptor–ligand complex," *Journal of Experimental Medicine*, vol. 190, no. 1, pp. 31–42, 1999.

[98] S. Qi, J. T. Groves, and A. K. Chakraborty, "Synaptic pattern formation during cellular recognition," *Proceedings of the National Academy of Sciences*, vol. 98, no. 12, pp. 6548–6553, 2001.

[99] S. J. Davis and P. A. van der Merwe, "The kinetic-segregation model: Tcr triggering and beyond," *Nature immunology*, vol. 7, no. 8, pp. 803–809, 2006.

[100] A. L. DeMond, K. D. Mossman, T. Starr, M. L. Dustin, and J. T. Groves, "T cell receptor microcluster transport through molecular mazes reveals mechanism of translocation," *Biophysical Journal*, vol. 94, no. 8, pp. 3286–3292, 2008.

[101] P. Beemiller and M. F. Krummel, "Regulation of t-cell receptor signaling by the actin cytoskeleton and poroelastic cytoplasm," *Immunological reviews*, vol. 256, no. 1, pp. 148–159, 2013.

[102] Y. Yu, A. A. Smoligovets, and J. T. Groves, "Modulation of t cell signaling by the actin cytoskeleton," *J Cell Sci*, vol. 126, no. 5, pp. 1049–1058, 2013.

[103] S. Kumari, S. Curado, V. Mayya, and M. L. Dustin, "T cell antigen receptor activation and actin cytoskeleton remodeling," *Biochimica et Biophysica Acta (BBA)-Biomembranes*, vol. 1838, no. 2, pp. 546–556, 2014.

[104] S. Murugesan, J. Hong, J. Yi, D. Li, J. R. Beach, L. Shao, J. Meinhardt, G. Madison, X. Wu, E. Betzig, and J. A. Hammer, "Formin-generated actomyosin arcs propel t cell receptor microcluster movement at the immune synapse," *J Cell Biol*, vol. 215, no. 3, pp. 383–399, 2016.

[105] J. Yi, X. S. Wu, T. Crites, and J. A. Hammer, "Actin retrograde flow and actomyosin ii arc contraction drive receptor cluster dynamics at the immunological synapse in jurkat t cells," *Molecular biology of the cell*, vol. 23, no. 5, pp. 834–852, 2012.

[106] J. A. Hammer III and J. K. Burkhardt, "Controversy and consensus regarding myosin ii function at the immunological synapse," *Current opinion in immunology*, vol. 25, no. 3, pp. 300–306, 2013.

[107] W. A. Comrie and J. K. Burkhardt, "Action and traction: cytoskeletal control of receptor triggering at the immunological synapse," *Frontiers in immunology*, vol. 7, p. 68, 2016.

[108] R. Varma, G. Campi, T. Yokosuka, T. Saito, and M. L. Dustin, "T cell receptor-proximal signals are sustained in peripheral microclusters and terminated in the central supramolecular activation cluster," *Immunity*, vol. 25, no. 1, pp. 117–127, 2006.

[109] G. Campi, R. Varma, and M. L. Dustin, "Actin and agonist mhc–peptide complex–dependent t cell receptor microclusters as scaffolds for signaling," *Journal of Experimental Medicine*, vol. 202, no. 8, pp. 1031–1036, 2005.

[110] Y. Kaizuka, A. D. Douglass, R. Varma, M. L. Dustin, and R. D. Vale, "Mechanisms for segregating t cell receptor and adhesion molecules during immunological synapse formation in jurkat t cells," *Proceedings of the National Academy of Sciences*, vol. 104, no. 51, pp. 20296–20301, 2007.

[111] A. Babich, S. Li, R. S. O'Connor, M. C. Milone, B. D. Freedman, and J. K. Burkhardt, "F-actin polymerization and retrograde flow drive sustained plcγ1 signaling during t cell activation," *J Cell Biol*, pp. jcb–201201018, 2012.

[112] P. Beemiller, J. Jacobelli, and M. F. Krummel, "Integration of the movement of signaling microclusters with cellular motility in immunological synapses," *Nature immunology*, vol. 13, no. 8, pp. 787–795, 2012.

[113] A. A. Smoligovets, A. W. Smith, H.-J. Wu, R. S. Petit, and J. T. Groves, "Characterization of dynamic actin associations with t-cell receptor microclusters in primary t cells," *J Cell Sci*, vol. 125, no. 3, pp. 735–742, 2012.

[114] M. Fritzsche, R. A. Fernandes, V. T. Chang, H. Colin-York, M. P. Clausen, J. H. Felce, S. Galiani, C. Erlenkämper, A. M. Santos, J. M. Heddleston, *et al.*, "Cytoskeletal actin dynamics shape a ramifying actin network underpinning immunological synapse formation," *Science Advances*, vol. 3, no. 6, p. e1603032, 2017.

[115] R. Basu and M. Huse, "Mechanical communication at the immunological synapse," *Trends in cell biology*, vol. 27, no. 4, pp. 241–254, 2017.

[116] W. A. Comrie, A. Babich, and J. K. Burkhardt, "F-actin flow drives affinity maturation and spatial organization of lfa-1 at the immunological synapse," *J Cell Biol*, pp. jcb–201406121, 2015.

[117] W. A. Comrie, S. Li, S. Boyle, and J. K. Burkhardt, "The dendritic cell cytoskeleton promotes t cell adhesion and activation by constraining icam-1 mobility," *J Cell Biol*, vol. 208, no. 4, pp. 457–473, 2015.

[118] E. M. Mace, W. W. Wu, T. Ho, S. S. Mann, H.-T. Hsu, and J. S. Orange, "Nk cell lytic granules are highly motile at the immunological synapse and require f-actin for post-degranulation persistence," *The Journal of Immunology*, p. 1201296, 2012.

[119] A. T. Ritter, Y. Asano, J. C. Stinchcombe, N. Dieckmann, B.-C. Chen, C. Gawden-Bone, S. van Engelenburg, W. Legant, L. Gao, M. W. Davidson, *et al.*, "Actin depletion initiates events leading to granule secretion at the immunological synapse," *Immunity*, vol. 42, no. 5, pp. 864–876, 2015.

[120] A. M. Beal, N. Anikeeva, R. Varma, T. O. Cameron, P. J. Norris, M. L. Dustin, and Y. Sykulev, "Protein kinase cθ regulates stability of the peripheral adhesion ring junction and contributes to the sensitivity of target cell lysis by ctl," *The Journal of Immunology*, vol. 181, no. 7, pp. 4815–4824, 2008.

[121] S. Kumari, D. Depoil, R. Martinelli, E. Judokusumo, G. Carmona, F. B. Gertler, L. C. Kam, C. V. Carman, J. K. Burkhardt, D. J. Irvine, *et al.*, "Actin foci facilitate activation of the phospholipase c-γ in primary t lymphocytes via the wasp pathway," *Elife*, vol. 4, p. e04953, 2015.

[122] N. B. Martín-Cófreces, F. Baixauli, and F. Sánchez-Madrid, "Immune synapse: conductor of orchestrated organelle movement," *Trends in cell biology*, vol. 24, no. 1, pp. 61–72, 2014.

[123] E. Kuokkanen, V. Šuštar, and P. K. Mattila, "Molecular control of b cell activation and immunological synapse formation," *Traffic*, vol. 16, no. 4, pp. 311–326, 2015.

[124] J. Lou, J. Rossy, Q. Deng, S. V. Pageon, and K. Gaus, "New insights into how trafficking regulates t cell receptor signaling," *Frontiers in cell and developmental biology*, vol. 4, p. 77, 2016.

[125] N. Blas-Rus, E. Bustos-Morán, F. Sánchez-Madrid, and N. B. Martín-Cófreces, "Analysis of microtubules and microtubule-organizing center at the immune synapse," in *The Immune Synapse*, pp. 31–49, Springer, 2017.

[126] N. B. Martin-Cofreces and F. Sánchez-Madrid, "Sailing to and docking at the immune synapse: Role of tubulin dynamics and molecular motors," *Frontiers in immunology*, vol. 9, p. 1174, 2018.

[127] J. Combs, S. J. Kim, S. Tan, L. A. Ligon, E. L. Holzbaur, J. Kuhn, and M. Poenie, "Recruitment of dynein to the jurkat immunological synapse," *Proceedings of the National Academy of Sciences*, vol. 103, no. 40, pp. 14883–14888, 2006.

[128] A. Hashimoto-Tane, T. Yokosuka, K. Sakata-Sogawa, M. Sakuma, C. Ishihara, M. Tokunaga, and T. Saito, "Dynein-driven transport of t cell receptor microclusters regulates immune synapse formation and t cell activation," *Immunity*, vol. 34, no. 6, pp. 919–931, 2011.

[129] T. Schnyder, A. Castello, C. Feest, N. E. Harwood, T. Oellerich, H. Urlaub, M. Engelke, J. Wienands, A. Bruckbauer, and F. D. Batista, "B cell receptor-mediated antigen gathering requires ubiquitin ligase cbl and adaptors grb2 and dok-3 to recruit dynein to the signaling microcluster," *Immunity*, vol. 34, no. 6, pp. 905–918, 2011.

[130] M. R. Kuhné, J. Lin, D. Yablonski, M. N. Mollenauer, L. I. R. Ehrlich, J. Huppa, M. M. Davis, and A. Weiss, "Linker for activation of t cells, ζ-associated protein-70, and src homology 2 domain-containing leukocyte protein-76 are required for tcr-induced microtubule-organizing center polarization," *The Journal of Immunology*, vol. 171, no. 2, pp. 860–866, 2003.

[131] C. A. Hartzell, K. I. Jankowska, J. K. Burkhardt, and R. S. Lewis, "Calcium influx through crac channels controls actin organization and dynamics at the immune synapse," *Elife*, vol. 5, p. e14850, 2016.

[132] E. Bustos-Morán, N. Blas-Rus, N. Martin-Cófreces, and F. Sánchez-Madrid, "Microtubule associated protein-4 (map4) controls nanovesicle dynamics and t cell activation," *J Cell Sci*, pp. jcs–199042, 2017.

[133] A. Stirnweiss, R. Hartig, S. Gieseler, J. A. Lindquist, P. Reichardt, L. Philipsen, L. Simeoni, M. Poltorak, C. Merten, W. Zuschratter, *et al.*, "T cell activation results in conformational changes in the src family kinase lck to induce its activation," *Sci. Signal.*, vol. 6, no. 263, pp. ra13–ra13, 2013.

[134] L. Philipsen, A. V. Reddycherla, R. Hartig, J. Gumz, M. Kästle, A. Kritikos, M. P. Poltorak, Y. Prokazov, E. Turbin, A. Weber, *et al.*, "De novo phosphorylation and conformational

opening of the tyrosine kinase lck act in concert to initiate t cell receptor signaling," *Sci. Signal.*, vol. 10, no. 462, p. eaaf4736, 2017.

[135] A. Rheinländer, B. Schraven, and U. Bommhardt, "Cd45 in human physiology and clinical medicine," *Immunology letters*, 2018.

[136] Y. X. Tan, B. N. Manz, T. S. Freedman, C. Zhang, K. M. Shokat, and A. Weiss, "Inhibition of the kinase csk in thymocytes reveals a requirement for actin remodeling in the initiation of full tcr signaling," *Nature immunology*, vol. 15, no. 2, p. 186, 2014.

[137] A. K. Chakraborty and A. Weiss, "Insights into the initiation of tcr signaling," *Nature immunology*, vol. 15, no. 9, p. 798, 2014.

[138] B. N. Manz, Y. X. Tan, A. H. Courtney, F. Rutaganira, E. Palmer, K. M. Shokat, and A. Weiss, "Small molecule inhibition of csk alters affinity recognition by t cells," *Elife*, vol. 4, p. e08088, 2015.

[139] D. Gil, A. G. Schrum, B. Alarcón, and E. Palmer, "T cell receptor engagement by peptide–mhc ligands induces a conformational change in the cd3 complex of thymocytes," *Journal of Experimental Medicine*, vol. 201, no. 4, pp. 517–522, 2005.

[140] W. W. Schamel, R. M. Risueño, S. Minguet, A. R. Ortíz, and B. Alarcón, "A conformation- and avidity-based proofreading mechanism for the tcr–cd3 complex," *Trends in immunology*, vol. 27, no. 4, pp. 176–182, 2006.

[141] S. Minguet, M. Swamy, B. Alarcón, I. F. Luescher, and W. W. Schamel, "Full activation of the t cell receptor requires both clustering and conformational changes at cd3," *Immunity*, vol. 26, no. 1, pp. 43–54, 2007.

[142] R. Blanco and B. Alarcón, "Tcr nanoclusters as the framework for transmission of conformational changes and cooperativity," *Frontiers in immunology*, vol. 3, p. 115, 2012.

[143] D. Moogk, A. Natarajan, and M. Krogsgaard, "T cell receptor signal transduction: affinity, force and conformational change," *Current opinion in chemical engineering*, vol. 19, pp. 43–50, 2018.

[144] B. Liu, W. Chen, B. D. Evavold, and C. Zhu, "Accumulation of dynamic catch bonds between tcr and agonist peptide-mhc triggers t cell signaling," *Cell*, vol. 157, no. 2, pp. 357–368, 2014.

[145] F. Baixauli, N. B. Martín-Cófreces, G. Morlino, Y. R. Carrasco, C. Calabia-Linares, E. Veiga, J. M. Serrador, and F. Sánchez-Madrid, "The mitochondrial fission factor dynamin-related protein 1 modulates t-cell receptor signalling at the immune synapse," *The EMBO journal*, vol. 30, no. 7, pp. 1238–1250, 2011.

[146] M. Nebel, B. Zhang, F. Odoardi, A. Flügel, B. V. Potter, and A. H. Guse, "Calcium signalling triggered by naadp in t cells determines cell shape and motility during immune synapse formation," *Messenger*, vol. 4, no. 1, pp. 104–111, 2015.

[147] M. van Ham, R. Teich, L. Philipsen, J. Niemz, N. Amsberg, J. Wissing, M. Nimtz, L. Gröbe, S. Kliche, N. Thiel, *et al.*, "Tcr signalling network organization at the immunological synapses of murine regulatory t cells," *European journal of immunology*, vol. 47, no. 12, pp. 2043–2058, 2017.

[148] D. Malinova, M. Fritzsche, C. R. Nowosad, H. Armer, P. M. Munro, M. P. Blundell, G. Charras, P. Tolar, G. Bouma, and A. J. Thrasher, "Wasp-dependent actin cytoskeleton stability at the dendritic cell immunological synapse is required for extensive, functional t cell contacts," *Journal of leukocyte biology*, vol. 99, no. 5, pp. 699–710, 2016.

[149] I. Maccari, R. Zhao, M. Peglow, K. Schwarz, I. Hornak, M. Pasche, A. Quintana, M. Hoth, B. Qu, and H. Rieger, "Cytoskeleton rotation relocates mitochondria to the immunological synapse and increases calcium signals," *Cell calcium*, vol. 60, no. 5, pp. 309–321, 2016.

[150] N. B. Martín-Cófreces, F. Baixauli, and F. Sánchez-Madrid, "Immune synapse: conductor of orchestrated organelle movement," *Trends in cell biology*, vol. 24, no. 1, pp. 61–72, 2014.

[151] F. Finetti, C. Cassioli, and C. T. Baldari, "Transcellular communication at the immunological synapse: a vesicular traffic-mediated mutual exchange," *F1000Research*, vol. 6, 2017.

[152] N. Blanchard, D. Lankar, F. Faure, A. Regnault, C. Dumont, G. Raposo, and C. Hivroz, "Tcr activation of human t cells induces the production of exosomes bearing the tcr/cd3/ζ complex," *The Journal of Immunology*, vol. 168, no. 7, pp. 3235–3241, 2002.

[153] M. Mittelbrunn, C. Gutiérrez-Vázquez, C. Villarroya-Beltri, S. González, F. Sánchez-Cabo, M. Á. González, A. Bernad, and F. Sánchez-Madrid, "Unidirectional transfer of microrna-loaded exosomes from t cells to antigen-presenting cells," *Nature communications*, vol. 2, p. 282, 2011.

[154] K. Choudhuri, J. Llodrá, E. W. Roth, J. Tsai, S. Gordo, K. W. Wucherpfennig, L. C. Kam, D. L. Stokes, and M. L. Dustin, "Polarized release of t-cell-receptor-enriched microvesicles at the immunological synapse," *Nature*, vol. 507, no. 7490, pp. 118–123, 2014.

[155] M. L. Dustin, "Cell adhesion molecules and actin cytoskeleton at immune synapses and kinapses," *Current opinion in cell biology*, vol. 19, no. 5, pp. 529–533, 2007.

[156] G. A. Azar, F. Lemaître, E. A. Robey, and P. Bousso, "Subcellular dynamics of t cell immunological synapses and kinapses in lymph nodes," *Proceedings of the National Academy of Sciences*, p. 200905901, 2010.

[157] H. D. Moreau, F. Lemaître, E. Terriac, G. Azar, M. Piel, A.-M. Lennon-Dumenil, and P. Bousso, "Dynamic in situ cytometry uncovers t cell receptor signaling during immunological synapses and kinapses in vivo," *Immunity*, vol. 37, no. 2, pp. 351–363, 2012.

[158] H. D. Moreau and P. Bousso, "In vivo imaging of t cell immunological synapses and kinapses in lymph nodes," in *The Immune Synapse: Methods and Protocols* (C. T. Baldari and M. L. Dustin, eds.), pp. 559–568, Springer, 2017.

[159] V. Mayya, E. Judokusumo, E. A. Shah, C. G. Peel, W. Neiswanger, D. Depoil, D. A. Blair, C. H. Wiggins, L. C. Kam, and M. L. Dustin, "Durable interactions of t cells with t cell receptor stimuli in the absence of a stable immunological synapse," *Cell reports*, vol. 22, no. 2, pp. 340–349, 2018.

[160] D. A. Schubert, S. Gordo, J. J. Sabatino, S. Vardhana, E. Gagnon, D. K. Sethi, N. P. Seth, K. Choudhuri, H. Reijonen, G. T. Nepom, *et al.*, "Self-reactive human cd4 t cell clones form unusual immunological synapses," *Journal of Experimental Medicine*, vol. 209, no. 2, pp. 335–352, 2012.

[161] D. R. Leach, M. F. Krummel, and J. P. Allison, "Enhancement of antitumor immunity by ctla-4 blockade," *Science*, vol. 271, no. 5256, pp. 1734–1736, 1996.

[162] E. J. Small, N. S. Tchekmedyian, B. I. Rini, L. Fong, I. Lowy, and J. P. Allison, "A pilot trial of ctla-4 blockade with human anti-ctla-4 in patients with hormone-refractory prostate cancer," *Clinical Cancer Research*, vol. 13, no. 6, pp. 1810–1815, 2007.

[163] P. Kvistborg, D. Philips, S. Kelderman, L. Hageman, C. Ottensmeier, D. Joseph-Pietras, M. J. Welters, S. van der Burg, E. Kapiteijn, O. Michielin, *et al.*, "Anti–ctla-4 therapy broadens the melanoma-reactive cd8+ t cell response," *Science translational medicine*, vol. 6, no. 254, pp. 254ra128–254ra128, 2014.

[164] J. Gao, L. Z. Shi, H. Zhao, J. Chen, L. Xiong, Q. He, T. Chen, J. Roszik, C. Bernatchez, S. E. Woodman, *et al.*, "Loss of ifn-γ pathway genes in tumor cells as a mechanism of resistance to anti-ctla-4 therapy," *Cell*, vol. 167, no. 2, pp. 397–404, 2016.

[165] M. G. Ruocco, K. A. Pilones, N. Kawashima, M. Cammer, J. Huang, J. S. Babb, M. Liu, S. C. Formenti, M. L. Dustin, and S. Demaria, "Suppressing t cell motility induced by anti–ctla-4 monotherapy improves antitumor effects," *The Journal of clinical investigation*, vol. 122, no. 10, pp. 3718–3730, 2012.

[166] S. Qi, J. T. Groves, and A. K. Chakraborty, "Synaptic pattern formation during cellular recognition," *Proceedings of the National Academy of Sciences*, vol. 98, no. 12, pp. 6548–6553, 2001.

[167] S.-J. E. Lee, Y. Hori, J. T. Groves, M. L. Dustin, and A. K. Chakraborty, "The synapse assembly model," *TRENDS in Immunology*, vol. 23, no. 10, pp. 500–502, 2002.

[168] Y. Hori, S. Raychaudhuri, and A. K. Chakraborty, "Analysis of pattern formation and phase separation in the immunological synapse," *The Journal of chemical physics*, vol. 117, no. 20, pp. 9491–9501, 2002.

[169] N. J. Burroughs and C. Wülfing, "Differential segregation in a cell-cell contact interface: the dynamics of the immunological synapse," *Biophysical journal*, vol. 83, no. 4, pp. 1784–1796, 2002.

[170] A. Carlson and L. Mahadevan, "Elastohydrodynamics and kinetics of protein patterning in the immunological synapse," *PLoS Comput Biol*, vol. 11, no. 12, p. e1004481, 2015.

[171] T. Weikl, J. Groves, and R. Lipowsky, "Pattern formation during adhesion of multicomponent membranes," *EPL (Europhysics Letters)*, vol. 59, no. 6, p. 916, 2002.

[172] T. R. Weikl and R. Lipowsky, "Pattern formation during t-cell adhesion," *Biophysical journal*, vol. 87, no. 6, pp. 3665–3678, 2004.

[173] N. Dharan and O. Farago, "Interplay between membrane elasticity and active cytoskeleton forces regulates the aggregation dynamics of the immunological synapse," *Soft matter*, vol. 13, no. 38, pp. 6938–6946, 2017.

[174] M. T. Figge and M. Meyer-Hermann, "Geometrically repatterned immunological synapses uncover formation mechanisms," *PLoS Comput Biol*, vol. 2, no. 11, p. e171, 2006.

[175] M. Figge and M. Meyer-Hermann, "Modeling receptor-ligand binding kinetics in immunological synapse formation," *The European Physical Journal D-Atomic, Molecular, Optical and Plasma Physics*, vol. 51, no. 1, pp. 153–160, 2009.

[176] P. K. Tsourkas, N. Baumgarth, S. I. Simon, and S. Raychaudhuri, "Mechanisms of b-cell synapse formation predicted by monte carlo simulation," *Biophysical journal*, vol. 92, no. 12, pp. 4196–4208, 2007.

[177] P. K. Tsourkas and S. Raychaudhuri, "Modeling of b cell synapse formation by monte carlo simulation shows that directed transport of receptor molecules is a potential formation mechanism," *Cellular and molecular bioengineering*, vol. 3, no. 3, pp. 256–268, 2010.

[178] J. C. Stinchcombe, G. Bossi, S. Booth, and G. M. Griffiths, "The immunological synapse of ctl contains a secretory domain and membrane bridges," *Immunity*, vol. 15, no. 5, pp. 751–761, 2001.

[179] A. Siokis, P. A. Robert, and M. Meyer-Hermann, "Mathematical modeling of synaptic patterns," in *The Immune Synapse: Methods and Protocols* (C. T. Baldari and M. L. Dustin, eds.), pp. 171–182, Springer, 2017.

[180] A. Siokis, P. A. Robert, P. Demetriou, M. L. Dustin, and M. Meyer-Hermann, "F-actin-driven cd28-cd80 localization in the immune synapse," *Cell reports*, vol. 24, no. 5, pp. 1151–1162, 2018.

[181] S. K. Bromley, W. R. Burack, K. G. Johnson, K. Somersalo, T. N. Sims, C. Sumen, M. M. Davis, A. S. Shaw, P. M. Allen, and M. L. Dustin, "The immunological synapse," *Annual review of immunology*, vol. 19, no. 1, pp. 375–396, 2001.

[182] M. Meyer-Hermann, E. Mohr, N. Pelletier, Y. Zhang, G. D. Victora, and K.-M. Toellner, "A theory of germinal center b cell selection, division, and exit," *Cell reports*, vol. 2, no. 1, pp. 162–174, 2012.

[183] R. M. Pielak, G. P. O'Donoghue, J. J. Lin, K. N. Alfieri, N. C. Fay, S. T. Low-Nam, and J. T. Groves, "Early t cell receptor signals globally modulate ligand: receptor affinities during antigen discrimination," *Proceedings of the National Academy of Sciences*, p. 201613140, 2017.

[184] M. L. Dustin, "The immunological synapse," *Cancer immunology research*, vol. 2, no. 11, pp. 1023–1033, 2014.

[185] K. G. Johnson, S. K. Bromley, M. L. Dustin, and M. L. Thomas, "A supramolecular basis for cd45 tyrosine phosphatase regulation in sustained t cell activation," *Proceedings of the National Academy of Sciences*, vol. 97, no. 18, pp. 10138–10143, 2000.

[186] M. L. Thomas and E. J. Brown, "Positive and negative regulation of src-family membrane kinases by cd45," *Immunology today*, vol. 20, no. 9, pp. 406–411, 1999.

[187] J. R. Seavitt, L. S. White, K. M. Murphy, D. Y. Loh, R. M. Perlmutter, and M. L. Thomas, "Expression of the p56 lck y505f mutation in cd45-deficient mice rescues thymocyte development," *Molecular and cellular biology*, vol. 19, no. 6, pp. 4200–4208, 1999.

[188] B. A. Freiberg, H. Kupfer, W. Maslanik, J. Delli, J. Kappler, D. M. Zaller, and A. Kupfer, "Staging and resetting t cell activation in smacs," *Nature immunology*, vol. 3, no. 10, pp. 911–917, 2002.

[189] Y. X. Tan, J. Zikherman, and A. Weiss, "Novel tools to dissect the dynamic regulation of tcr signaling by the kinase csk and the phosphatase cd45," in *Cold Spring Harbor symposia on quantitative biology*, vol. 78, pp. 131–139, Cold Spring Harbor Laboratory Press, 2013.

[190] V. T. Chang, R. A. Fernandes, K. A. Ganzinger, S. F. Lee, C. Siebold, J. McColl, P. Jönsson, M. Palayret, K. Harlos, C. H. Coles, *et al.*, "Initiation of t cell signaling by cd45 segregation at'close contacts'," *Nature immunology*, 2016.

[191] H. Shenoi, J. Seavitt, A. Zheleznyak, M. L. Thomas, and E. J. Brown, "Regulation of integrin-mediated t cell adhesion by the transmembrane protein tyrosine phosphatase cd45," *The Journal of Immunology*, vol. 162, no. 12, pp. 7120–7127, 1999.

[192] U. D'Oro and J. D. Ashwell, "Cutting edge: the cd45 tyrosine phosphatase is an inhibitor of lck activity in thymocytes," *The Journal of Immunology*, vol. 162, no. 4, pp. 1879–1883, 1999.

[193] M. A. Al-Aghbar, Y.-S. Chu, B.-M. Chen, and S. R. Roffler, "High affinity ligands can trigger t cell receptor signaling without cd45 segregation," *Frontiers in immunology*, vol. 9, p. 713, 2018.

[194] C. Irles, A. Symons, F. Michel, T. R. Bakker, P. A. van der Merwe, and O. Acuto, "Cd45 ectodomain controls interaction with gems and lck activity for optimal tcr signaling," *Nature immunology*, vol. 4, no. 2, pp. 189–197, 2003.

[195] N. C. Hartman, J. A. Nye, and J. T. Groves, "Cluster size regulates protein sorting in the immunological synapse," *Proceedings of the National Academy of Sciences*, vol. 106, no. 31, pp. 12729–12734, 2009.

[196] T. Yokosuka, W. Kobayashi, K. Sakata-Sogawa, M. Takamatsu, A. Hashimoto-Tane, M. L. Dustin, M. Tokunaga, and T. Saito, "Spatiotemporal regulation of t cell costimulation by tcr-cd28 microclusters and protein kinase c θ translocation," *Immunity*, vol. 29, no. 4, pp. 589–601, 2008.

[197] B. Graf, T. Bushnell, and J. Miller, "Lfa-1-mediated t cell costimulation through increased localization of tcr/class ii complexes to the central supramolecular activation cluster and exclusion of cd45 from the immunological synapse," *The Journal of Immunology*, vol. 179, no. 3, pp. 1616–1624, 2007.

[198] C. B. Carbone, N. Kern, R. A. Fernandes, E. Hui, X. Su, K. C. Garcia, and R. D. Vale, "In vitro reconstitution of t cell receptor-mediated segregation of the cd45 phosphatase," *Proceedings of the National Academy of Sciences*, vol. 114, no. 44, pp. E9338–E9345, 2017.

[199] C. J. Wang, F. Heuts, V. Ovcinnikovs, L. Wardzinski, C. Bowers, E. M. Schmidt, A. Kogimtzis, R. Kenefeck, D. M. Sansom, and L. S. Walker, "Ctla-4 controls follicular helper t-cell differentiation by regulating the strength of cd28 engagement," *Proceedings of the National Academy of Sciences*, vol. 112, no. 2, pp. 524–529, 2015.

[200] D. M. Sansom and L. S. Walker, "The role of cd28 and cytotoxic t-lymphocyte antigen-4 (ctla-4) in regulatory t-cell biology," *Immunological reviews*, vol. 212, no. 1, pp. 131–148, 2006.

[201] O. Acuto and F. Michel, "Cd28-mediated co-stimulation: a quantitative support for tcr signalling," *Nature Reviews Immunology*, vol. 3, no. 12, pp. 939–951, 2003.

[202] N. Beyersdorf, T. Kerkau, and T. Hünig, "Cd28 co-stimulation in t-cell homeostasis: a recent perspective," *ImmunoTargets and therapy*, vol. 4, p. 111, 2015.

[203] J. M. Slavik, J. E. Hutchcroft, and B. E. Bierer, "Cd80 and cd86 are not equivalent in their ability to induce the tyrosine phosphorylation of cd28," *Journal of Biological Chemistry*, vol. 274, no. 5, pp. 3116–3124, 1999.

[204] T. Pentcheva-Hoang, J. G. Egen, K. Wojnoonski, and J. P. Allison, "B7-1 and b7-2 selectively recruit ctla-4 and cd28 to the immunological synapse," *Immunity*, vol. 21, no. 3, pp. 401–413, 2004.

[205] S. K. Bromley, A. Iaboni, S. J. Davis, A. Whitty, J. M. Green, A. S. Shaw, A. Weiss, and M. L. Dustin, "The immunological synapse and cd28-cd80 interactions," *Nature immunology*, vol. 2, no. 12, p. 1159, 2001.

[206] S.-Y. Tseng, M. Liu, and M. L. Dustin, "Cd80 cytoplasmic domain controls localization of cd28, ctla-4, and protein kinase cθ in the immunological synapse," *The Journal of Immunology*, vol. 175, no. 12, pp. 7829–7836, 2005.

[207] M. Sanchez-Lockhart, B. Graf, and J. Miller, "Signals and sequences that control cd28 localization to the central region of the immunological synapse," *The Journal of Immunology*, vol. 181, no. 11, pp. 7639–7648, 2008.

[208] S.-Y. Tseng, J. C. Waite, M. Liu, S. Vardhana, and M. L. Dustin, "T cell-dendritic cell immunological synapses contain tcr-dependent cd28-cd80 clusters that recruit protein kinase cθ," *The Journal of Immunology*, vol. 181, no. 7, pp. 4852–4863, 2008.

[209] R. Tavano, R. L. Contento, S. J. Baranda, M. Soligo, L. Tuosto, S. Manes, and A. Viola, "Cd28 interaction with filamin-a controls lipid raft accumulation at the t-cell immunological synapse," *Nature cell biology*, vol. 8, no. 11, p. 1270, 2006.

[210] K. Hayashi and A. Altman, "Filamin a is required for t cell activation mediated by protein kinase c-θ," *The Journal of Immunology*, vol. 177, no. 3, pp. 1721–1728, 2006.

[211] P. A. van der Merwe, D. L. Bodian, S. Daenke, P. Linsley, and S. J. Davis, "Cd80 (b7-1) binds both cd28 and ctla-4 with a low affinity and very fast kinetics," *Journal of Experimental Medicine*, vol. 185, no. 3, pp. 393–404, 1997.

[212] P. A. Van Der Merwe, A. N. Barclay, D. W. Mason, E. A. Davies, B. P. Morgan, M. Tone, A. Krishnam, C. Ianelli, and S. J. Davis, "Human cell-adhesion molecule cd2 binds cd58 (lfa-3) with a very low affinity and an extremely fast dissociation rate but does not bind cd48 or cd59.," *Biochemistry*, vol. 33, no. 33, pp. 10149–10160, 1994.

[213] K. Badour, J. Zhang, F. Shi, M. K. McGavin, V. Rampersad, L. A. Hardy, D. Field, and K. A. Siminovitch, "The wiskott-aldrich syndrome protein acts downstream of cd2 and the cd2ap and pstpip1 adaptors to promote formation of the immunological synapse," *Immunity*, vol. 18, no. 1, pp. 141–154, 2003.

[214] O. Milstein, S.-Y. Tseng, T. Starr, J. Llodra, A. Nans, M. Liu, M. K. Wild, P. A. van der Merwe, D. L. Stokes, Y. Reisner, *et al.*, "Nanoscale increases in cd2-cd48-mediated intermembrane spacing decrease adhesion and reorganize the immunological synapse," *Journal of Biological Chemistry*, vol. 283, no. 49, pp. 34414–34422, 2008.

[215] T. Shao, W. Shi, J.-y. Zheng, C. Li, X.-X. Xu, A.-f. Lin, L. Xiang, and J.-Z. Shao, "Costimulatory function of cd58/cd2 interaction in adaptive humoral immunity in a zebrafish model," *Frontiers in immunology*, vol. 9, p. 1204, 2018.

[216] P. Demetriou and M. L. Dustin, "Unpublished data regarding the localization and pattern formation of cd2-cd58 pairs." unpublished, 2019.

[217] P. A. van der Merwe, M. H. Brown, S. Davis, and A. Barclay, "Affinity and kinetic analysis of the interaction of the cell adhesion molecules rat cd2 and cd48.," *The EMBO journal*, vol. 12, no. 13, p. 4945, 1993.

[218] P. A. van der Merwe, P. N. McNamee, E. A. Davies, A. N. Barclay, and S. J. Davis, "Topology of the cd2–cd48 cell-adhesion molecule complex: implications for antigen recognition by t cells," *Current Biology*, vol. 5, no. 1, pp. 74–84, 1995.

[219] M. L. Dustin, L. M. Ferguson, P.-Y. Chan, T. A. Springer, and D. E. Golan, "Visualization of cd2 interaction with lfa-3 and determination of the two-dimensional dissociation constant for adhesion receptors in a contact area.," *The Journal of Cell Biology*, vol. 132, no. 3, pp. 465–474, 1996.

[220] M. L. Dustin, D. E. Golan, D.-M. Zhu, J. M. Miller, W. Meier, E. A. Davies, and P. A. van der Merwe, "Low affinity interaction of human or rat t cell adhesion molecule cd2 with its ligand aligns adhering membranes to achieve high physiological affinity," *Journal of Biological Chemistry*, vol. 272, no. 49, pp. 30889–30898, 1997.

[221] D.-M. Zhu, M. L. Dustin, C. W. Cairo, H. S. Thatte, and D. E. Golan, "Mechanisms of cellular avidity regulation in cd2–cd58-mediated t cell adhesion," *ACS chemical biology*, vol. 1, no. 10, pp. 649–658, 2006.

[222] E. V. Tibaldi, R. Salgia, and E. L. Reinherz, "Cd2 molecules redistribute to the uropod during t cell scanning: implications for cellular activation and immune surveillance," *Proceedings of the National Academy of Sciences*, vol. 99, no. 11, pp. 7582–7587, 2002.

[223] N. Espagnolle, D. Depoil, R. Zaru, C. Demeur, E. Champagne, M. Guiraud, and S. Valitutti, "Cd2 and tcr synergize for the activation of phospholipase cγ1/calcium pathway at the immunological synapse," *International immunology*, vol. 19, no. 3, pp. 239–248, 2007.

[224] J.-h. Wang, A. Smolyar, K. Tan, J.-h. Liu, M. Kim, J. S. Zhen-yu, G. Wagner, and E. L. Reinherz, "Structure of a heterophilic adhesion complex between the human cd2 and cd58 (lfa-3) counterreceptors," *Cell*, vol. 97, no. 6, pp. 791–803, 1999.

[225] M. Sanders, M. Makgoba, S. Sharrow, D. Stephany, T. Springer, H. Young, and S. Shaw, "Human memory t lymphocytes express increased levels of three cell adhesion molecules (lfa-3, cd2, and lfa-1) and three other molecules (uchl1, cdw29, and pgp-1) and have enhanced ifn-gamma production.," *The Journal of Immunology*, vol. 140, no. 5, pp. 1401–1407, 1988.

[226] A. Hashimoto-Tane, M. Sakuma, H. Ike, T. Yokosuka, Y. Kimura, O. Ohara, and T. Saito, "Micro–adhesion rings surrounding tcr microclusters are essential for t cell activation," *Journal of Experimental Medicine*, vol. 213, no. 8, pp. 1609–1625, 2016.

[227] A. Hashimoto-Tane, T. Yokosuka, and T. Saito, "Analyzing the dynamics of signaling microclusters," in *The Immune Synapse: Methods and Protocols*, pp. 51–64, Springer, 2017.

[228] K. Karjalainen, "High sensitivity, low affinity—paradox of t-cell receptor recognition," *Current opinion in immunology*, vol. 6, no. 1, pp. 9–12, 1994.

[229] J. A. Siller-Farfán and O. Dushek, "Molecular mechanisms of t cell sensitivity to antigen," *Immunological reviews*, vol. 285, no. 1, pp. 194–205, 2018.

[230] J. Huang, M. Brameshuber, X. Zeng, J. Xie, Q.-j. Li, Y.-h. Chien, S. Valitutti, and M. M. Davis, "A single peptide-major histocompatibility complex ligand triggers digital cytokine secretion in cd4+ t cells," *Immunity*, vol. 39, no. 5, pp. 846–857, 2013.

[231] J. D. Stone, A. S. Chervin, and D. M. Kranz, "T-cell receptor binding affinities and kinetics: impact on t-cell activity and specificity," *Immunology*, vol. 126, no. 2, pp. 165–176, 2009.

[232] N. Martin-Blanco, R. Blanco, C. Alda-Catalinas, E. Bovolenta, C. Oeste, E. Palmer, W. Schamel, G. Lythe, C. Molina-París, M. Castro, *et al.*, "A window of opportunity for cooperativity in the t cell receptor," *Nature communications*, vol. 9, no. 1, p. 2618, 2018.

[233] E. Molnár, S. Deswal, and W. W. Schamel, "Pre-clustered tcr complexes," *FEBS letters*, vol. 584, no. 24, pp. 4832–4837, 2010.

[234] W. W. Schamel and B. Alarcón, "Organization of the resting tcr in nanoscale oligomers," *Immunological reviews*, vol. 251, no. 1, pp. 13–20, 2013.

[235] E. Sherman, V. Barr, S. Manley, G. Patterson, L. Balagopalan, I. Akpan, C. K. Regan, R. K. Merrill, C. L. Sommers, J. Lippincott-Schwartz, *et al.*, "Functional nanoscale organization of signaling molecules downstream of the t cell antigen receptor," *Immunity*, vol. 35, no. 5, pp. 705–720, 2011.

[236] T. A. Springer and M. L. Dustin, "Integrin inside-out signaling and the immunological synapse," *Current opinion in cell biology*, vol. 24, no. 1, pp. 107–115, 2012.

[237] R. J. Faull and M. H. Ginsberg, "Inside-out signaling through integrins.," *Journal of the American Society of Nephrology*, vol. 7, no. 8, pp. 1091–1097, 1996.

[238] J.-P. Changeux and S. J. Edelstein, "Allosteric mechanisms of signal transduction," *Science*, vol. 308, no. 5727, pp. 1424–1428, 2005.

[239] W. W. Schamel, B. Alarcon, T. Höfer, and S. Minguet, "The allostery model of tcr regulation," *The Journal of Immunology*, vol. 198, no. 1, pp. 47–52, 2017.

[240] E. Carrizosa, T. S. Gomez, C. M. Labno, D. A. K. Dehring, X. Liu, B. D. Freedman, D. D. Billadeau, and J. K. Burkhardt, "Hematopoietic lineage cell-specific protein 1 is recruited to the immunological synapse by il-2-inducible t cell kinase and regulates phospholipase cγ1

microcluster dynamics during t cell spreading," *The Journal of Immunology*, pp. jimmunol–0900973, 2009.

[241] A. Braiman, M. Barda-Saad, C. L. Sommers, and L. E. Samelson, "Recruitment and activation of plcγ1 in t cells: a new insight into old domains," *The EMBO journal*, vol. 25, no. 4, pp. 774–784, 2006.

[242] M. Coué, S. L. Brenner, I. Spector, and E. D. Korn, "Inhibition of actin polymerization by latrunculin a," *FEBS letters*, vol. 213, no. 2, pp. 316–318, 1987.

[243] B. Nolen, N. Tomasevic, A. Russell, D. Pierce, Z. Jia, C. McCormick, J. Hartman, R. Sakowicz, and T. Pollard, "Characterization of two classes of small molecule inhibitors of arp2/3 complex," *Nature*, vol. 460, no. 7258, p. 1031, 2009.

[244] B. Hetrick, M. S. Han, L. A. Helgeson, and B. J. Nolen, "Small molecules ck-666 and ck-869 inhibit actin-related protein 2/3 complex by blocking an activating conformational change," *Chemistry & biology*, vol. 20, no. 5, pp. 701–712, 2013.

[245] T. Yokosuka and T. Saito, "Dynamic regulation of t-cell costimulation through tcr–cd28 microclusters," *Immunological reviews*, vol. 229, no. 1, pp. 27–40, 2009.

[246] N. Martínez-Martín, R. M. Risueño, A. Morreale, I. Zaldívar, E. Fernández-Arenas, F. Herranz, A. R. Ortiz, and B. Alarcón, "Cooperativity between t cell receptor complexes revealed by conformational mutants of cd3ϵ," *Sci. Signal.*, vol. 2, no. 83, pp. ra43–ra43, 2009.

[247] T. M. Fahmy, J. G. Bieler, M. Edidin, and J. P. Schneck, "Increased tcr avidity after t cell activation: a mechanism for sensing low-density antigen," *Immunity*, vol. 14, no. 2, pp. 135–143, 2001.

[248] J. F. Dixon, J. L. Law, and J. J. Favero, "Activation of human t lymphocytes by crosslinking of anti-cd3 monoclonal antibodies," *Journal of leukocyte biology*, vol. 46, no. 3, pp. 214–220, 1989.

[249] M. L. Dustin and T. A. Springer, "T-cell receptor cross-linking transiently stimulates adhesiveness through lfa-1," *Nature*, vol. 341, no. 6243, p. 619, 1989.

[250] G. Dong, R. Kalifa, P. R. Nath, S. Gelkop, and N. Isakov, "Tcr crosslinking promotes crk adaptor protein binding to tyrosine-phosphorylated cd3ζ chain," *Biochemical and biophysical research communications*, vol. 488, no. 3, pp. 541–546, 2017.

[251] E. Cai, K. Marchuk, P. Beemiller, C. Beppler, M. G. Rubashkin, V. M. Weaver, A. Gérard, T.-L. Liu, B.-C. Chen, E. Betzig, *et al.*, "Visualizing dynamic microvillar search and stabilization during ligand detection by t cells," *Science*, vol. 356, no. 6338, p. eaal3118, 2017.

[252] Y. Jung, I. Riven, S. W. Feigelson, E. Kartvelishvily, K. Tohya, M. Miyasaka, R. Alon, and G. Haran, "Three-dimensional localization of t-cell receptors in relation to microvilli

using a combination of superresolution microscopies," *Proceedings of the National Academy of Sciences*, vol. 113, no. 40, pp. E5916–E5924, 2016.

[253] M. de la Roche, Y. Asano, and G. M. Griffiths, "Origins of the cytolytic synapse," *Nature Reviews Immunology*, vol. 16, no. 7, p. 421, 2016.

[254] D. V. Köster and S. Mayor, "Cortical actin and the plasma membrane: inextricably intertwined," *Current opinion in cell biology*, vol. 38, pp. 81–89, 2016.

[255] T. L. Walunas, C. Y. Bakker, and J. A. Bluestone, "Ctla-4 ligation blocks cd28-dependent t cell activation.," *Journal of Experimental Medicine*, vol. 183, no. 6, pp. 2541–2550, 1996.

[256] L. E. Marengère, P. Waterhouse, G. S. Duncan, H.-W. Mittrücker, G.-S. Feng, and T. W. Mak, "Regulation of t cell receptor signaling by tyrosine phosphatase syp association with ctla-4," *Science*, vol. 272, no. 5265, pp. 1170–1173, 1996.

[257] J. G. Egen and J. P. Allison, "Cytotoxic t lymphocyte antigen-4 accumulation in the immunological synapse is regulated by tcr signal strength," *Immunity*, vol. 16, no. 1, pp. 23–35, 2002.

[258] P. S. Linsley, J. Bradshaw, J. Greene, R. Peach, K. L. Bennett, and R. S. Mittler, "Intracellular trafficking of ctla-4 and focal localization towards sites of tcr engagement," *Immunity*, vol. 4, no. 6, pp. 535–543, 1996.

[259] S. Khailaie, B. Rowshanravan, P. A. Robert, E. Waters, N. Halliday, J. D. B. Herrera, L. S. Walker, D. M. Sansom, and M. Meyer-Hermann, "Characterization of ctla4 trafficking and implications for its function," *Biophysical journal*, vol. 115, no. 7, pp. 1330–1343, 2018.

[260] O. S. Qureshi, Y. Zheng, K. Nakamura, K. Attridge, C. Manzotti, E. M. Schmidt, J. Baker, L. E. Jeffery, S. Kaur, Z. Briggs, *et al.*, "Trans-endocytosis of cd80 and cd86: a molecular basis for the cell-extrinsic function of ctla-4," *Science*, vol. 332, no. 6029, pp. 600–603, 2011.

[261] C. B. Thompson and J. P. Allison, "The emerging role of ctla-4 as an immune attenuator," *Immunity*, vol. 7, no. 4, pp. 445–450, 1997.

[262] G. J. Freeman, A. J. Long, Y. Iwai, K. Bourque, T. Chernova, H. Nishimura, L. J. Fitz, N. Malenkovich, T. Okazaki, M. C. Byrne, *et al.*, "Engagement of the pd-1 immunoinhibitory receptor by a novel b7 family member leads to negative regulation of lymphocyte activation," *Journal of Experimental Medicine*, vol. 192, no. 7, pp. 1027–1034, 2000.

[263] Y. Latchman, C. R. Wood, T. Chernova, D. Chaudhary, M. Borde, I. Chernova, Y. Iwai, A. J. Long, J. A. Brown, R. Nunes, *et al.*, "Pd-l2 is a second ligand for pd-1 and inhibits t cell activation," *Nature immunology*, vol. 2, no. 3, p. 261, 2001.

[264] P. C. Tumeh, C. L. Harview, J. H. Yearley, I. P. Shintaku, E. J. Taylor, L. Robert, B. Chmielowski, M. Spasic, G. Henry, V. Ciobanu, *et al.*, "Pd-1 blockade induces responses by inhibiting adaptive immune resistance," *Nature*, vol. 515, no. 7528, p. 568, 2014.

[265] S. M. Ansell, A. M. Lesokhin, I. Borrello, A. Halwani, E. C. Scott, M. Gutierrez, S. J. Schuster, M. M. Millenson, D. Cattry, G. J. Freeman, *et al.*, "Pd-1 blockade with nivolumab in relapsed or refractory hodgkin's lymphoma," *New England Journal of Medicine*, vol. 372, no. 4, pp. 311–319, 2015.

[266] J. M. Zaretsky, A. Garcia-Diaz, D. S. Shin, H. Escuin-Ordinas, W. Hugo, S. Hu-Lieskovan, D. Y. Torrejon, G. Abril-Rodriguez, S. Sandoval, L. Barthly, *et al.*, "Mutations associated with acquired resistance to pd-1 blockade in melanoma," *New England Journal of Medicine*, vol. 375, no. 9, pp. 819–829, 2016.

[267] S. J. Rodig, D. Gusenleitner, D. G. Jackson, E. Gjini, A. Giobbie-Hurder, C. Jin, H. Chang, S. B. Lovitch, C. Horak, J. S. Weber, *et al.*, "Mhc proteins confer differential sensitivity to ctla-4 and pd-1 blockade in untreated metastatic melanoma," *Science translational medicine*, vol. 10, no. 450, p. eaar3342, 2018.

[268] N. A. Rizvi, J. Mazières, D. Planchard, T. E. Stinchcombe, G. K. Dy, S. J. Antonia, L. Horn, H. Lena, E. Minenza, B. Mennecier, *et al.*, "Activity and safety of nivolumab, an anti-pd-1 immune checkpoint inhibitor, for patients with advanced, refractory squamous non-small-cell lung cancer (checkmate 063): a phase 2, single-arm trial," *The Lancet Oncology*, vol. 16, no. 3, pp. 257–265, 2015.

[269] N. A. Rizvi, M. D. Hellmann, A. Snyder, P. Kvistborg, V. Makarov, J. J. Havel, W. Lee, J. Yuan, P. Wong, T. S. Ho, *et al.*, "Mutational landscape determines sensitivity to pd-1 blockade in non–small cell lung cancer," *Science*, vol. 348, no. 6230, pp. 124–128, 2015.

[270] C. D. Schmeitz, E. A. Hernandez-Vargas, R. Fliegert, A. H. Guse, and M. Meyer-Hermann, "A mathematical model of t lymphocyte calcium dynamics derived from single transmembrane protein properties," *Frontiers in immunology*, vol. 4, p. 277, 2013.

[271] J. C. Nolz, T. S. Gomez, P. Zhu, S. Li, R. B. Medeiros, Y. Shimizu, J. K. Burkhardt, B. D. Freedman, and D. D. Billadeau, "The wave2 complex regulates actin cytoskeletal reorganization and crac-mediated calcium entry during t cell activation," *Current biology*, vol. 16, no. 1, pp. 24–34, 2006.

[272] D. E. Clapham, "Calcium signaling," *Cell*, vol. 131, no. 6, pp. 1047–1058, 2007.

[273] M. Hoth, "Crac channels, calcium, and cancer in light of the driver and passenger concept," *Biochimica et Biophysica Acta (BBA)-Molecular Cell Research*, vol. 1863, no. 6, pp. 1408–1417, 2016.

[274] L. Simeoni, "Lck activation: puzzling the pieces together," *Oncotarget*, vol. 8, no. 61, p. 102761, 2017.